Influence of Reinforcing Steel Parameters on the Formation of the Passive Layer

Laura J. Smolinski

Thesis submitted to the faculty of the Virginia Polytechnic Institute and State University
in partial fulfillment of the requirements for the degree of

Master of Science
In
Civil and Environmental Engineering

Richard E. Weyers, Chair
Carin L. Roberts-Wollmann
David Mokarem

February 15, 2007
Blacksburg, VA

Keywords: Corrosion, Macrocell Corrosion, Reinforced Concrete, Passive Layer

Influence of Reinforcing Steel Parameters on the Formation of the Passive Layer

Laura J. Smolinski

Abstract

Corrosion in reinforced concrete bridge decks has always been a concern amongst engineers. However, as structures continue to increase in size and in the amount of reinforcement present, consideration must be given to parameters such as the clear spacing arrangements between bars, the presence and absence of stay-in-place (SIP) forms, and differences in the cathode bar to anode bar ratios. Limited research has been performed to determine the effects of the parameters (Shiessel, P. 1986).

Research has been conducted on the effects of macrocell corrosion compared to microcell corrosion. Previous studies have shown that the measured microcell corrosion is not augmented greatly by the macrocell current (Andrade et al. 1991). In this study, twenty-seven specimens were cast with reinforcing steel to represent reinforcing mats at the top and bottom of each specimen. Top and bottom spacing arrangements were approximately 51, 76, 102 mm (2, 3, and 4-inches), cathode-to-anode bar (C/A) ratios were 2 and 1, and the presence and absence of SIP were considered. Macrocell currents, resistivity measurements, half-cell potential measurements, and corrosion current densities were recorded over a 273 day time period to compare the differences that existed amongst the three different parameters.

Based upon the data that was collected, no significant differences were recorded when comparisons were made between the spacing arrangements, the absence and presence of SIP, and differences in C/A ratios. The formation of the passive layer was confirmed by the corrosion current densities and half-cell potentials. The rate of the formation of the passive layer occurred in two distinct periods, a rapid rate from casting to about 105 days and a significantly slower rate beyond 105 days after casting. There was no detected influence of the macrocell activity on the formation of the passive layer throughout the 273 day study period.

ACKNOWLEDGEMENTS

I would first like to thank Dr. Richard Weyers for his guidance, patience and understanding throughout the completion of my masters degree and the opportunity to participate in a research project. You have provided me with an invaluable wealth of knowledge that I will greatly benefit upon for the rest of my professional career.

I would also like to thank the countless hours of mentorship from my peers, Gregory Williamson and Andrei Ramniceanu. Without your assistance and outstanding sense of humor I would have been unable to complete such an extensive project in such a short amount of time.

Last, I would like to thank my parents Henry and Diane Smolinski as well as my sister Lynn. Their constant love and support were my motivation to return for my degree as well as its completion. I love you and want you to know that your encouragement and advice are a driving force throughout my future endeavors.

TABLE OF CONTENTS

LIST OF TABLES

LIST OF FIGURES

INTRODUCTION

Corrosion damage to bridges has long been a problem in the United States. A turning point that led to closer scrutiny of the problem occurred when the Silver Bridge collapsed on December 15, 1967. The collapse of the bridge prompted a national concern over the safety and condition of existing bridges and led to the establishment of the National Bridge Inspection Standards under the Federal-Aid Highway Act of 1968 and the Special Bridge Replacement Program under the Federal-Aid Highway Act of 1970 (Weingroff, R.F. 1996). Since then, billions of dollars have been spent on protecting, repairing and replacing damages caused by corrosion.

One of the largest maintenance, repair, and rehabilitation problems is the corrosion of reinforcing steel in concrete as a result of winter maintenance activities. The United States uses over 10 million tons of deicing salts per year on the highway system (Broomfield, J.P. 1997). According to a 1991 Transportation Research Board Report, the annual cost of bridge deck repairs as attributed to deicing salts was estimated between $50 to $200 million (Broomfield, J.P. 1997). Fifteen years later, this trend continues to increase as bridges within the United States continue to experience rapid and severe deterioration as well as an increase in the maintenance demands because of the effects of corrosion.

In recent years, numerous studies have been performed to investigate methods that may effectively reduce the rate of corrosion and its associated costs. However, little basic research has been conducted on the controlling factors which influence the chloride initiation and subsequent corrosion rate. One such factor is when truss bars are utilized which increase the cathode area within concrete bridge decks. This study will address the effects of the cathode area on the macrocell corrosion in simulated concrete bridge decks. Macrocell corrosion is defined as the top mat of reinforcing steel being the anode and the bottom mat being the cathode.

LITERATURE REVIEW

Concrete Reinforcement Corrosion

The damage and economic strain that result from corrosion of reinforcing steel in concrete can be categorized as the largest single infrastructure problem facing industrialized countries (Broomfield, J.P. 1997). Because of its significant economical impact, an increase in demand for studies on the prevention of corrosion has occurred. The subject of corrosion especially came to light once it was discovered that an appreciable number of structures were suffering from damages of corrosion at a premature age. Several structures were found to be experiencing severe effects of corrosion at as early an age as 20 years out of a 120-year life span (Berke, N.S. and Hicks, M.C. 1996). Such early ages of failure only meant greater economic losses, which pressured engineers to determine why structures were not able to provide an acceptable level of service throughout their design life span.

The most common causes of corrosion in reinforced concrete structures develop from the intrusion of chlorides and through carbonation. Experiments have been performed in the past to analyze different variables such as the spacing between reinforcing bars, different reinforcing bar materials, different admixtures, and numerous methods to identify ideal rehabilitation methods to be used for reinforced concrete structures (Andrade, C. et al 1991 and Raupach, M. 1996). Research continues today to expand upon what is known.

Corrosion Mechanism in Concrete

In order to understand how to reduce or prevent corrosion in reinforced concrete, a basic understanding of the reactions and processes that take place is necessary.

Electrochemical Process

An electrochemical process occurs once steel reinforcement corrodes within the concrete. The products of corrosion are created through the electrochemical reaction of iron, water, and oxygen. This electrochemical reaction is generally composed of four processes.

The first reaction is the anodic process in which the oxidation of iron occurs at the anode area of the steel. At the anode areas of the steel, electrons are lost and metallic ions are formed on the steel surface which is represented by the following reaction:

$$Fe \rightarrow Fe^{2+} + 2e^{-} \qquad \text{(Equation 1)}$$

Actual metal loss will occur at the anode area. During the anodic reaction, electrons are deposited on the surface of the steel, increasing the electrical potential (Bentur, A. et al 1997). The ferrous ions that are produced dissolve in the water solution surrounding the steel and produce acidic conditions as shown in the following reaction:

$$Fe^{2+} + 2H_2O \rightarrow Fe(OH)_2 + 2H^{+} \qquad \text{(Equation 2)}$$

The electrons that are lost during the anodic reaction are consumed by the cathodic reaction, the second electrochemical reaction needed in order for corrosion to take place. The reduction of oxygen occurs and can be represented by the following reactions:

$$O_2 + 2H_2O + 4e^{-} \rightarrow 4OH^{-} \qquad \text{(Equation 3)}$$

The third process occurs with "the transport of electrons within the metal from the anodic regions, where they become available, to the cathodic regions where they are consumed" (Bertolini, L. et al 2004). The electrons that are deposited on the surface of the steel will migrate toward a lower electrical potential, the cathode area. The flow of electrons from the anode, through the steel, to the cathode creates an electrical current within the steel reinforcing bar and forms a closed loop with the hydroxyl ion migrating to the anode

area, sometimes referred to as galvanic corrosion, which also represents the fourth process (Chess, P. 1998).

All four processes must occur at the same rate and must be equal in order for corrosion to occur. The corrosion rate will be controlled by the slowest of the four processes mentioned above. The anode and cathode reactions must also be balanced in order for the corrosion process to continue. The number of electrons that are received by the cathode area must equal the number or electrons that are contributed by the anode area (Bentur A. et al 1997).

However, the reactions that take place at the anode and cathode do not complete the process to create rust. There are several more reactions that must be explained in order to fully understand the formation of rust. The additional reactions needed are as follows:

$$Fe^{2+} + 2OH^- \rightarrow Fe(OH)_2 \qquad \text{(Equation 4)}$$

$$4Fe(OH)_2 + O_2 + 2H_2O \rightarrow 4Fe(OH)_3 \qquad \text{(Equation 5)}$$

$$2Fe(OH)_3 \rightarrow Fe_2O_3H_2O + 2H_2O \qquad \text{(Equation 6)}$$

In equation 4, ferrous hydroxide is formed. The ferrous hydroxide then forms ferric hydroxide which in turn forms hydrated ferric oxide which is more commonly referred to as rust, equation 5. The ferric oxide that is produced in equation 6 has a volume that is twice that of steel (Broomfield, J.P. 1997). Once the ferric oxide hydrates, it swells, becoming more porous. This increase in volume may eventually create a pressure great enough to exceed the tensile capacity of the concrete which can lead to cracking, spalling, and delamination of the cover concrete (ACI Committee 222 1996).

Figure 1 provides a graphical description of the corrosion process:

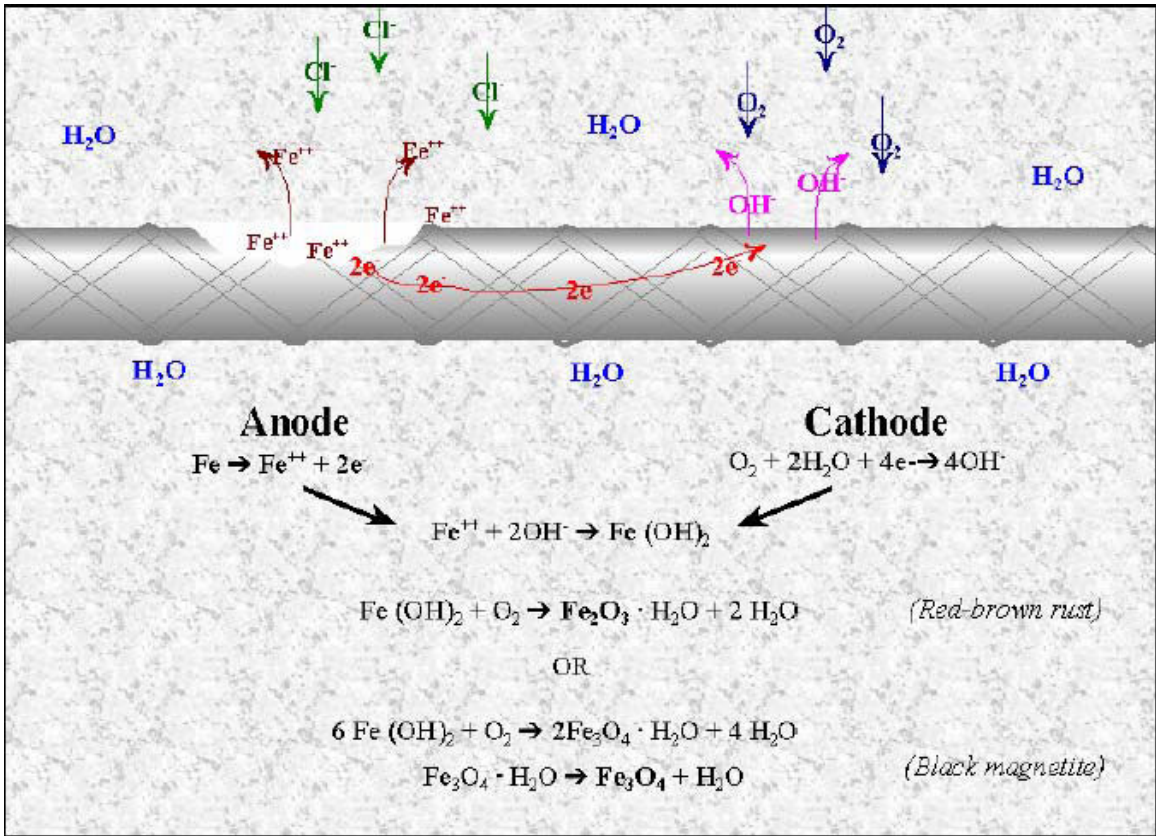

Figure 1 – Electrochemical Process of Steel Corrosion in Concrete (Brown, M.C. 2002)

The most common occurrences of corrosion in reinforced concrete structures, as stated earlier, are the intrusion of chlorides and carbonation. Both processes are detrimental once present at the depth of the reinforcing steel. Measures must be taken to minimize both in order to prevent the premature failure of structures.

Chlorides

Chlorides can be introduced during the mixing of concrete or once concrete is already hardened. During the mixing process, chlorides may enter the mix as chloride-contaminated aggregates, sea water, or as an admixture component (usually $CaCl_2$) (Weingroff, R.F. 1996 and Bentur, A. et al 1997). Once concrete has hardened, chlorides can still diffuse into the material from external sources such as sea water, salt spray, or deicing salts (Weingroff, R.F. 1996 and Bentur, A. et al 1997). Once sufficient chlorides are present, it is difficult to eliminate corrosion; hence precautions must be taken to

prevent the excess addition and to reduce the effects of atmospheric exposure to chloride environments.

Several chemical reactions must occur in order for corrosion of the steel to occur within the concrete. The chlorides must first penetrate or disrupt a passive layer that exists on the reinforcing steel. The hydroxides in concrete create a very alkaline condition when mixed with water and create the passive layer on the surface of the steel (Bentur, A. et al 1997). The passive layer is formed in concrete when the steel reacts with oxygen to form oxides which in turn form hydroxides, and is only a few nanometers in thickness (Broomfield, J.P. 1997). The final form of the passive layer is the gamma phase of ferric oxide. This passive layer will remain intact as long as it stays in contact with the concrete pore solution and will resist further corrosion. As chlorides come in contact with and break down this passive layer, they become a catalyst for corrosion. Chlorides will continue to break apart the passive layer surrounding the reinforcing bar, commencing the corrosion process.

Carbonation

Carbon dioxide is one of the most common gases that can penetrate concrete and destroy the protective passive layer of steel reinforcement. Carbonation occurs when the carbon dioxide within the atmosphere reacts with the water inside the pores of the concrete to form carbonic acid (Revie, R.W. 2000). The acid then reacts with the calcium and other hydroxides to form solid carbonates (Revie, R.W. 2000). Carbonation can be a result of poor concrete cover, poor concrete quality, and poor consolidation. The following reaction is associated with carbonation:

$$CO_2 + Ca(OH)_2 \xrightarrow{H_2O,NaOH} CaCO_3 + H_2O \qquad \text{(Equation 7)}$$

Carbonation will initially attack the surface of the concrete and then gradually move inwards. The pH levels in the pore solution within the concrete will decrease from a pH level of approximately 12 to a pH level of approximately 8, approaching neutrality

(Bertolini, L. 2004). The decrease in the pH levels decreases the stability of the passive layer. The instability of the passive layer leads to a breakdown of this passive layer which will initiate corrosion.

The rate that corrosion will occur as a result of carbonation depends on environmental factors and factors related to the concrete. Environmental factors include humidity, temperature, and the concentration levels of carbon dioxide while factors related to the concrete involve the alkalinity levels and the permeability of the concrete (Bertolini, L. 2004). The following equation describes the rate of carbonation which decreases with time:

$$d = k * t^{\frac{1}{2}} \qquad \text{(Equation 8)}$$

where, d = depth of carbonation (mm)

t = time (years)

k = carbonation coefficient ($mm/y^{1/2}$)

Electrical Potential

As stated before, in order for corrosion to occur, the passive layer along the steel must be disrupted. A conservative chloride concentration required to commence the deterioration of the passive layer has been reported to be between 0.6 to 1.2 kilograms of chloride ion per cubic meter of concrete for uninhibited systems (Berke, N.S. and Hicks, M.C. 1996 and Zemajtis, J. 1998).

ASTM C 867 provides a manner in which to interpret half cell potentials in the field. The values are compared against a copper/copper sulfate half cell. The corroding electrode potential is measured against a standard reference probe, the copper/copper sulfate electrode (Broomfield, J.P. 1997 and Shiessel, P. 1998). The half cell potentials are not corrosion rate measurements, but instead are utilized to indicate the likeliness that corrosion may be occurring (Broomfield, J.P. 1997). The table listed below represents

the ASTM C 876-91 criteria for corrosion of steel in concrete for the copper/copper sulfate half cell:

Potential Readings (mV)	**Probability of Corrosion**
$x \geq -200$	Low Probability→ less than 10%
$-200 > x > -350$	Uncertain Probability
$x \leq -350$	High Probability → 90% or greater

The Influence of Micro and Macro-cell Corrosion

Two mechanisms of corrosion that are often overlooked are those of microcells and macrocells. Different spatial locations of both the anode and the cathode leads to different forms of corrosion of the reinforcing steel in concrete (Elsener, B. 2002).

Microcell Corrosion

Microcell corrosion is observed when the anodic and cathodic reactions take place adjacent to one another. Microcell corrosion is commonly referred to as localized corrosion and occurs at isolated locations along the bar as pitting corrosion. Because the reactions are in such close proximity, uniform iron dissolution occurs over a relatively large area of the surface. The pairs of adjacent anodes and cathodes give the appearance that the removal of steel is uniform (Elsener, B. 2002 and Raupach, M. 1996). The uniform corrosion is generally a result of carbonation of the concrete or of very high chloride contents in the area of the reinforcing steel (Elsener, B. 2002 and Raupach, M. 1996). Knowledge of the effects of microcell corrosion is important as they can augment the effects of macrocell corrosion.

Macrocell Corrosion

Macrocells often develop as a result of the presence of large anodic reinforcement areas that are in electrical contact with the cathodic areas (Andrade, C. et al 1991 and Keddam, M. et al 1994). The concrete acts as the electrolyte in order to complete the galvanic cell. The macrocells tend to form in anodic areas where the critical chloride content has been attained, often leading to pitting (Elsener, B. 2002 and Raupach, M. 1996). One important aspect that has gained much attention is that the microcell corrosion should not be disregarded when macrocells are present (Felier, S. et al 2005 and Clemena, G. 2003). In order to accurately reflect the corrosion occurring within the structure, the corrosive actions of the microcells should be added to that of the macrocells (Andrade, C. et al 1991). This is especially significant when the cathodic area is much larger than the anodic area such as in bridge decks especially where truss bars are utilized.

The macrocell current is difficult to predict due to the many influencing factors that must be analyzed. Most researchers prefer to analyze four key elements needed to evaluate the effects of macrocell activity (Schiessl, P. 1986). These elements are I_{corr}, E_{corr}, I_g, and R. The corrosions current, I_{corr} represents the combined activity of the micro plus macrocell activity and can be represented by the following equation:

$$I_{corr} = \frac{B}{R_p \times s} \quad \text{(Equation 9)}$$

Where, B is a constant that is dependant upon whether or not the corrosion is active or not, R_p is the polarization resistance, and s is the size of the steel area that is exposed to the corrosion attack (Castro, P. et al 2003). R_p is the ratio of the change in corrosion potential over the change in the electrical current polarizing the metallic area (Castro, P. et al 2003). While I_{corr} provides information on both the micro and macrocell corrosion mechanisms, I_g, the galvanic current, only provides information on the macrocell corrosion. The corrosion potential, E_{corr}, and resistivity, R, are also needed to interpret macrocell activity.

The Effects of Differences in Clear Spacing on Macrocell Corrosion

Bertolini contests that concrete that has a low resistivity permits cathodic current to travel distances in the range of one meter to the local anode (Bertolini, L. 2004). However, research performed by Schiessel reported that anode to cathode distances of 80 to 640 millimeters had practically no effect on macrocell corrosion in the case of Portland Cement Concrete (Schiessel, P. 1998).

The Effects of Increased Cathode Area on Macrocell Corrosion

Those that have studied and researched the effects of macrocell corrosion have been led to believe that the ratio of the cathode area to the anode area greatly affects the rate of corrosion. According to Andrade, et al 1991, corrosion in small samples of reinforced concrete is entirely attributed to that of microcells. However, it is believed that once the dimensions of the structure become larger, the presence of macrocells cannot be overlooked but must instead be added to the action of the microcells. These large structures provide an environment where chlorides may penetrate the outside areas of the structure but allow the inside to remain chloride-free and passive. These passive areas may be much greater than that of the active outer areas of reinforcement. The greater the ratio of the cathode area to the anode area, the greater the contribution of the macrocell to that of corrosion. Very large macrocells may accelerate the rate of corrosion, making the process of great concern to researchers (Elsener, B. 2002). The increased rate of corrosion may be as great as 0.5 to 1.0 mm/year (0.02 to 0.04 in/year) (Elsener, B 2002).

However, experimentation has shown that only when the cathodic area is in the range of 41 times greater than the anodic area, the macrocell corrosion is three to six times greater than that of the microcells (Andrade, et al, 1991). The results support the hypothesis that macrocell corrosion will most likely form in very large structures that have very large passive areas in comparison to that of the anode areas and that microcell corrosion is most often the dominant corrosion mechanism measured.

The Effects of Stay-in-Place Forms on Macrocell Corrosion

In the case of stay-in-place forms in bridge decks, only one surface of the deck will be exposed to air. If stay-in-place forms are omitted, both surfaces of the bridge deck will be exposed to the atmosphere. Raupach's research supports the hypothesis that a bridge deck that lacks stay-in-place forms will increase the effects of macrocell corrosion since one side of the deck will be exposed to the atmosphere while the other side will be exposed to chlorides, such as deicing salts (Raupach, M. 1996). The macrocell activity is a result of the anode having a very low potential because of its exposure to high chloride content, the depassivation of the steel, and the high-water content, and of the cathode possessing a very high potential because of its exposure to high oxygen content and the passivity of the steel surface (Raupach, M. 1996). The differences in the potentials of the anode and cathode (usually the reinforcing mats in the top and bottom of the bridge deck) separated by some distance lend to the formation of a corrosion macrocell.

Methods Used to Measure Corrosion Activity

Of the test methods that are available to predict corrosion in reinforced concrete, it is uncommon to rely on only one. Instead, a combination of testing methods are performed and analyzed to predict the presence of corrosion and the rate at which it is occurring. Four of the most commonly used methods are discussed below.

Resistivity

It is important to measure the resistivity of concrete as it assists in the determination of the magnitude of the corrosion rate at specific locations (Berkeley, K. and Pathmanaban, S. 1990). As stated before, ions must flow from the anode to the cathode for corrosion to occur, referred to as an ionic current. The ionic current created by corrosion will in turn affect the resistivity of the concrete (Broomfield, J.P. 1997). Resistivity will also be influenced by the pore structure composition of the concrete such as water to cement ratio, additional moisture, and the size of the pore system (Berkeley, K. and Pathmanaban, S. 1990).

There are several different ways to measure resistivity including the four-probe resistivity meter (Wenner Probe), two-probe system, or single electrode system. The most commonly used is the four-probe resistivity meter, see Figure 2. Originally developed to measure soil resistivity, the Wenner Probe is a spring-loaded hand-held instrument that is pushed upon until it comes in contact with the concrete surface (Broomfield, J.P. 1997). Once in contact with the concrete, a current is applied between the outer probes and the potential difference is measure across the inner probes. Wetted wooden plugs are sometimes placed at the end of the probes of some models to increase conductivity. Placement of the probes should be in a manner that prevents contact with the steel reinforcement and avoids the edges of the concrete. If steel reinforcement cannot be avoided, the instrument should be placed at right angles to the reinforcement.

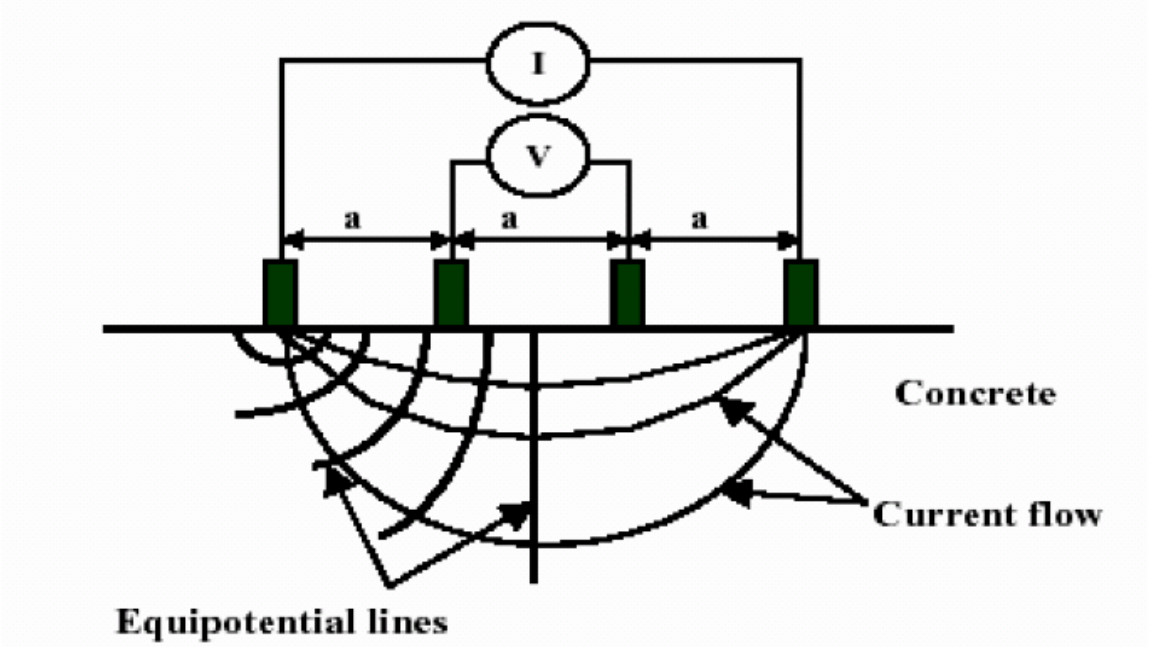

Figure 2 – Four-Probe Resistivity Meter or Wenner Probe (Ramniceanu, A. 2004)

The two-probe resistivity meter is lower in cost but is considered less accurate than the four-probe model (Broomfield, J.P. 1997). The probes are inserted into holes that have been drilled into the concrete. This is done to improve the electrical contact by

surpassing any impurities that might be on the surface of the concrete (Broomfield, J.P. 1997). For the two-probe instrument, voltage and current are supplied from one pin.

Last, a single electrode can be placed on the surface of the concrete to measure resistivity. This method is the newest approach of the three and uses the reinforcement mat as one electrode and a small surface probe as the other. The single electrode instrument measures the resistivity in the concrete cover only.

The Wenner Probe will be used throughout this study. As explained earlier, once the instrument is applied to the surface, a small current is ejected and the potential difference is measured across the inner probes (Mehta, K.P. 2005). The measured resistance is used in the following equation:

$$\rho = 2\pi aR \quad \text{(Mehta, K.P. 2005)} \qquad \text{(Equation 10)}$$

Where,
ρ = the calculated resistivity (ohm – cm)
a = the spacing measured between the electrodes or probes (cm)
R = the resistance obtained from the Wenner Probe (ohms)

While this resistivity measurement cannot determine if corrosion has begun, it will predict the capacity of the concrete to allow corrosion to occur through ionic conduction as listed below and prepared by the Comite Euro-International du Beton (CE-192) (Mehta, K.P. 2005):

Concrete Resistivity (Ω - m)	Likely Corrosion Rate
> 200	Negligible
100 – 200	Low
50 – 100	High
< 50	Very High

Corrosion Potential

The half cell potential test method is most commonly used to predict the likelihood of corrosion of uncoated steel reinforcement in concrete structures. This test is the most commonly used test in the field because it is quick and inexpensive (Mehta, K.P. 2005).

The equipment used in this test is presented in Figure 3.

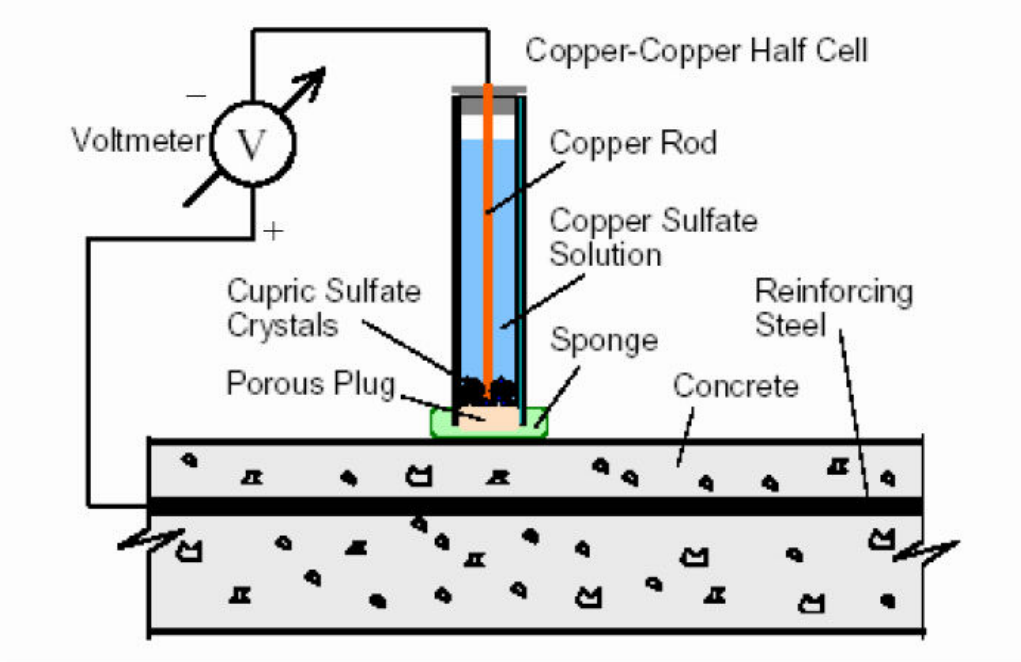

Figure 3 – Half-Cell Potential Apparatus (Ramniceanu, A. 2004)

A standard half cell such as copper/copper sulfate with a porous plug that remains moist as a result of capillary action is commonly used in laboratory and field testing (ASTM C 876-91 2004). Silver/silver chloride and mercury/mercury oxides are examples of other half cells that may be used in the field and laboratory (Broomfield, J.P. 1997). The copper/copper sulfate half cell contains a copper rod that is immersed in a saturated solution of cupric sulfate crystals and deionized water. The half cell is connected to the negative terminal of a high impedance voltmeter and the steel reinforcement is connected

to the positive terminal (Mehta, K.P. 2005). The half cell is placed upon a sponge that is wetted to maintain a low electrical resistance bridge between the concrete surface and the half cell (ASTM C 876-91 2004). The half cell is then moved along the reinforcement embedded within the concrete.

The voltmeter reads the potential difference between the steel reinforcement and the reference electrode, the copper/copper sulfate half cell. The potentials are then compared to the values presented in Table 1.

Table 1 – ASTM Criteria for Corrosion of Steel Reinforcement in Concrete for a Copper/Copper Sulfate Half Cell (Ramniceanu, A. 2004)

Measured Potential (mV vs. CSE)	Corrosion Probability
> -200	Low, less than 10%
-200 to -350	Uncertain
< -350	High, greater than 90%

Linear Polarization

The linear polarization method determines the general corrosion rate of the steel reinforcement embedded within the concrete. The fastest method to measure the corrosion rate is the three electrode polarization (3LP) or the polarization resistance method. The method is widely used in the field and laboratory.

Figure 4 – 3LP Apparatus

The 3LP method uses three electrodes to calculate the corrosion rate. The first electrode, the working electrode, is the steel that is embedded in the concrete and the second is the counter electrode which is a "metallic object used to apply a polarizing current" (Clear, K.C. 1989). The last electrode, or the reference electrode, is a standard half cell which senses potential changes in the steel reinforcement created by the current applied by the counter electrode (Clear, K.C. 1989). Figure 4 is an example of the arrangement of an unguarded 3LP apparatus. As the counter and reference electrodes are placed on the surface of the concrete over the steel reinforcement, current is applied and the associated change in potential is recorded and used in the Stern and Geary equation to calculate current corrosion density (corrosion rate).

$$R_p = \frac{B}{i_{corr}} \quad \text{(Equation 11)}$$

where,

R_p = polarization resistance in ohms = change in potential/applied current (mV/μA)

i_{corr} = corrosion rate current (μA/cm^2)

B = constant between 26 and 52 (mV)

$$B = \frac{\beta_a \beta_c}{2.3(\beta_a + \beta_c)} = 40 \qquad \text{(Equation 12)}$$

where,

β_a = anodidc Tafel slope = 150 mV/decade

β_c = cathodic Tafel slope = 250 mV/decade

The measured corrosion current cannot be considered constant with time but is instead the corrosion current of the steel surface at that instant in time (Clear, K.C. 1989). The calculated unguarded 3LP values, established by Kenneth C. Clear can be compared to the values in Table 2 below to determine the relative rate of corrosion.

Table 2 – Predicted Corrosion Rates (Ramniceanu, A. 2004)

No corrosion expected: I_{corr} < 0.2 μA/cm^2

Corrosion possible in 10-15 years: I_{corr} 0.2 to 1.0 μA/cm^2

Corrosion expected in 2 – 10 years: I_{corr} 1.0 to 10 μA/cm^2

Corrosion expected in 2 years or less: I_{corr} > 10 μA/cm^2

PURPOSE & SCOPE OF WORK

Studies have been performed in the past to verify that recording galvanic current alone is not enough to determine macrocell activity. Instead, the corrosion current density and corrosion potential must be combined with the galvanic current to accurately reflect macrocell activity (Zemajtis, J. 1998). The scope of the study involved the preparation of 27 total specimens via 9 separate batches of concrete, 3 specimens per bath. Each batch was subjected to tests to record resistivities, macrocell potentials, half-cell potentials, and corrosion current densities. The data was then statiscally analyzed using MINITAB Statistical Analysis Software.

The purposes of this study are:

- Determining the microcell current and whether or not it augments the macrocell current significantly.

- Determining the effects of an increased number of cathode bars in reinforced concrete bridge decks and whether they will increase the micro and/or macrocell activity.

- Determining the effects of increased spacing between anode and cathode bars in reinforced concrete bridge decks and its effect on micro and/or macrocell activity.

- Determining the influence of stay-in-place forms (SIP) on limiting the oxygen to the cathode.

- Determining the influence of increased spacing arrangements, increased C/A ratios, and influence of SIP on the formation of the passive layer.

METHODS & MATERIALS

The testing method outlined in the American Standards for Testing of Materials (ASTM) G 109-99a, The Standard Test Method for Determining the Effects of Chemical Admixtures on the Corrosion of Embedded Steel Reinforcement in Concrete Exposed to Chloride Environments, was utilized. The procedure was slightly modified in order to meet the objective of the proposed project.

Concrete Specimens

Twenty-seven specimens were cast in the form of a prism that had dimensions of 318 mm (12.5 in) in length, 356 mm (14.0 in) in width and 152 mm (6.0 in) in height, see Figure 5. The specimens were divided into three groups: specimens without stay-in-place (SIP) forms with a cathode to anode bar ratio of 2 to 1 (C/A = 2/1), with SIP with C/A = 2/1, and with SIP with C/A = 1/1. Those specimens that represent the presence of SIP forms were coated with a low-viscosity epoxy on all sides with the exception of the top of the prism. This study had 9 specimens without SIP forms and 18 specimens with SIP forms, see Table 3. All specimens were cast in an inverted position in order to reduce the effects of subsidence cracking and any defects that may occur as a result of hand finishing.

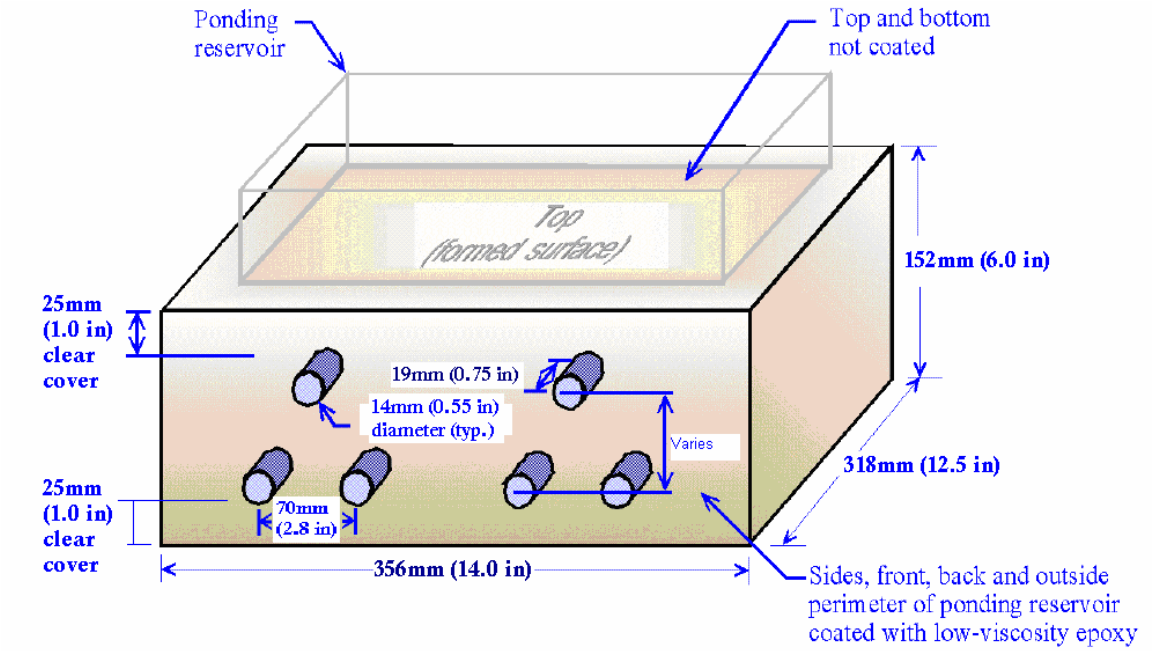

Figure 5 – Modified ASTM G 109-99a Concrete Prism Dimensions (Brown, M.C. 1999)

Of the 9 specimens that represented decks without stay-in-place forms, all possessed a bar arrangement that contained 6 pieces of reinforcing steel as two sets of C/A = 2/1, See Figure 6. Each piece of reinforcing steel is 356 mm (14.0 in) in length and 14 mm (0.55 in) in diameter (No. 5 bar). Each steel bar extends out of the concrete prism approximately 19 mm (0.75 in). Instead of the single triad of bars listed in ASTM G 109-99a, these specimens contained two triads of reinforcing steel placed side by side in the prism. The two sets of bars within a specimen and three specimens representing each group is to assess the variability within and between batches. The C/A = 2 and 1 represents areas of a bridge deck where C/A = 2 or 1, with an example being where the truss bar section is in the bottom mat (C/A = 2) and where the truss bar section is in the top mat (C/A = 1). The spacing between the top and bottom reinforcing steel varied between 50.8 mm, 76.2 mm, and 101.6 mm (2, 3, and 4-inches) for all three groups and represented the possible spacing between mats in a deck. The clear cover over the top bars was 25 mm. Three specimens without SIP were cast with a C/A = 2/1 at each spacing arrangement, see Table 3.

Table 3 – Test Matrix of Specimen Arrangement

Clear Bar Spacing mm (in)	Number of Specimens Without SIP	**Number of Specimens With SIP**	
	2 Cathode Bars	2 Cathode Bars	1 Cathode Bar
50.8 (2)	3	3	3
76.2 (3)	3	3	3
101.6 (4)	3	3	3
Total	9	9	9

Of the remaining 18 specimens which represented SIP forms, 9 were cast with an arrangement of 4 pieces of reinforcing steel, C/A = 1, and 9 were cast with the same triad arrangement as in those specimens that represented decks without SIP forms, C/A = 2. The 4-bar arrangement of reinforcing steel consisted of 1 pair of reinforcing bar at the top of the specimen and the other pair at the bottom, see Figure 7. The bar spacing once

again varied between 50.8 mm, 76.2 mm, and 101.6 mm (2, 3, and 4-inches) and three specimens were cast for each spacing arrangement, see Table 3.

All of the specimens contained a 100-ohm resistor that connected the top reinforcing bars to the bottom reinforcing bars, see Figures 6 and 7. In the C/A = 2 arrangement, the bottom two bars were connected by a jumper in order to make them electrically continuous. The two bottom bars were then connected to the top bar for each triad via a 100-ohm resistor that extended from the top bar to the bottom bar on the right side. In the C/A = 1 arrangement, the bottom bar was connected to the top bar via a 100-ohm resistor.

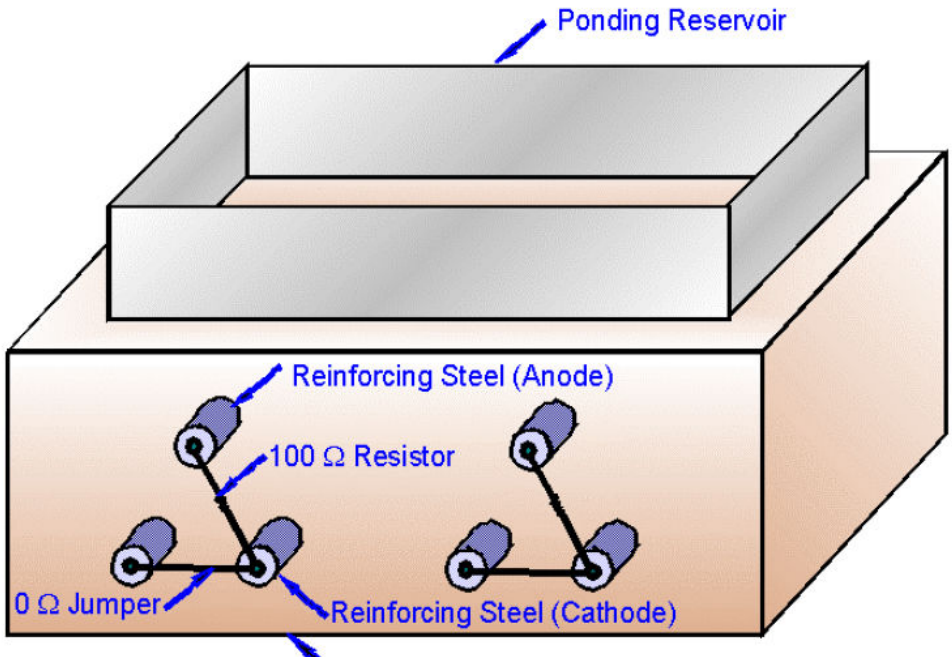

Figure 6 – Resistor Configuration of Concrete Specimen (Brown, M.C. 1999)

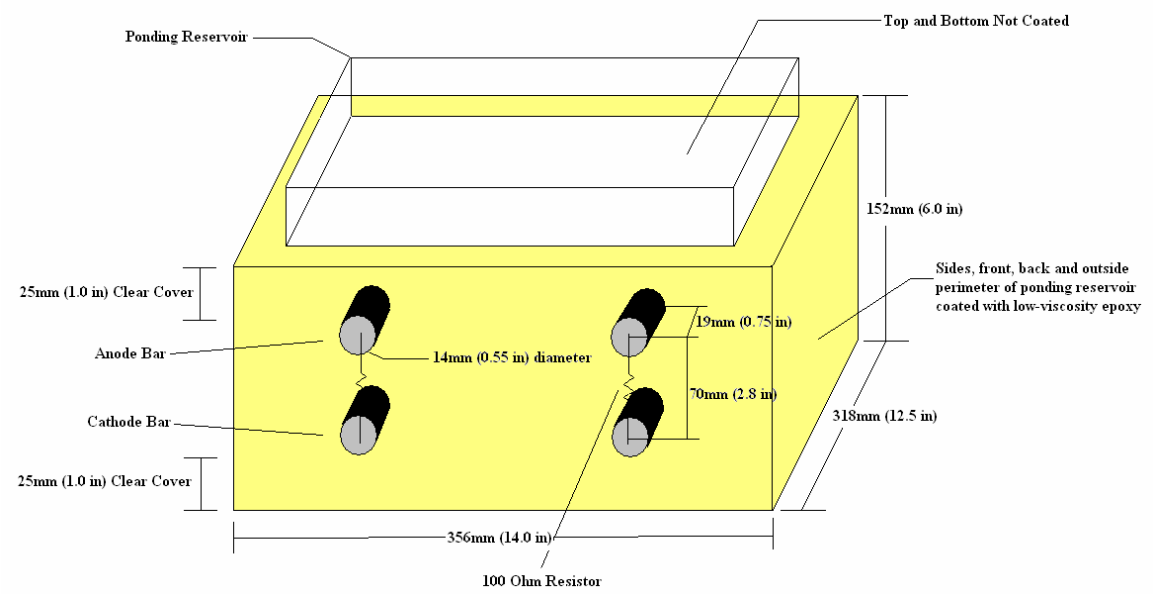

Figure 7 – Modified ASTM G 109-99a Concrete Prism Dimensions (4-bar Arrangement)

The concrete used to cast all the specimens was mixed in accordance with ASTM C 192/C 192M, Practice for Making and Curing Concrete Test Specimens in the Laboratory. Nine separate batches of concrete were made throughout the experiment. The water-to-cement (w/c) ratio did not exceed 0.5 with each batch containing approximately kilograms 600 lb (272 kg) of cement per cubic yard of concrete. The minimum slump value was 50 millimeters (2 in) with the actual slump ranging from 76 mm (3.0 in) to 197 mm (7.75 in). Air content ranges were from 5.5 to 6.9 percent. Approximately 26 mL of high-range water reducing admixtures per cubic foot of concrete from W.R. Grace were utilized in each batch. Approximately, 9 mL of air entraining admixtures per cubic foot of concrete from W.R. Grace were incorporated per batch.

Appendix A presents the mixture proportions and test results for each of the nine batches of concrete. The aggregate used in each batch of concrete was oven dried in the laboratory for at least 8 hours. Additional water was added to account for absorption percentages of both the fine and coarse aggregates.

Procedures

Preparation of Forms and Steel Reinforcement

The steel reinforcing bars utilized were of bare steel and obtained from the local building materials supply center. Approximately half of the reinforcement had thin ribbing and the other half a thicker sized ribbing. Only reinforcement of the same sized ribbing were placed in each specimen to prevent inconsistencies. Each steel reinforcing bar was cut in the laboratory to 356 mm (14.0 in) lengths. One end of each piece of reinforcement was drilled and tapped to facilitate a stainless steel screw. The bars were then cleaned of surface rust with a wire brush or light sandblasting and then soaked in hexane before being hand dried with a lint free cloth. Fifty-one mm (2 in) of each end of each reinforcing bar was covered in electroplaters tape leaving 254 mm (10.0 in) of exposed reinforcing steel in the concrete. Electroplaters tape was used in order to expose a predetermined length of reinforcement during linear polarization measurements. Fifty-one mm (2.0 in) of neoprene rubber was also placed over the electroplaters tape to further isolate the area of reinforcement exposed to polarization. Figure 8 provides a generalized plan view of the specimen and the exposed area of steel.

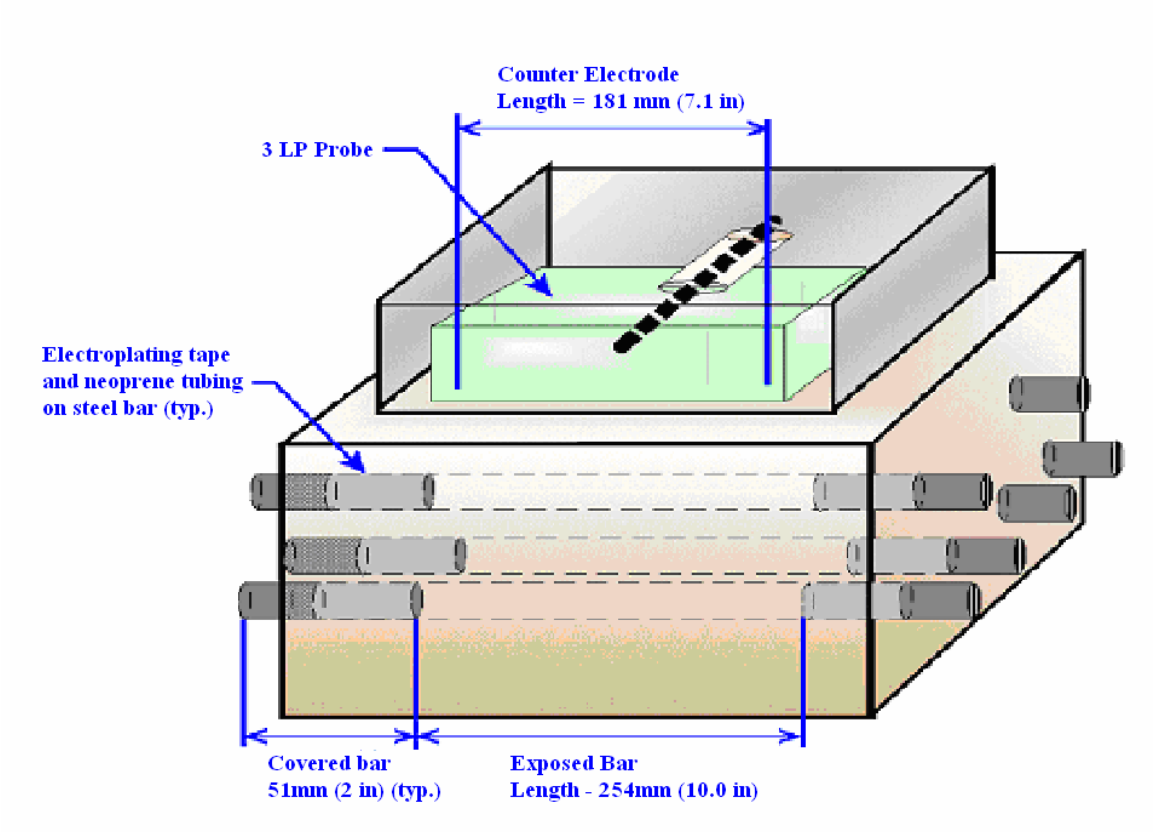

Figure 8 - Plan View of Exposed Reinforcement Area (Brown, M.C. 1999)

A two part commercial epoxy was also applied over the exposed ends of reinforcement once the stainless steel screws were in place and the specimen had been cast. The epoxy was applied in order to prevent the exposed ends of the steel reinforcement from corroding. Figure 9 details the ends of the steel reinforcing bars placed in each specimen.

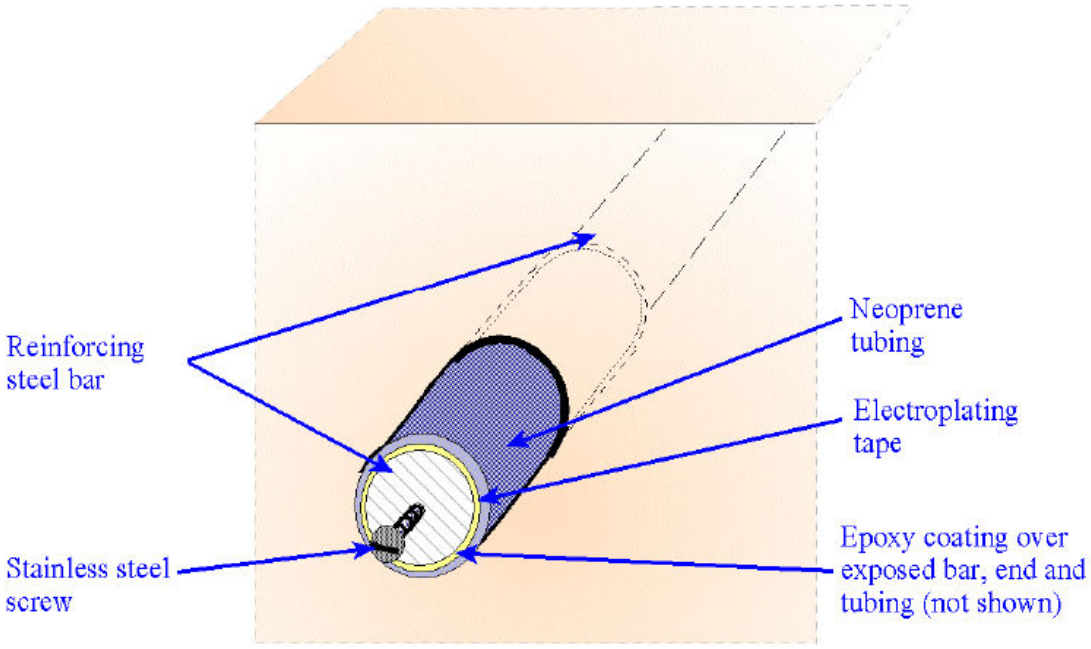

Figure 9 – Detail of Reinforcement Ends (Brown, M.C. 1999)

Materials Preparation

The coarse limestone aggregate, maximum size of 12.5 mm (0.5 in), was obtained from the CON-Rock ready-mix plant in Blacksburg, Virginia. The fine aggregate was local natural sand from Wytheville, Virginia and was also obtained from the CON-Rock ready-mix plant in Blacksburg, Virginia. The specific gravity and absorption for the coarse aggregate were 2.82 and 0.30% respectively. The specific gravity and absorption for the fine aggregate were 2.61 and 0.80% respectively.

The amount of mixing water was adjusted for the absorptions of the aggregate which were oven dried overnight at 110 degrees Centigrade (230ºF) and then allowed to cool to room temperature during the day before mixing.

Batching and Mixing

In order to stagger the number of corrosion test measurements taken at one time and because of the capacity limitations of the laboratory mixing equipment, six specimens were cast in one day per week. Only three specimens were cast in the first, second, and ninth weeks.

Batches were prepared by weighing all bulk materials on a digital scale to the nearest 0.01 kilogram in five-gallon plastic buckets that were covered and stored overnight. Both the AEA and HRWR were measured immediately prior to mixing to the nearest 0.1 mL in a container with water from the batch mixing water. Each batch was mixed in a tub-type mixer which has a capacity of approximately 0.07 cubic meters (2.5 ft^3).

In order to test the compressive strength of the concrete, three test cylinders were cast per batch. Each cylinder measured 102 mm (4.0 in) in diameter and 204 mm (8.0 in) in length and were cast in accordance with ASTM C 192-95 and ASTM C 39-96. One cylinder per batch was tested for each 7, 14, and 28 day strengths. Each strength was recorded and can be found in Appendix A for mix design.

Curing and Ponding

After casting, each specimen was covered with moist burlap which was in turn covered by a polyethylene sheet. Each specimen was moist cured for only 72-hours in order to increase the rate of chloride penetration once ponding begins. After 72-hours, each specimen was removed from the form and inverted once again upon a non conducting base in a temperature and humidity controlled environment

Approximately 72-hours later, each specimen was also coated with epoxy as required for the representation of with and without stay-in-place forms. Plexiglass dams were placed on each specimen after the epoxy has been allowed to cure for 24-hours. Base measurements were taken on the 6^{th} day. Finally, ponding commenced on the 7^{th} day

with a chloride solution of 3 parts of sodium chloride and 97 parts water by mass in accordance with ASTM G109-99a.

After 7 days of ponding, the 14th day of the cycle, the specimen was allowed to surface dry for 24 hours. On the 15th day of the cycle, the first set of measurements was taken. Ponding commenced again on the 21st day of each cycle and then was repeated in two week cycles until the average integrated macrocell current was 150 coulombs or greater (ASTM G 109-99a).

Corrosion Testing

Several different measurements were recorded 24 hours after the ponding solution was removed from each specimen.

Macro-Cell Corrosion Current

The most simple of tests performed was utilized to calculate the difference in potentials between the top (anode) bar and the bottom (cathode bar). A high impedance voltmeter was attached to the resistor from the top bar to the bottom bar in order to obtain the difference in potential. Using Ohm's Law (Equation 13), the current obtained from the voltmeter was determined because the resistance was known. The current is an estimation of what is known as I_{corr} or the macro-cell corrosion current. The greater the difference in potential between the anode and the cathode, the greater the estimation of the macro-cell corrosion current.

$$V = IR \quad \text{(Equation 13)}$$

where, V = Electrical Potential Difference/Voltage Across the Resistor (millivolts)
I = Electrical Current Flow/Estimated I_{corr} (milliamperes)
R = Electrical Resistance to Flow (ohms)

Half-Cell Potentials

Next, the electrical potential was measured utilizing the standard procedure outlined in ASTM C876-91, Standard Test Method for Half-Cell Potentials of Uncoated Reinforcing Steel in Concrete. The measurement revealed the potential that corrosive activity may occur. The magnitude of the electrical potential of the reinforcing steel was compared against a standard reference probe, the copper-copper sulfate electrode (CSE). (Schiessel, P. 1998). The steel reinforcement will act as an electrode, and the pore solution of the concrete will act as the electrolyte. A high impedance voltmeter is attached to the anode bar and the probe which rests on a moistened sponge completes the electrical circuit.

The half-cell potential was recorded while the anode bar was connected to the cathode bar via the 100-ohm resistor and with the anode bar in an unconnected state. The measurement in the unconnected state was taken in order to record the microcell corrosion activity on the anode bar. An adequate amount of time was allowed between the connected and unconnected measurements to allow the system to stabilize. The microcell values were then be subtracted from the connected readings to isolate the contribution of the macrocell corrosion.

Linear Polarization (3LP)

Last, the 3LP (or linear polarization) test was performed to estimate the progress of the corrosion reactions, micro plus macrocell corrosion. The test helped to estimate the rate of metal loss. The device used to measure the linear polarization of the reinforced concrete was developed by Kenneth C. Clear and is one of the most recent utilized in the prediction of corrosion using the unguarded 3LP. As discussed previously, this method yields a corrosion current density that predicts the rate of metal loss due to corrosion.

Linear polarization readings were taken with the anode bar connected to the cathode bar. As with the half-cell potentials, an additional set of measurements were taken once the top bar was disconnected from the bottom bar. Again, an adequate amount of time was

provided between the connected and unconnected measurements to allow the system to stabilize. The test was performed in the unconnected state in order to record the microcell corrosion activity on the anode bar. The microcell values can then be subtracted from the connected readings to isolate the contribution of the macrocell corrosion.

Resistivity

The Wenner four-probe resistivity meter was used to measure concrete resistivity. The spacing between the probes was set at 50.8 mm (2 in). The concrete resistivity measurements were taken parallel to and midway between the top reinforcing bars to avoid any influence from the reinforcing steel.

RESULTS, ANALYSIS, & DISCUSSION

Concrete Specimens

Concrete Specimens were grouped to represent concrete bridge decks with SIP, without SIP, C/A = 2/1, C/A = 1/1, and typical clear spacing arrangements between reinforcing mats. Overall, 9 separate batches of concrete, 0.07 cubic meters (2.5 ft^3) in volume, were batched over a time period of 6 weeks.

Concrete Characteristics

Compressive strength, air entrainment, and slump tests were performed for each batch of concrete to ensure each exhibited similar characteristics to limit variability during the observation period.

Slump Testing

Slump tests were performed for each batch of concrete during the batching process. Table 4 lists the results of the slump test of each batch of concrete. Each batch was required to meet a minimum slump of 50.8mm (2 in) as given in ASTM G 109-99a.

Slump between batches were relatively constant except for batches 2 and 6 which were 177.8mm (7 in) or greater. However, the w/c was kept constant at 0.5 for all 9 batches. Differences between the batches are the results of varying amounts of high range water reducer (HRWR).

Table 4 – Slump Test Measurements

Batch	Slump mm (in)
1	88.9 (3.5)
2	196.9 (7.75)
3	101.6 (4.0)
4	114.3 (4.5)
5	76.2 (3.0)
6	177.8 (7.0)
7	114.3 (4.5)
8	114.3 (4.5)
9	139.7 (5.5)
Average Slump of 9 Batches	127.0 (5.0)

Air Entrainment

The air entrainment for each batch of concrete was also recorded in order to have continuity amongst batches for later comparisons. Table 5 lists the air content for each batch of concrete. All batches were required to meet 6 ± 1% as given in ASTM G 109-99a. Air entrainment values appeared relatively consistent throughout the 9 batches.

Table 5 – Air Entrainment Measurements

Batch	Air Entrainment (%)
1	6.4
2	6.2
3	6.4
4	6.4
5	6.6
6	5.5
7	6.4
8	6.9
9	6.4
Average Air Entrainment	6.4

Compressive Strength

Last, the compressive strength for each batch was recorded. No specific requirement was set forth by ASTM G 109-99a with the exception that it must conform to the standards set forth in the Annual Book of ASTM Standards, Vol 14.02. Table 6 lists the recorded compressive strengths for each batch. Compressive strengths were compared to ensure that one batch of concrete did not differ significantly from the others. Compressive strengths were relatively uniform between the 9 batches at 7 and 28 days.

Table 6 – Compressive Strength Measurements

Batch	Compressive Strength MPa (psi)	
	7-day	28-day
1	27.4 (3980)	35.1 (5090)
2	24.1 (3500)	29.9 (4340)
3	27.4 (3980)	34.0 (4930)
4	26.9 (3900)	34.4 (4990)
5	27.4 (3980)	31.6 (4580)
6	25.8 (3740)	31.4 (4560)
7	27.4 (3980)	34.8 (5050)
8	29.1 (4220)	34.3 (4970)
9	27.4 (3980)	34.7 (5030)
Average Compressive Strength	27.0 (3920)	33.4 (4840)

Corrosion Measurements

Measurements were recorded in order to determine the rate of corrosion, the probability that corrosion would occur, and to ensure that the concrete itself would support corrosion. Data was also collected to determine whether different spacing arrangements, the presence of SIP, and differences in the cathode bar to anode bar ratio would affect the magnitude of macrocell corrosion as well as the formation of the passive layer. The resistivities, macrocell potentials, half-cell potentials, and corrosion current densities were observed and compared in order to detect such differences.

Resistivities

All resistivity measurements were taken with the Wenner Probe. In order for corrosion to occur, the concrete must sustain a resistivity level less than 200 Ohm-meters. To compare the test group concrete resistivities, all spacing arrangements were combined to form 3 plots that represented resistivities with SIP with C/A = 2/1, without SIP with C/A = 2/1 and with SIP with C/A = 1/1. The comparison would determine whether the concrete resistivity was influencing the corrosion measurements and thus would have to

be accounted for in the comparison of the corrosion measurement between and within the groups.

Figure 10 represents resistivities observed with SIP with C/A = 1/1 and includes 50.8 mm, 76.2 mm, and 101.6 mm (2 in, 3 in, and 4 in) spacings. Initially, the resistivities of the specimens all increased steadily until approximately day 105 where they began to remain relatively constant between 150 and 170 ohm-meters. From casting to 273 days, the resistivities remained less than the 200 ohm-meter level required to sustain corrosion. Few differences were observed between the different spacing arrangements, as shown in Figure 10.

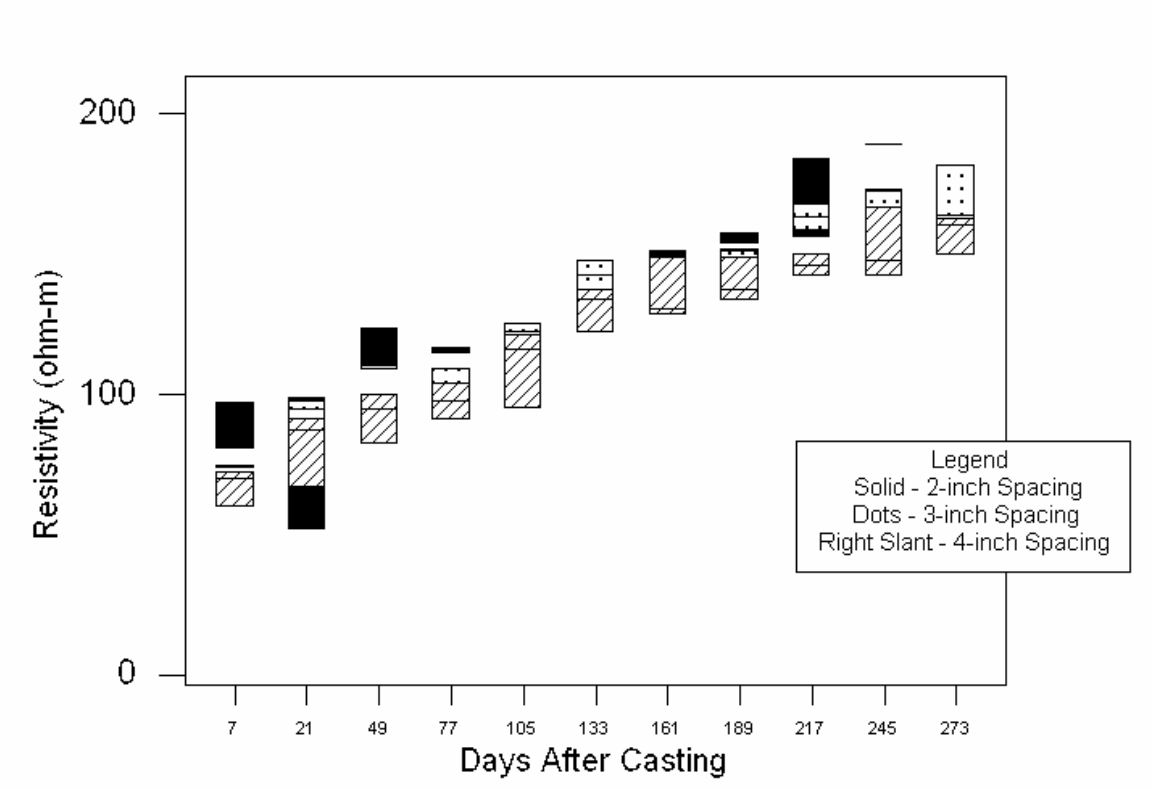

Figure 10 – Resistivity With SIP With One Cathode Bar

Resistivities were also measured for the specimens with SIP with 2 cathode bars. The resistivities all increased steadily until approximately day 105 where the resistivities remained relatively constant between 150 and 170 ohm-meters as presented in Figure 11.

At day 273, the observed resitivities were within the range needed to sustain corrosion. Few differences existed between the resistivities of the reinforcing steel spacings, 50.8 mm, 76.2 mm, and 101.6 mm (2 in, 3 in, and 4 in).

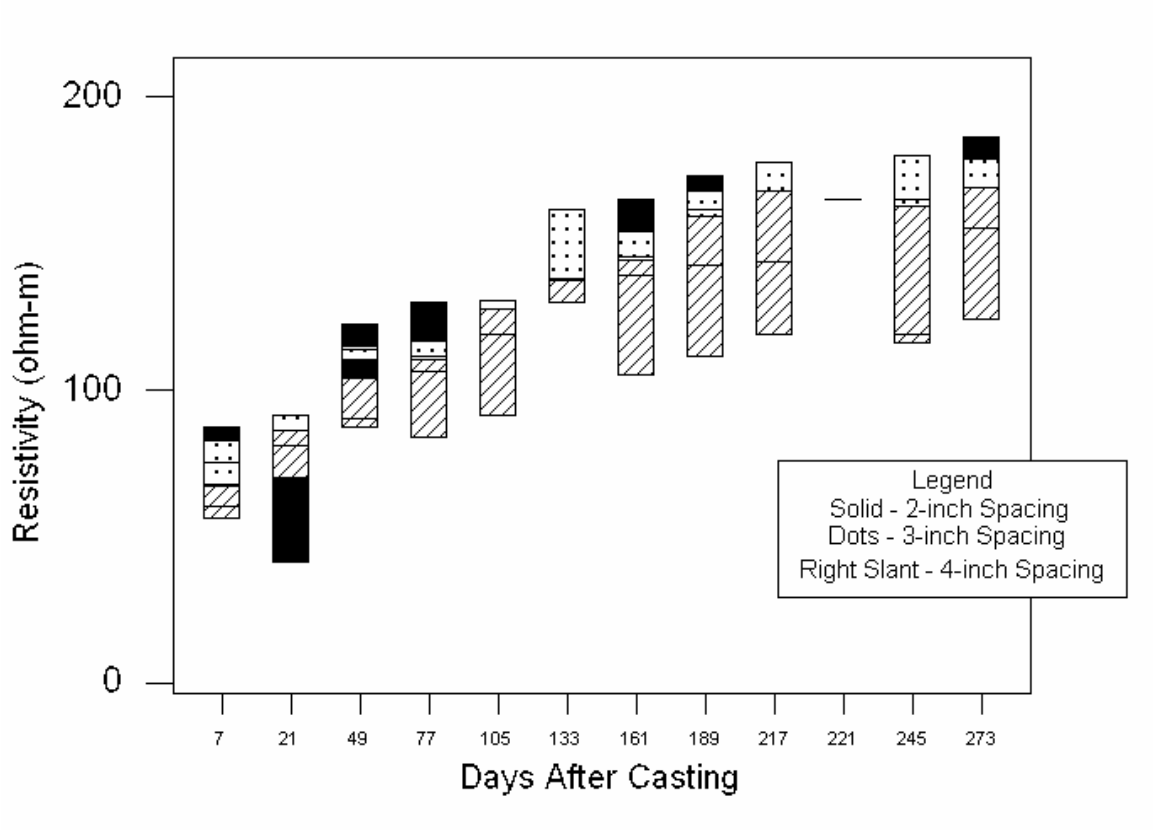

Figure 11 – Resistivity With SIP With Two Cathode Bars

The last set of measurements were those specimens that did not have SIP and had C/A = 2/1. Figure 12, represents the resistivities for all spacing arrangements combined. The resistivities initially increased steadily until day 105 where they remained relatively constant between 150 and 190 ohm-meters. All resistivities observed without SIP with C/A = 2/1 were below the maximum value required to sustain corrosion. Few differences existed amongst the resistivities of the reinforcing steel spacing.

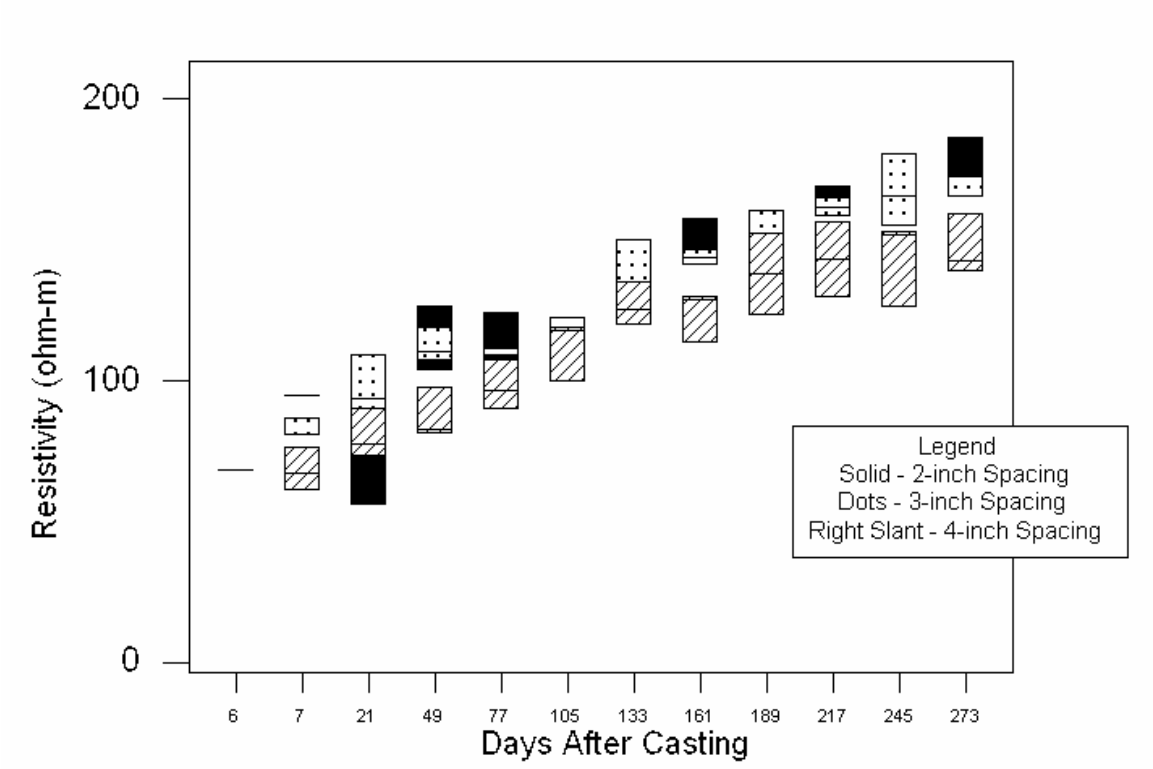

Figure 12 – Resistivity Without SIP With Two Cathode Bars

With few differences detected between group resitivities as shown in Figures 10, 11, and 12, between spacing arrangements, more detailed observations were required. Spacing arrangements, the presence of SIP, and the number of cathode bars to anode bars were separately evaluated at 3 distinct days after casting and compared amongst one another. Resistivities were observed and compared at days 105, 189, and 245, as the variability of the resistivity of concrete decreased with age. There would be little use in statistically comparing measurements less than 105 days after casting because of the relatively large variations at earlier ages.

Spacing Arrangement Differences

In order to determine if any significant differences existed in the resistivities of each specimen, the spacing arrangements were compared within each group of resistivities with SIP with C/A = 2/1, with SIP with C/A = 1/1, and without SIP with C/A = 2/1. The MINITAB statistical analyses for all of the following study comparison are summarized in Appendix F.

The differences in the mean resistivities varied only slightly for each specified day after casting for each group of specimens as displayed in Table 7. The coefficients of variation for each group of specimens are relatively small as well. The basic statistical data, Table 7, showed that the spacing arrangement differences had an insignificant effect upon the measured resistivities at specified days after casting.

Table 7 – Basic Statistics for the Resistivities of Different Spacing Arrangements

Days After Casting	Spacing Arrangement mm (in)	Number of Measurements (N)	Mean Resistivity (Ω-m)	Standard Deviation	Coefficient of Variation (%)
105	50.8 (2)	9	113.96	9.51	8.35
105	76.2 (3)	9	121.53	5.94	4.89
105	101.6 (4)	9	112.07	18.50	16.51
189	50.8 (2)	9	148.60	13.10	8.82
189	76.2 (3)	9	153.21	8.51	5.55
189	101.6 (4)	9	138.72	14.72	10.61
245	50.8 (2)	9	174.61	12.02	6.88
245	76.2 (3)	9	168.58	8.6	5.10
245	101.6 (4)	9	143.07	18.50	12.93

Stay-in Place Forms

As with spacing arrangements, the variable of SIP must be considered in order to determine if differences existed amongst each batch of concrete. Table 8 lists the resistivity of specimens, C/A = 2/1 with SIP and without SIP at a specified spacing arrangement and day after casting.

Table 8 also displays the basic statistical data for the resistivities measured for specimens with and without SIP. All spacing arrangements possessed similar mean resistivities regardless of SIP with the exception of the 101.6 mm (4 in) spacing arrangement at day 105. Here a 30 ohm-meter difference existed between the mean resistivities of those specimen with and without SIP. However, at days 189 and 245, the data is once again similar. As shown in Appendix B, the increase in the mean can be attributed to outlying data. Therefore, the difference in the means can be considered insignificant. The mean

resistivities for the specimens with and without SIP were very similar and possessed relatively small coefficients of variation. The statistical analysis supports the statement that the presence of SIP and spacing arrangements did not effect the resistivity measurements.

Table 8 – Resistivity Measurements for Specimen, C/A = 2/1, With SIP and Without SIP

Days After Casting	Clear Spacing mm (in)	SIP				NSIP			
		Number of Measurements (N)	Mean Resistivity (Ω-m)	Standard Deviation	Coefficient of Variation (%)	Number of Measurements (N)	Mean Resistivity (Ω-m)	Standard Deviation	Coefficient of Variation (%)
105	50.8 (2)	6	114.73	10.90	9.50	3	112.42	7.70	6.85
105	76.2 (3)	6	121.64	7.42	6.10	3	121.29	1.84	1.52
105	101.6 (4)	6	111.89	21.35	19.08	3	143.99	10.76	7.47
189	50.8 (2)	6	149.66	15.12	10.10	3	146.47	10.23	6.98
189	76.2 (3)	6	154.80	7.15	4.62	3	150.02	9.75	6.50
189	101.6 (4)	6	139.02	16.17	11.63	3	138.10	14.58	10.56
245	50.8 (2)	6	176.79	13.85	7.83	3	170.23	7.45	4.38
245	76.2 (3)	6	169.17	7.15	4.23	3	167.40	12.82	7.66
245	101.6 (4)	6	142.60	21.35	14.97	3	143.99	15.06	10.46

Cathode Bar to Anode Bar Ratio

The last variable compared in the experiment was the difference in resistivity between the ratio of the cathode bar to the anode bar. Table 9 lists the mean resistivities for specimens with C/A = 2/1 and C/A = 1/1 at different spacing arrangements and specified days since placement. Relatively small differences were observed and the coefficients of variations are relatively small. Statistical analyses demonstrated that the C/A ratio and the specified spacing arrangements do not influence the measured resistivities.

Table 9 – Resistivity Measurements for Different Cathode-to-Anode Ratios

Days After Casting	Clear Spacing mm (in)	C/A = 2/1				C/A = 1/1			
		SIP				NSIP			
		Number of Measurements (N)	Mean Resistivity (Ω-m)	Standard Deviation	Coefficient of Variation (%)	Number of Measurements (N)	Mean Resistivity (Ω-m)	Standard Deviation	Coefficient of Variation (%)
105	50.8 (2)	3	113.49	15.28	13.46	3	115.97	7.67	6.61
105	76.2 (3)	3	120.58	11.28	9.35	3	122.71	2.68	2.18
105	101.6 (4)	3	112.8	18.9	16.76	3	111.01	13.47	12.13
189	50.8 (2)	3	147.5	22.5	15.25	3	151.79	7.25	4.78
189	76.2 (3)	3	158.88	10.92	6.87	3	150.73	1.63	1.08
189	101.6 (4)	3	138.00	24.3	17.60	3	140.09	7.84	5.60
245	50.8 (2)	3	176.6	17.8	10.08	3	176.97	12.78	7.22
245	76.2 (3)	3	169.17	9.28	5.49	3	169.17	6.47	3.82
245	101.6 (4)	3	132.7	26.1	19.67	3	152.50	12.87	8.44

As presented earlier, the resistivity differences in spacing arrangement was relatively insignificant. Therefore, SIP and C/A ratio can be combined.

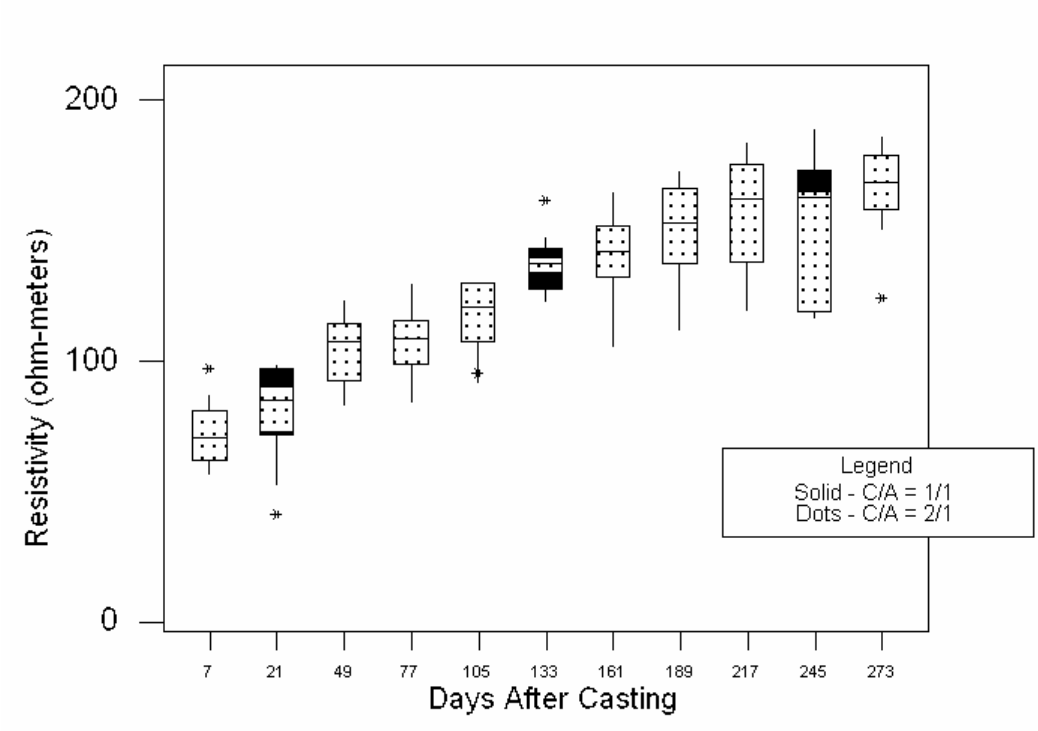

Figure 13 – Resistivity Measurements With SIP (C/A = 2/1 and C/A = 1/1)

As shown in Figure 13, the differences between the shaded areas, C/A = 2/1, and unshaded areas, C/A = 1/1, are small. The rate of increase began to decrease at approximately day 105 and was in the range of 90 to 130 ohm-meters from casting until day 105. The variability is relatively consistent throughout the testing period. Further comparisons were also made between the resistivities of specimens with SIP with C/A = 2/1 and specimens without SIP with C/A = 2/1, Figure 14.

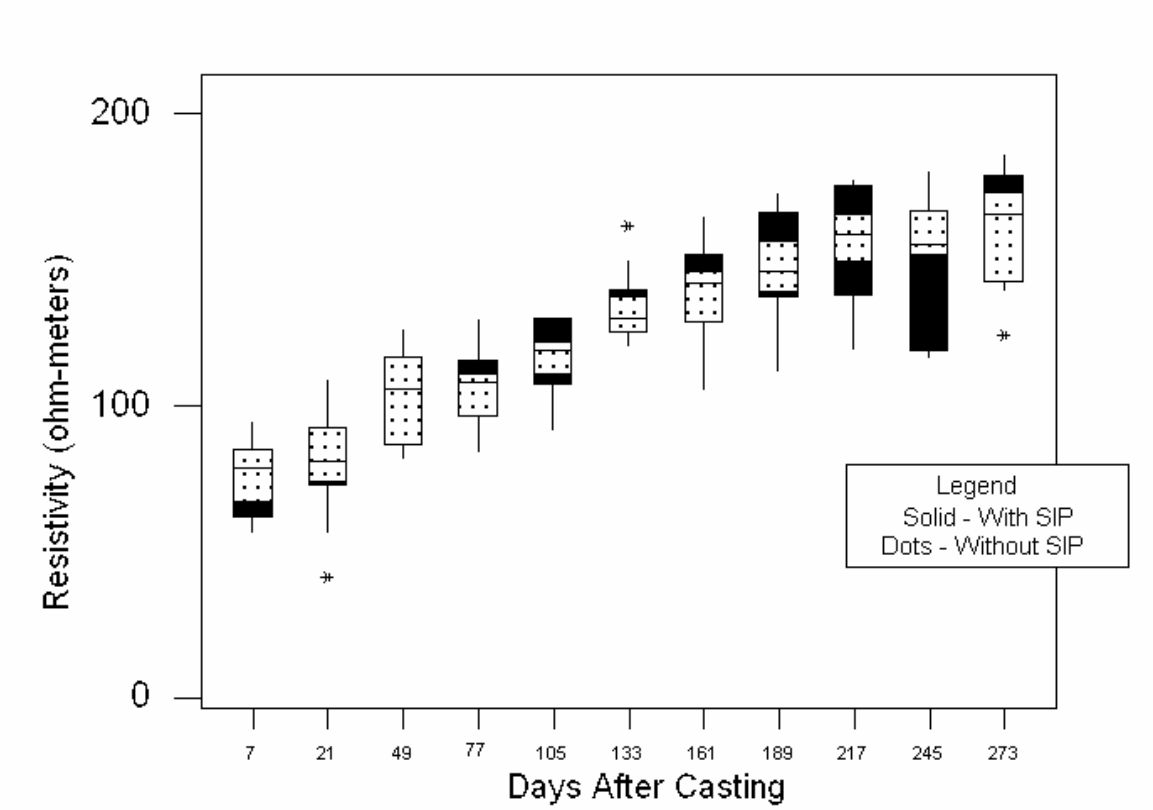

Figure 14 – Resistivity Measurements with C/A = 2/1 (With and Without SIP)

As can be seen from Figure 14, few differences existed between specimens with C/A = 2/1 with and without SIP. The combined resistivities show a relatively rapid rate of increase to day 105, afterwards the rate decreases and the resistivity measurements ranged between 180 to 220 ohm-meters. The variability was relatively consistent throughout the 273 day time period. The variability throughout the experiment for resistivities can be attributed to the slight differences in probe placement on the concrete

surface at the time the measurements were taken. With no significant differences between resistivity measurements when comparing the C/A ratios and the presence of SIP, all the resistivity measurements can be combined, Figure 15.

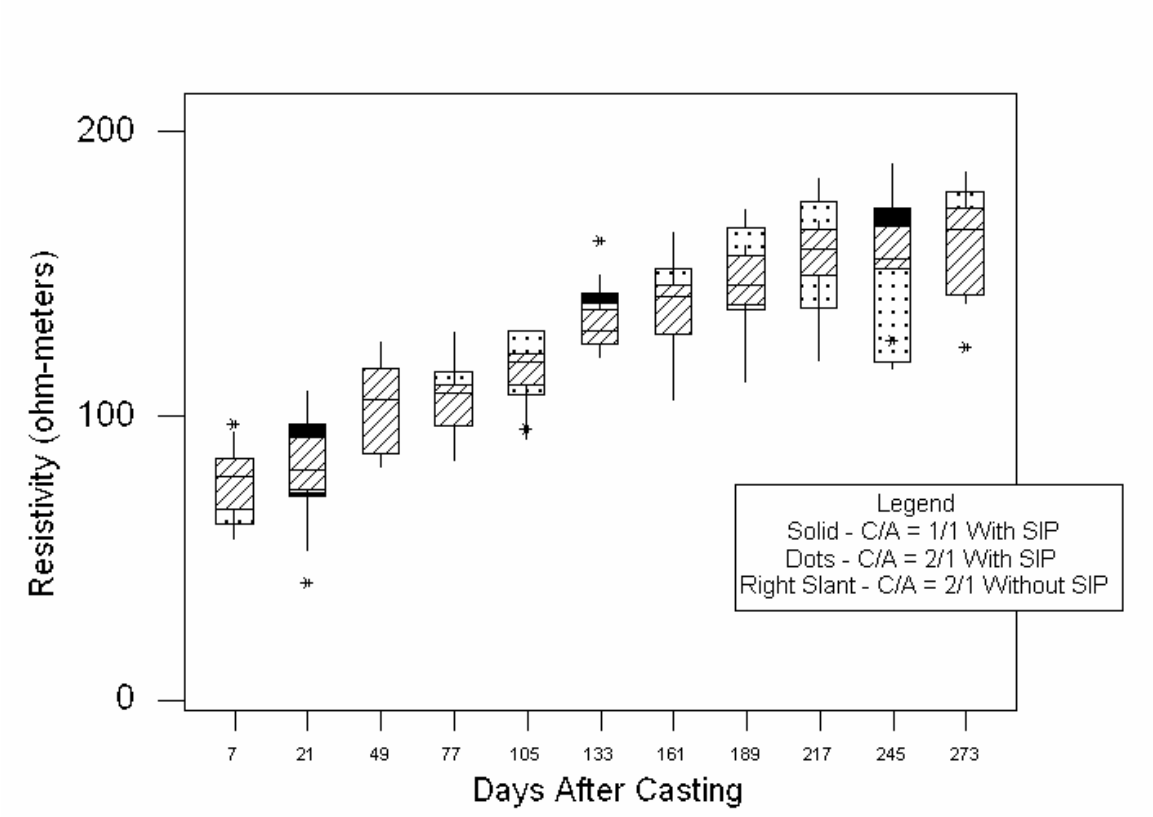

Figure 15 – Combined Resistivity Measurements

As shown in Figure 15, the differences between all resistivities were relatively small and may be considered insignificant. When combined, the data follows the trend of initially increasing until approximately 105 days and then the rate of increase begins to decrease. Then, regardless of differences in spacing arrangements, the presence of SIP, and the C/A ratio, the resistivites are the same as no significant differences were detected.

The lack of significant differences amongst resistivities supports the consistencies amongst the mixture parameters for each batch of concrete. If the batch mixtures were dissimilar, the resistivities would be inconsistent and the aforementioned figures would show a large variability in the measurements. Consistent batch to batch mixture parameters are important as they ensure that any corrosion that occurs can be attributed to

the intended variables of the experiment which, in this case, are reinforcing steel spacing, the presence of SIP, and the C/A ratio.

It is also important to note that the resistivity measured is that of approximately the first 50.8 mm (2 in) in depth in the concrete. The Wenner Probe measures a depth in the concrete equivalent to the spacing of the probes, which in this experiment was 50.8 mm (2 in). Each concrete specimen has a 25 mm (1 in) cover and each steel reinforcing bar is a No. 5 bar meaning that the range of the resistivity meter measures to a depth just below the top reinforcing bar (Mehta, K.P. 2006). It is expected that any chloride induced corrosion that might occur would occur first on the top bar (the anode bar) because that is the passive layer that the chlorides would encounter and breach first. Since all resistivity readings support the probability that corrosion can occur, it confirms that corrosion can occur in the top 50.8 mm (2 in) of the specimens.

Half-Cell Potentials

A potential more negative than -350 mV indicates a 90-percent probability that corrosion is occurring. Measurements were taken connected and unconnected in order to record the potential differences between macrocell corrosion and microcell corrosion. Connected, the half-cell potentials may include the microcell and macrocell corrosion and unconnected the microcell corrosion. In this report, microcell corrosion is defined as the corrosion occurring on the top bar only. For the purpose of comparison, the data has been separated into groups of potentials with SIP with C/A = 1/1, SIP with C/A = 2/1, and NSIP with C/A = 2/1.

The first set of data presented is the half-cell potential readings with SIP, and C/A = 1/1, connected and unconnected. As shown in Figures 16 and 17, the initial values were less than the -200 mV level but were greater than the threshold of a 90-percent probability that corrosion was occurring, -350 mV. The measurements were within the uncertain active corrosion range of -350 to -200 mV.

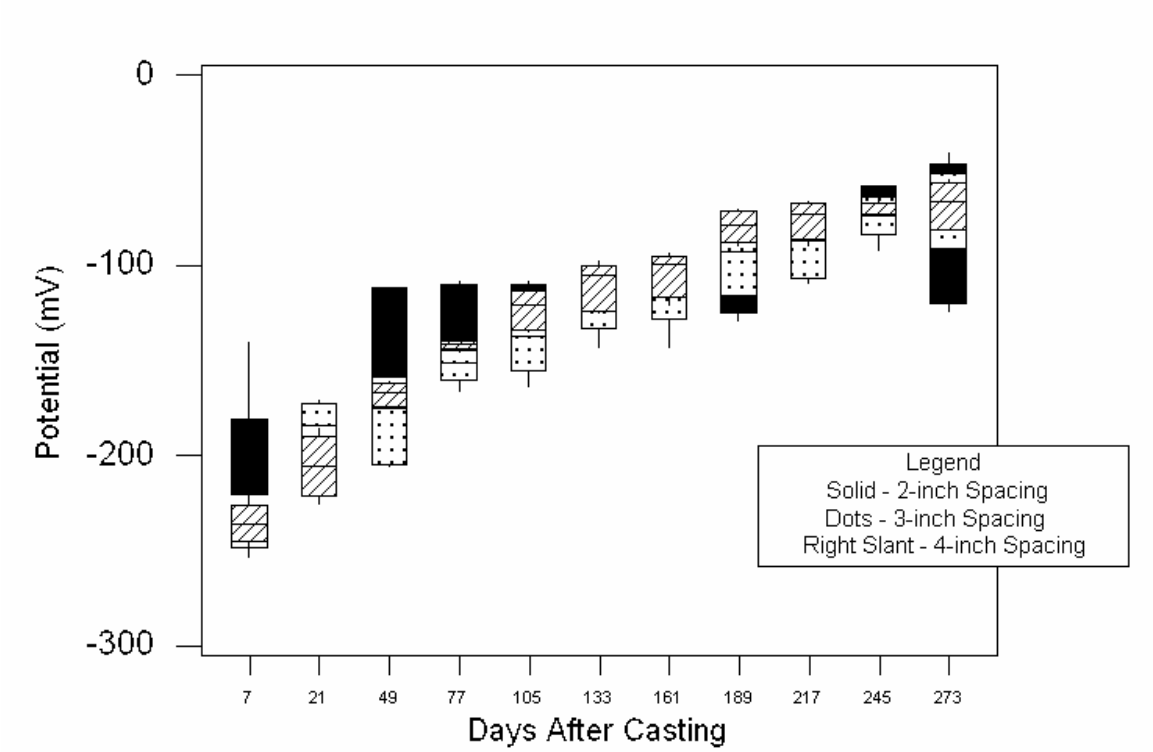

Figure 16 – Connected Half-Cell Potentials with SIP with C/A = 1/1

With time, the corrosion potentials became less negative and increased to approximately day 105. After 105 days, the half-cell potentials became relatively constant, varying between -140 to -75 mV. These values were similar in both the connected and unconnected states as shown in Figures 16 and 17.

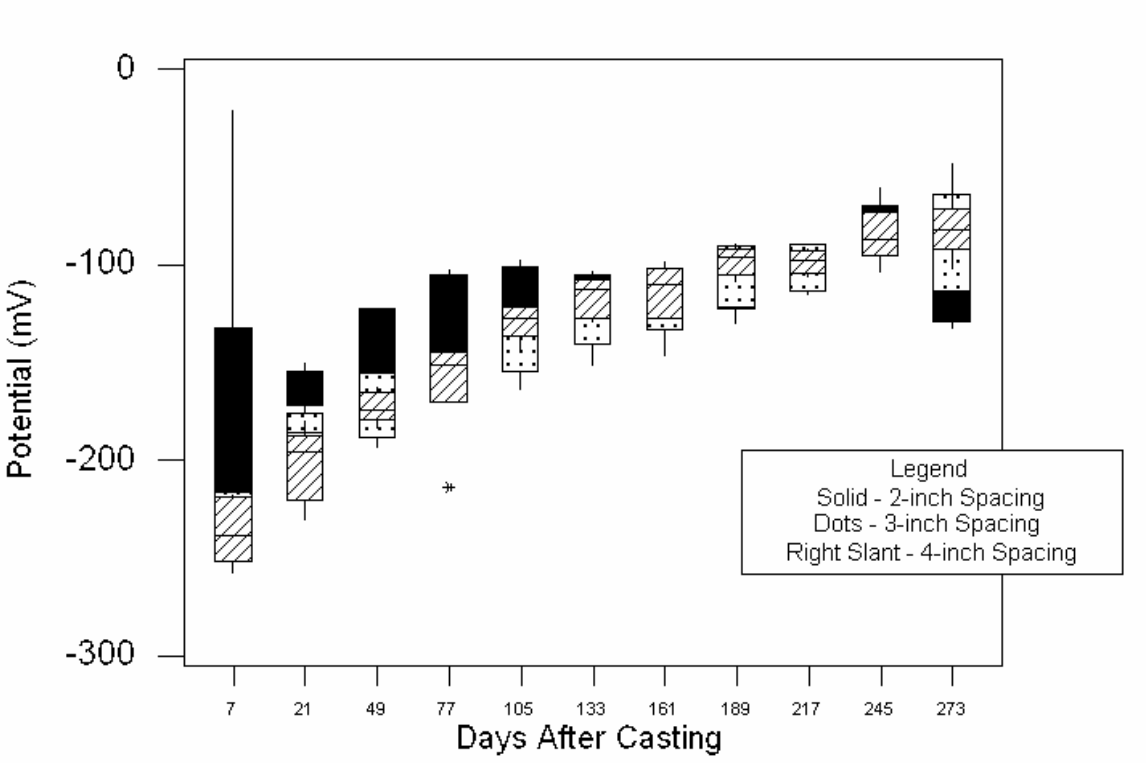

Figure 17 – Unconnected Half-Cell Potentials with SIP with C/A = 1/1

Few measurements were observed in the range of -350 mV to -200 mV which does not exclude the possibility of active corrosion. At approximately day 105, the values remained more positive than -200 mV which represents a 90% probability that chloride induced corrosion is not occurring. It is interesting to note that the half-cell and the resistivity measurements began to remain relatively constant at about the same time, approximately 105 days after casting.

The next set of presented data represents half-cell potentials with SIP, C/A = 2/1, connected and unconnected. As shown in Figures 18 and 19, the potentials initially were more negative than -200 mV and became relatively constant at day 105 between -150 and -130 mV.

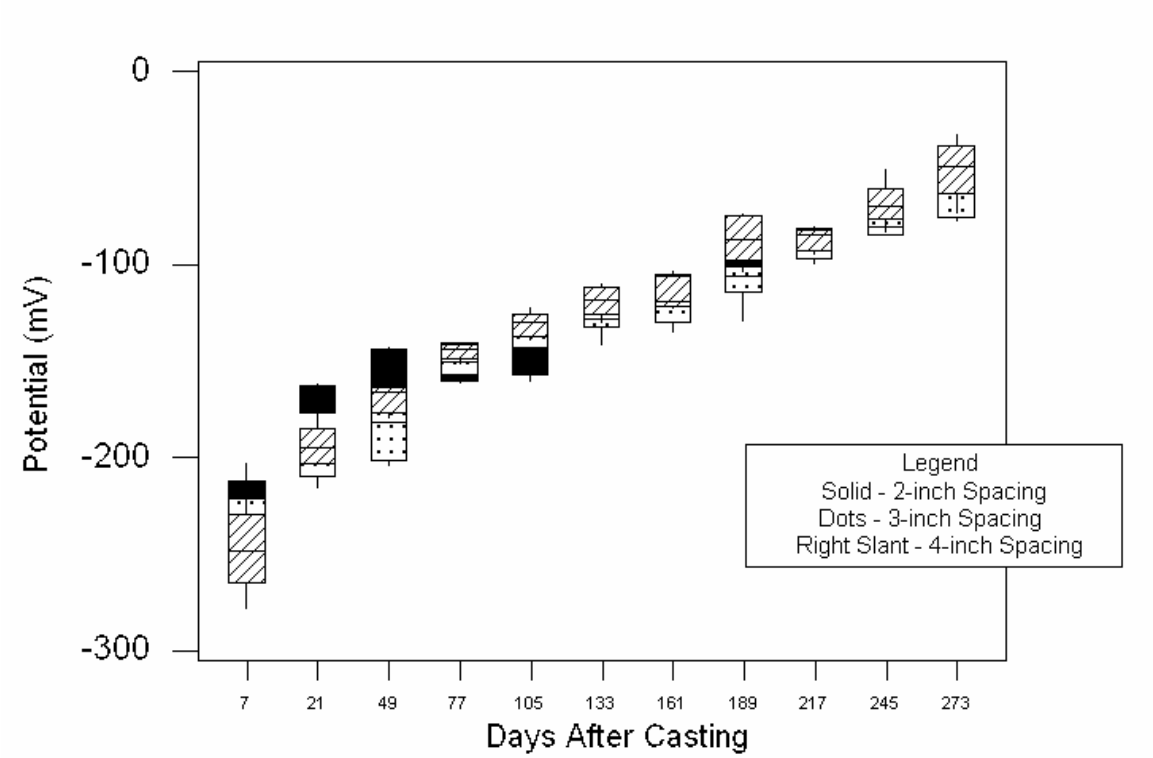

Figure 18 – Connected Half-Cell Potentials with SIP with C/A = 2/1

Measured potentials for both the connected and unconnected states became less negative than -200 mV after day 105. Approximately 75% of the observed values were less negative than -200 mV which indicated that there was a 10% or less chance that corrosion was occurring. As the measured potentials stabilized, the connected and unconnected values ranged from -150 mV to -90 mV. As time increased, the variability of the measured potentials also decreased. Few differences existed between the values measured for the connected and unconnected states as shown in Figures 18 and 19.

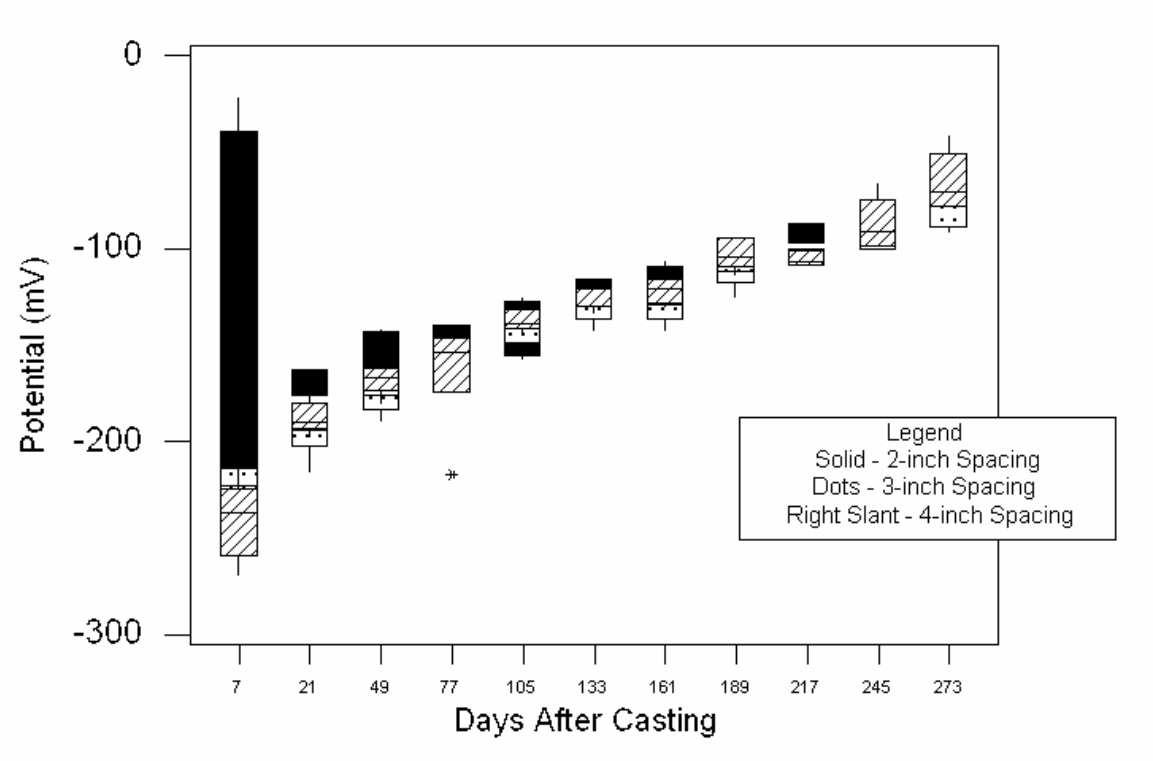

Figure 19 – Unconnected Half-Cell Potentials with SIP with C/A = 2/1

The last set of half-cell potentials are for specimens without SIP C/A = 2/1 in the connected and unconnected states. Figures 20 and 21 present the measured half-cell potentials for the connected and unconnected condition, respectively. The half-cell potentials became less negative until day 105 where the potentials began to stabilize. The values stabilized in a range of -150 mV to -90 mV. Before day 105, the observed values ranged from -290 mV to -150 mV. Few differences existed in the measured values between the connected and unconnected states. Approximately 75 - 80% of the values on both the connected and unconnected conditions were more positive than -200 mV while the other 20 – 25% of the data was classified as having an uncertain probability of active corrosion between -200 and -350 mV.

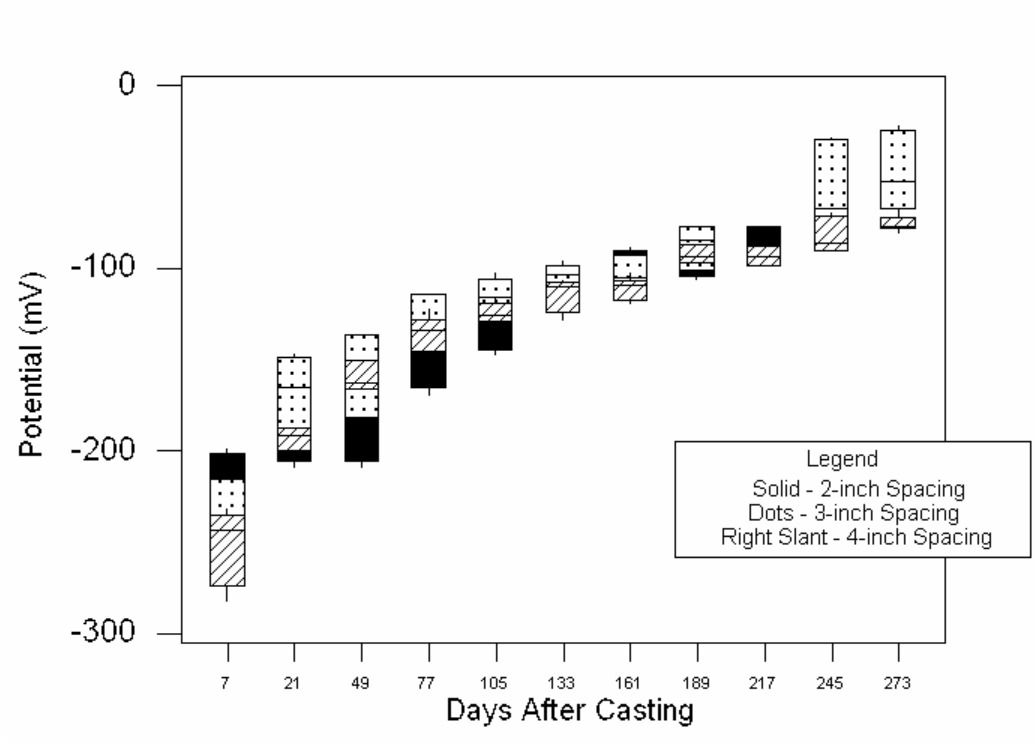

Figure 20 – Connected Half-Cell Potentials Without SIP with C/A = 2/1

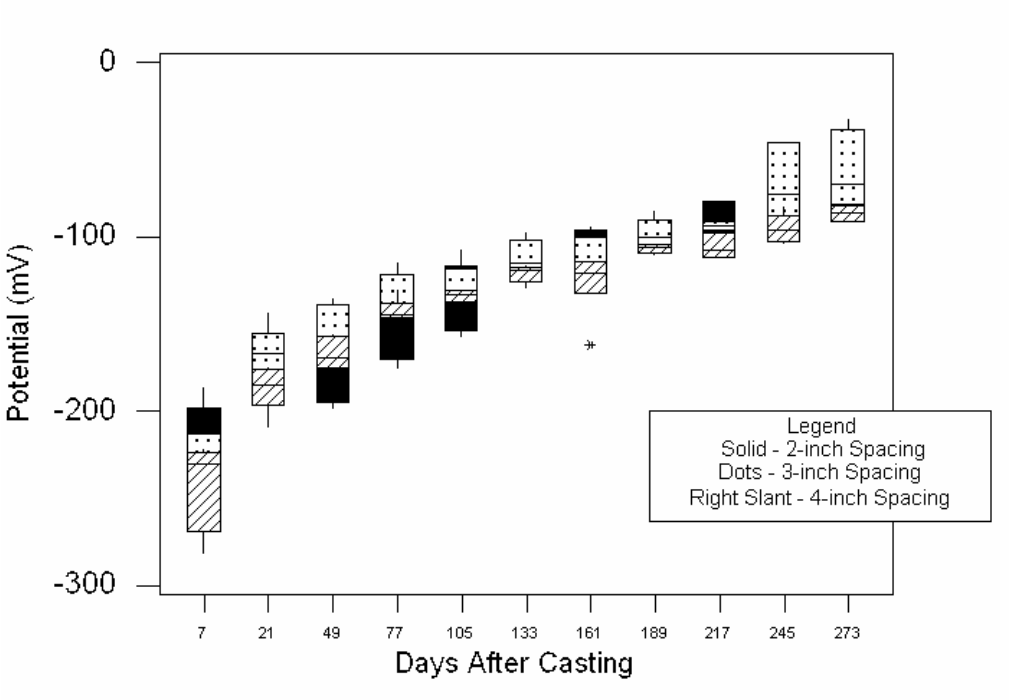

Figure 21 – Unconnected Half-Cell Potentials Without SIP with C/A = 2/1

In order to more closely examine the half-cell potentials, three specific periods of time were chosen. Half-cell potentials in the connected and unconnected states were observed with the three variables of different spacing arrangements, the presence of and absence of SIP, and differences in cathode bar to anode bar ratios. With few significant differences observed in Figures 16 through 21, the specimens were compared at days 105, 189, and 245 to more closely examine the data when subjected to the aforementioned variables.

Spacing Arrangement Differences

Each spacing arrangement was observed at days 105, 189, and 245 in order to examine the differences in half-cell potentials. Table 10 summarizes the half-cell potentials for all spacing arrangements in the connected and unconnected states. Relatively little difference existed between the connected and unconnected conditions for the three spacing factors for both means and coefficients of variations at the three ages. Statistical analyses of the data presented in Table 10 supports the statement that the spacing arrangement at specified days after casting does not affect the difference between the connected and unconnected potentials. This also means that the macrocell effect is insignificant in this comparison during the formation of the passive layer.

Table 10 – Half-Cell Potentials for Different Spacing Arrangements

Days After Casting	Clear Spacing mm (in)	Connected Half-Cell Potentials (mV)				Unconnected Half-Cell Potentials (mV)			
		Number of Measurements (N)	Mean Potential (mV)	Standard Deviation	Coefficient of Variation (%)	Number of Measurements (N)	Mean Potential (mV)	Standard Deviation	Coefficient of Variation (%)
105	50.8 (2)	18	-126.00	15.08	11.97	18	-129.17	15.48	11.98
105	76.2 (3)	18	-131.39	15.47	11.77	18	-135.83	13.12	9.66
105	101.6 (4)	18	-125.83	8.10	6.44	18	-133.56	6.96	5.21
189	50.8 (2)	18	-103.67	9.85	9.50	18	-107.50	7.67	7.13
189	76.2 (3)	18	-97.94	16.17	16.51	18	-105.22	12.62	11.99
189	101.6 (4)	18	-86.39	10.24	11.85	18	-102.72	7.04	6.85
245	50.8 (2)	18	-83.39	18.26	21.90	18	-91.22	20.89	22.90
245	76.2 (3)	18	-68.83	17.29	25.12	18	-80.17	16.49	20.57
245	101.6 (4)	18	-74.06	10.52	14.20	18	-89.39	11.09	12.41

Stay-in-Place Forms

The next set of corrosion potentials is for SIP and NSIP conditions. Tables 11 and 12 list the mean and basic statistics of the half-cell potentials for specimens with and without SIP, at different spacing arrangements, and at specified days after casting in the connected and unconnected states.

Table 11 – Half-Cell Potentials for Specimen With SIP

Days After Casting	Clear Spacing mm (in)	SIP							
		Connected Half-Cell Potentials (mV)				Unconnected Half-Cell Potentials (mV)			
		Number of Measurements (N)	Mean Potential (mV)	Standard Deviation	Coefficient of Variation (%)	Number of Measurements (N)	Mean Potential (mV)	Standard Deviation	Coefficient of Variation (%)
105	50.8 (2)	12	-126.08	16.68	13.23	12	-126.67	17.56	13.86
105	76.2 (3)	12	-138.75	11.43	8.24	12	-140.50	12.03	8.56
105	101.6 (4)	12	-126.58	9.23	7.29	12	-133.33	8.29	6.22
189	50.8 (2)	12	-105.58	10.97	10.39	12	-109.75	7.51	6.84
189	76.2 (3)	12	-102.83	16.08	15.64	12	-108.75	13.17	12.11
189	101.6 (4)	12	-83.25	10.91	13.11	12	-100.67	7.73	7.68
245	50.8 (2)	12	-86.42	20.78	24.05	12	-94.50	22.48	23.79
245	76.2 (3)	12	-72.75	10.69	14.69	12	-89.83	8.09	9.01
245	101.6 (4)	12	-86.50	11.49	13.28	12	-86.50	11.49	13.28

Table 12 – Half-Cell Potentials for Specimen Without SIP

Days After Casting	Clear Spacing mm (in)	NSIP							
		Connected Half-Cell Potentials (mV)				Unconnected Half-Cell Potentials (mV)			
		Number of Measurements (N)	Mean Potential (mV)	Standard Deviation	Coefficient of Variation (%)	Number of Measurements (N)	Mean Potential (mV)	Standard Deviation	Coefficient of Variation (%)
105	50.8 (2)	6	-125.83	12.67	10.07	6	-131.33	15.79	12.02
105	76.2 (3)	6	-116.67	11.66	9.99	6	-126.50	10.48	8.28
105	101.6 (4)	6	-124.33	5.61	4.51	6	-134.00	3.58	2.67
189	50.8 (2)	6	-99.83	6.24	6.25	6	-103.00	6.29	6.11
189	76.2 (3)	6	-88.17	12.14	13.77	6	-98.17	8.38	8.54
189	101.6 (4)	6	-92.67	4.89	5.28	6	-106.83	2.64	2.47
245	50.8 (2)	6	-77.33	10.84	14.02	6	-84.67	17.17	20.28
245	76.2 (3)	6	-58.33	23.31	39.96	6	-71.00	21.11	29.73
245	101.6 (4)	6	-82.50	9.65	11.70	6	-95.17	8.26	8.68

For each specified day and spacing arrangement, the difference between half-cell potentials must initially be compared locally amongst each spacing arrangement and then globally amongst the presence of SIP. Again, there is relatively little difference between spacing factors and the connected and unconnected conditions between the means and the coefficients of variation. Tables 11 and 12 show that regardless of the presence of SIP at a specified spacing arrangement and age, that the connected and unconnected potentials vary slightly. This observation supports the hypothesis that the macrocell presence throughout the analysis period was insignificant.

Cathode Bar to Anode Bar Ratio

The last variable observed was the cathode-to-anode ratio for each specimen at a specified day, spacing arrangement, and with the presence of SIP for both the connected and unconnected states. Tables 13 and 14 list the mean half-cell measurements for the cathode-to-anode ratio for days 105, 189, and 245.

Table 13 – Half-Cell Potential Measurements for Different C/A = 2/1

Days After Casting	Clear Spacing mm (in)	C/A = 2/1							
		SIP							
		Connected Half-Cell Potentials (mV)				Unconnected Half-Cell Potentials (mV)			
		Number of Measurements (N)	Mean Potential (mV)	Standard Deviation	Coefficient of Variation (%)	Number of Measurements (N)	Mean Potential (mV)	Standard Deviation	Coefficient of Variation (%)
105	50.8 (2)	6	-129.00	22.11	17.14	6	-134.00	16.36	12.21
105	76.2 (3)	6	-137.67	5.28	3.84	6	-142.33	8.21	5.77
105	101.6 (4)	6	-130.67	6.50	3.84	6	-137.17	5.85	4.26
189	50.8 (2)	6	-103.17	6.85	6.64	6	-110.67	4.32	3.90
189	76.2 (3)	6	-108.00	11.97	11.08	6	-113.00	7.10	6.28
189	101.6 (4)	6	-87.00	12.71	14.61	6	-103.33	7.74	7.49
245	50.8 (2)	6	-88.83	22.44	25.26	6	-97.20	27.3	28.09
245	76.2 (3)	6	-78.75	7.14	9.07	6	-93.00	7.62	8.19
245	101.6 (4)	6	-68.50	11.48	16.76	6	-87.33	12.86	14.73

Table 14 – Half-Cell Potential Measurements for C/A = 1/1

Days After Casting	Clear Spacing mm (in)	C/A = 1/1							
		SIP							
		Connected Half-Cell Potentials (mV)				Unconnected Half-Cell Potentials (mV)			
		Number of Measurements (N)	Mean Potential (mV)	Standard Deviation	Coefficient of Variation (%)	Number of Measurements (N)	Mean Potential (mV)	Standard Deviation	Coefficient of Variation (%)
105	50.8 (2)	6	-123.17	10.15	8.24	6	-122.17	14.33	11.73
105	76.2 (3)	6	-139.83	16.02	11.46	6	-138.67	15.58	11.24
105	101.6 (4)	6	-122.50	10.25	8.37	6	-129.50	9.05	6.99
189	50.8 (2)	6	-108.00	14.27	13.21	6	-108.83	10.17	9.34
189	76.2 (3)	6	-97.67	19.02	19.47	6	-104.50	16.97	16.24
189	101.6 (4)	6	-79.50	8.14	10.24	6	-98.00	7.38	7.53
245	50.8 (2)	6	-84.00	20.79	24.75	6	-91.83	18.74	20.41
245	76.2 (3)	6	-74.00	12.68	17.14	6	-84.17	14.92	17.73
245	101.6 (4)	6	-71.17	4.31	6.06	6	-85.67	11.09	12.95

For each specified day since placement, the C/A ratio will first be compared to the spacing arrangement. If significant differences amongst the spacings cannot be determined, then the potentials will be compared globally utilizing only the C/A ratio. As shown with the other groups of data, there is little difference between spacing factors in the connected and unconnected conditions at the various ages between the means and coefficients of variation. This data further supports the observation that the macrocell effect is insignificant when potentials are compared with the presence of SIP, C/A ratios, and connected and unconnected states at specified spacing arrangements and ages.

In order to determine further if differences in the measured potentials existed, the data was divided into two groups similar to the resistivity comparisons, C/A = 2/1 and 1/1 and SIP and NSIP. Since it was observed that the differences between reinforcing bar spacing and the connected and unconnected states are insignificant, all the data was combined. Figure 22 represents those specimens with SIP.

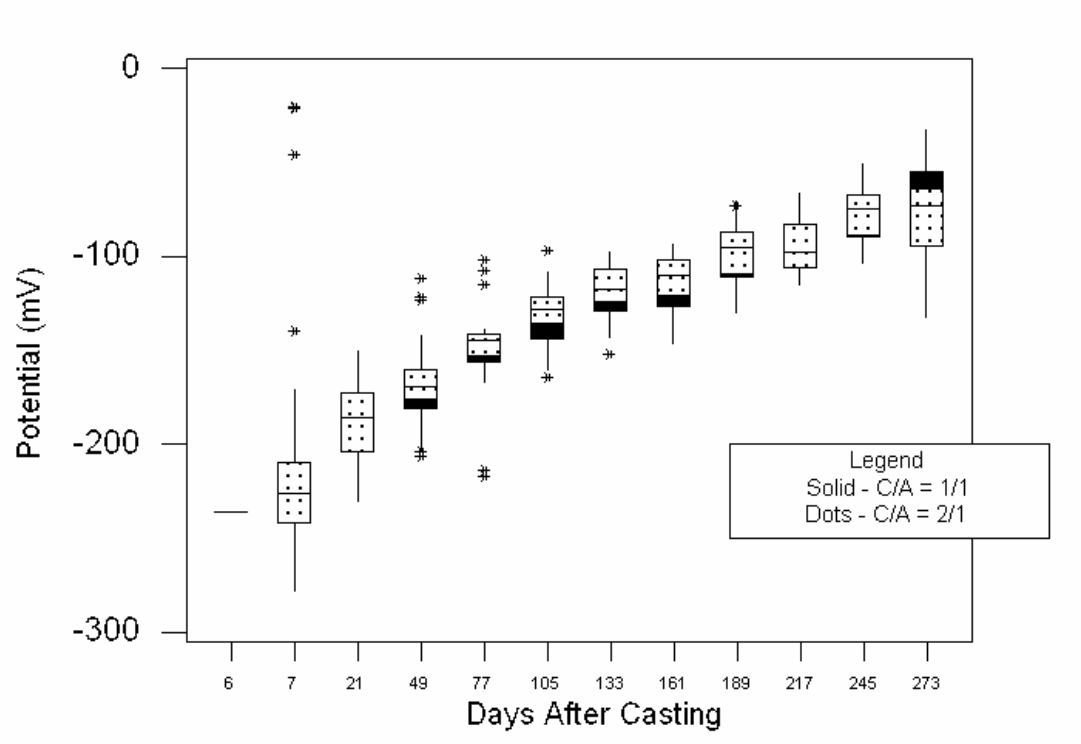

Figure 22 – Half-Cell Potentials With SIP (C/A = 2/1 v. C/A = 1/1)

A large variability existed in the first 7 days of the measured potentials. This may be attributed to the operator becoming familiar with the equipment. After the initial 7 day period, the variability was relatively consistent throughout the remainder of the testing period. Initially, the potentials became more positive until they reached day 105 where they remained within the range of -150 to -50 mV. Also, few differences can be detected between those specimens with two cathode bars and those specimens with only one cathode bar. The lack of significant differences between those specimens with a C/A = 2/1 and a C/A = 1/1 supports the statement that an increase in the cathode area of 50% does not necessarily increase the rate of formation of the passive layer nor does it affect the potentials throughout the 273 day period.

One last comparison is made because of a lack of significant differences observed in Figures 22. All the half-cell measurements for SIP regardless of the C/A ratio are compared to all specimens without SIP in Figure 23.

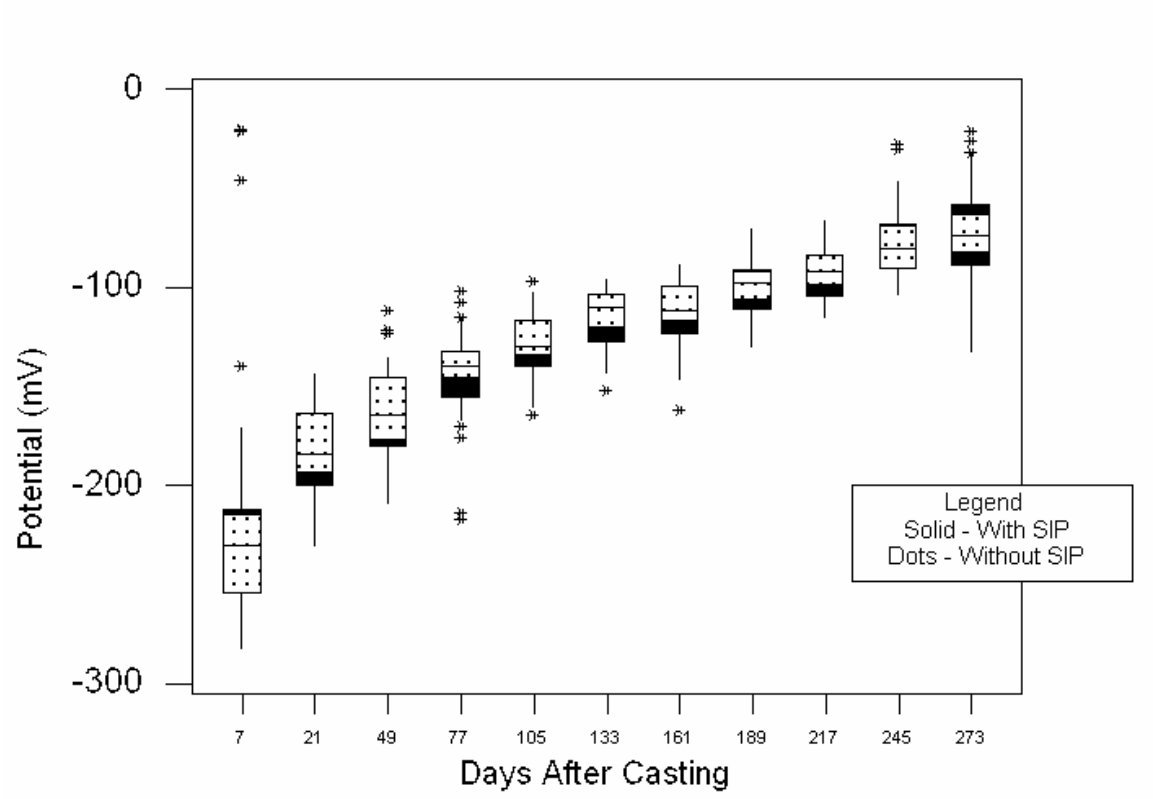

Figure 23 – Half-Cell Potentials (SIP v. NSIP)

The trend continued in the graph as it did in previous figures. The potentials initially became more positive until about day 105, afterwards they ranged between -150 and -60 mV. The variability after 7 days casting was relatively consistent over the 273 day time period. Few differences existed between those specimen that possessed SIP versus those specimen that did not regardless of the spacing arrangement and the C/A ratio. The results support the statement that the potentials measured are those from the top bar or the anode bar due to a lack of significant differences between the connected and unconnected readings. Additionally, the increase of the cathode area by 50% and the presence of SIP did not have a significant effect over a 273 day time period and did not increase the rate of the formation of the passive layer.

Corrosion Current Density

Kenneth C. Clear has performed extensive testing in field environments (Clear, K.C., 1989). Therefore, the interpretation of the corrosion rates that he presents may differ from the interpretation of the measurements in laboratory experiments such as this one.

Corrosion current density was observed with different spacing arrangements, the presence of SIP, and different cathode bar to anode bar ratios. All three variables were compared in order to detect any differences that might have existed between specimens. The first group of specimen observed were those with SIP with C/A = 1/1 in the connected and unconnected states.

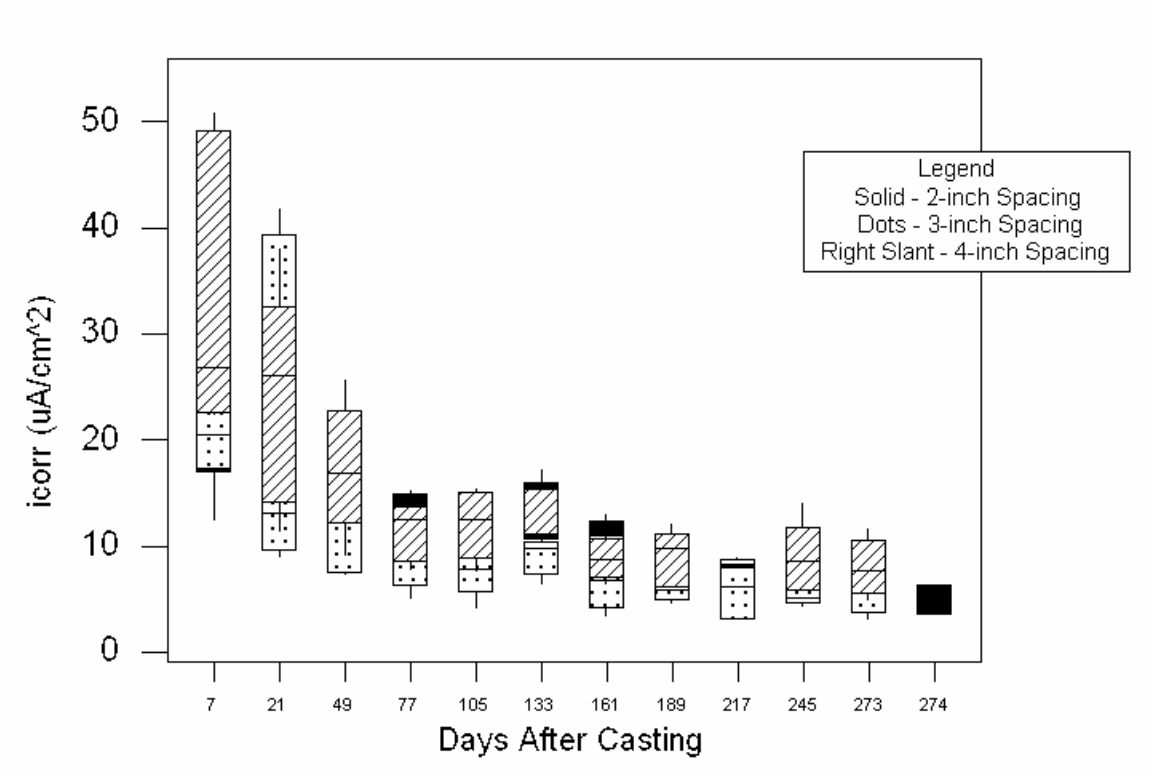

Figure 24 – Connected Corrosion Current Density with SIP with C/A = 1/1

As shown in Figure 24, corrosion current density values ranged from 52 to 12 uA/cm^2 for the first 105 days after casting, decreasing with increasing time after casting. The rate of change in corrosion current density decreased at approximately day 105, afterwards ranging from 18 to 5 uA/cm^2. Few differences existed between spacing arrangements over the 273 day time period. The variability also was more uniform after day 21. The large variability up to day 21 may be attributed to the operator becoming familiar with the equipment.

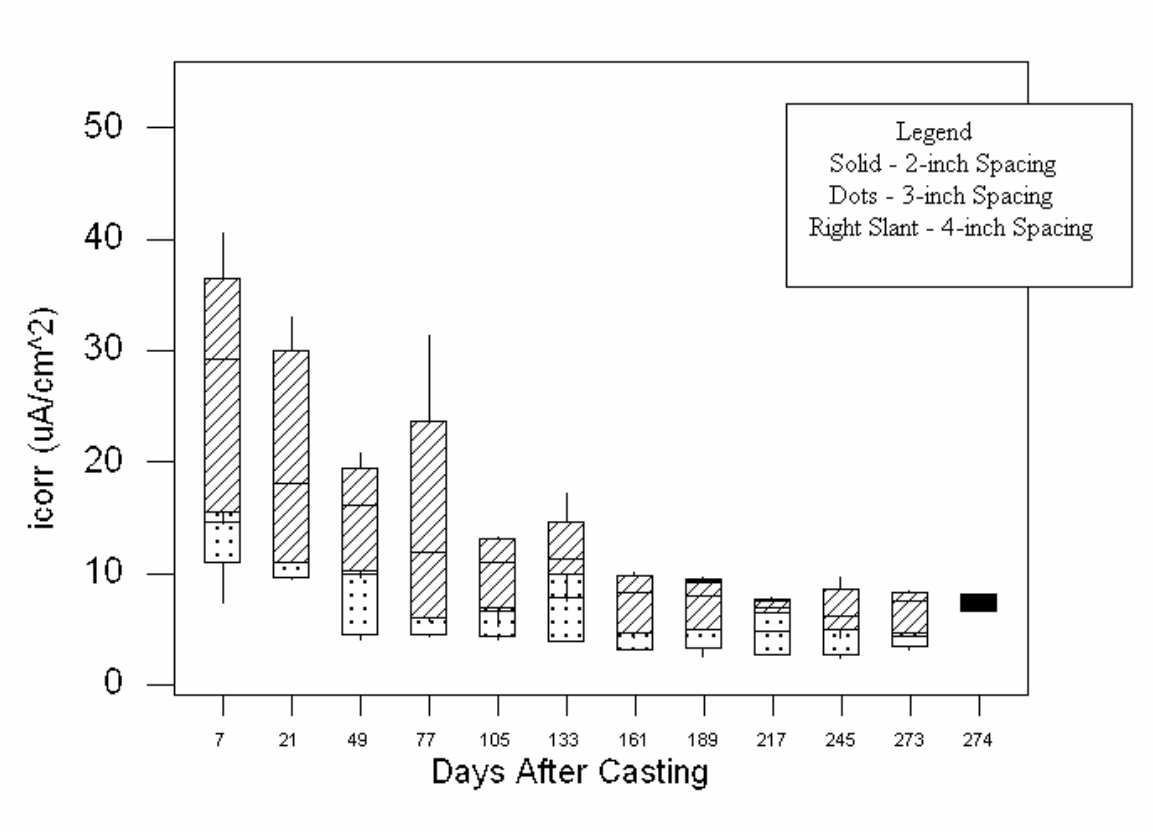

Figure 25 – Unconnected Corrosion Current Density with SIP with C/A = 1/1

As illustrated in Figure 25, corrosion current density values initially ranged from 42 to 7 uA/cm^2 and decreased with time after casting. As in Figure 24, the corrosion current density rate of change decreased at about day 105 where the values ranged from 35 to 3 uA/cm^2 to 273 days as shown in Figures 24 and 25. Few differences were visually detected between the connected and unconnected states of SIP, C/A = 1/1. Therefore, it was inferred that the measured corrosion current density is mostly attributed to that of the top bar (anode bar).

The next specimen group is displayed in Figures 26 and 27 which represented the corrosion current density measurements with SIP with C/A = 2/1. In the unconnected state as well as in the connected state, measured corrosion current densities decreased initially at a relatively rapid rate until approximately day 105 where they became more uniform.

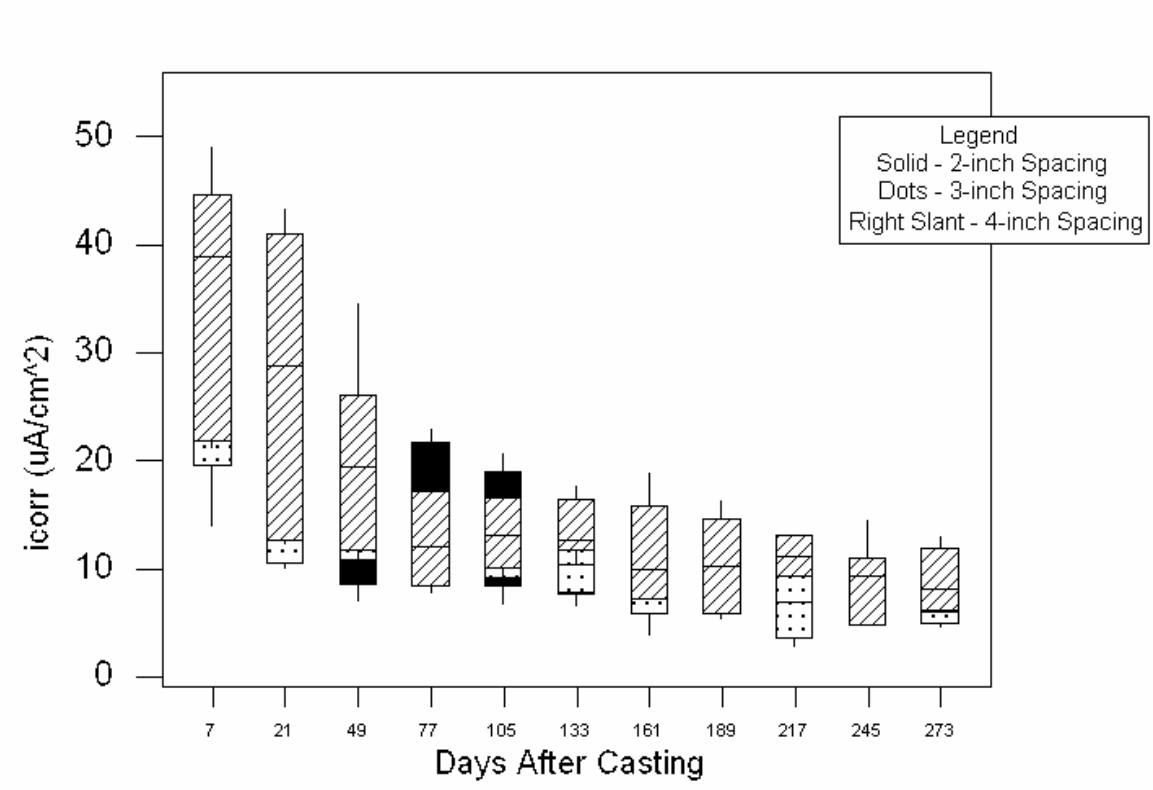

Figure 26 – Connected Corrosion Current Density with SIP with C/A = 2/1

Few differences were visually observed between Figures 26 and 27. Both graphs contained values that ranged between 50 and 8 uA/cm^2. The rate of change in corrosion current density measurements decreased at about 105 days and remained in the range of 25 and 9 uA/cm^2 afterwards. After day 105, the variability remained relatively uniform throughout day 273.

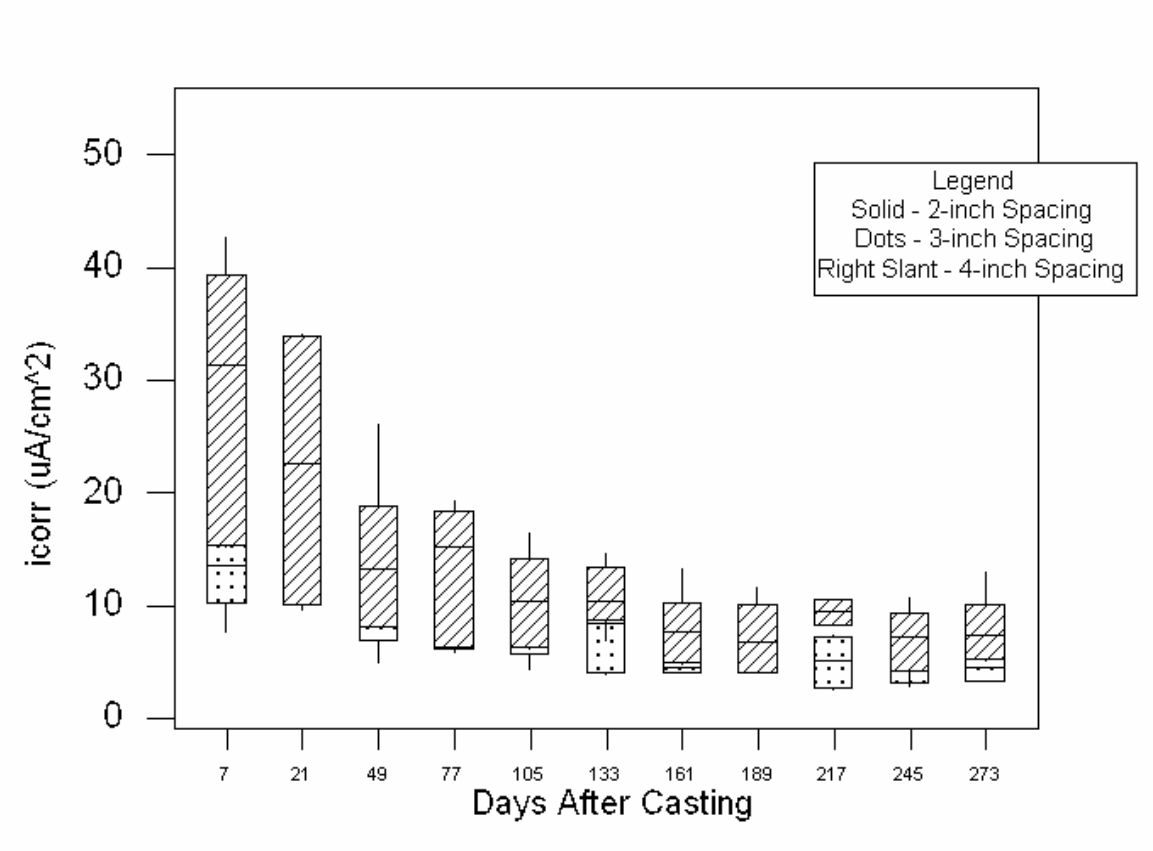

Figure 27 – Unconnected Corrosion Current Density with SIP with C/A = 2/1

Figures 28 and 29 display the corrosion current density with C/A = 2/1 without SIP in the connected and unconnected states. The observed values for corrosion current densities without SIP with C/A = 2/1 were 42 to 11 uA/cm^2. The values, as in previous figures decreased at a relatively rapid rate until about day 105 and then became more uniform after day 105. After 105 days, corrosion current density values ranged between 23 to 5 uA/cm^2. Few differences existed between the connected and unconnected states.

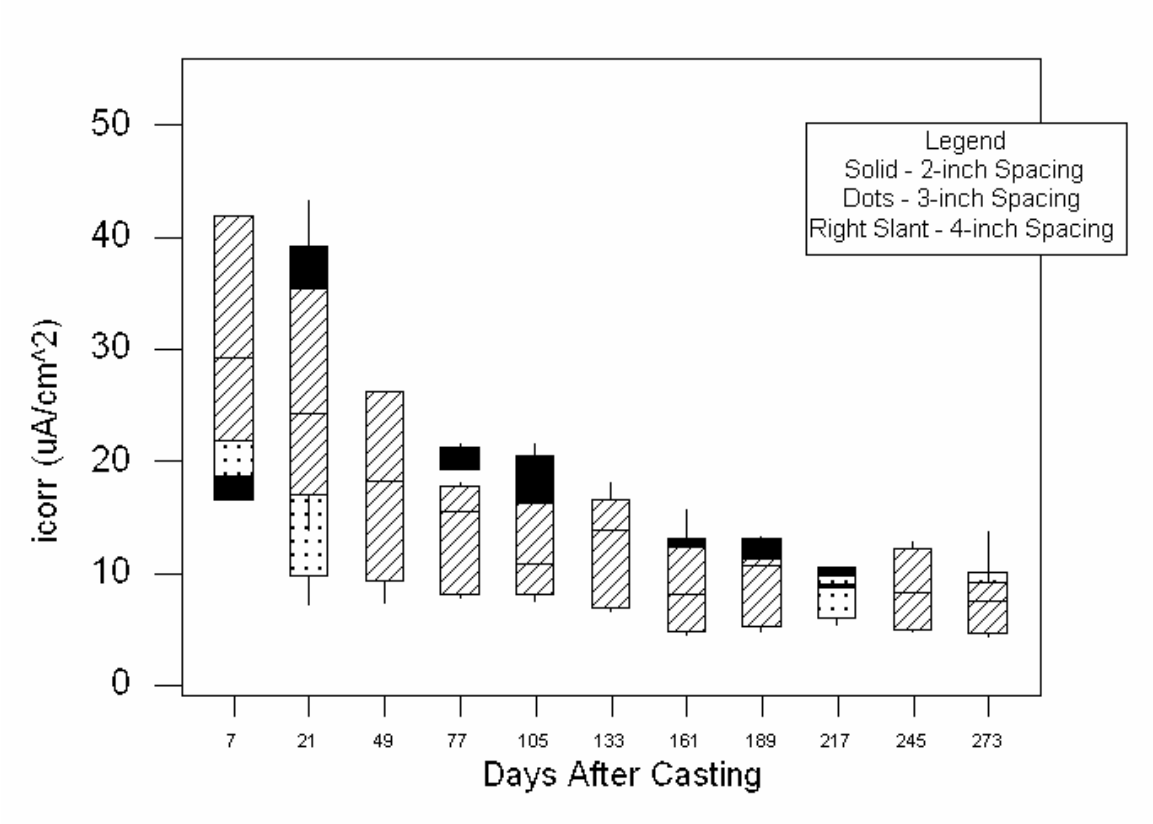

Figure 28 – Connected Corrosion Current Density without SIP with C/A = 2/1

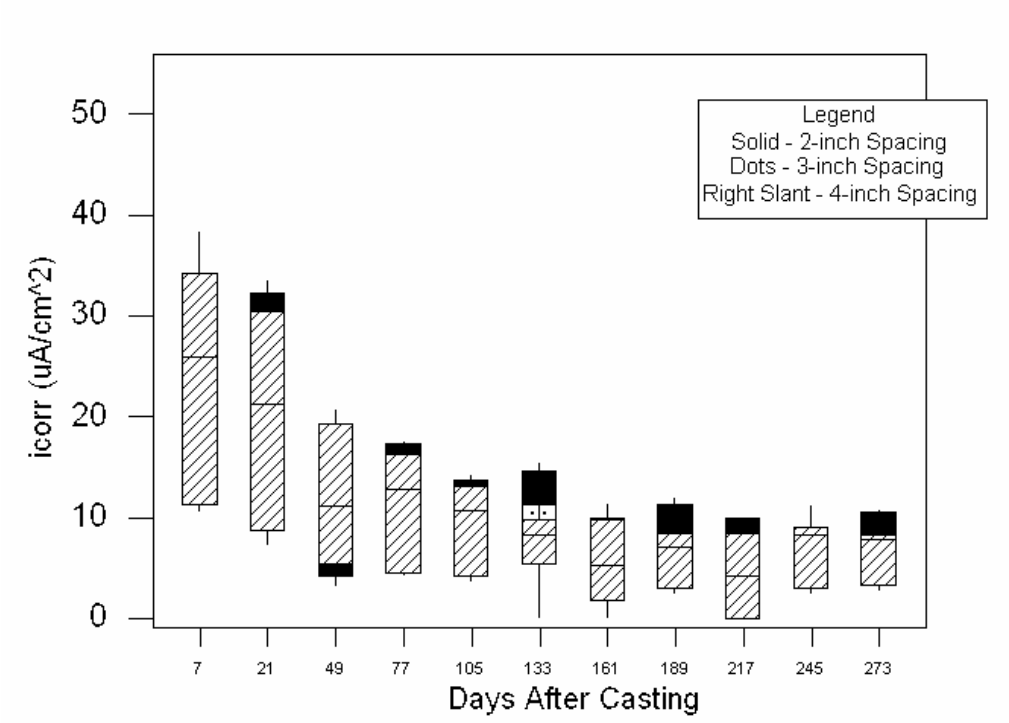

Figure 29 – Unconnected Corrosion Current Density without SIP with C/A = 2/1

Insignificant differences were observed visually from Figures 24 through 29. The lack of differences between corrosion current densities supports the statement that for different spacing arrangements, the macrocell effect is insignificant regardless of the presence of SIP and C/A ratio over 273 days after casting. In order for the data to be examined more closely, three distinct days after casting were chosen and compared. Spacing arrangement differences, the presence of SIP, and differences in the cathode bar to anode bar ratios were compared at days 105, 189, and 245 days after casting for each specimen group.

Spacing Arrangement Differences

Table 15 displays data to examine differences that existed at specified days since casting at different spacing arrangements for the corrosion current density in the connected and unconnected states. Kenneth C. Clear states that corrosion damage will possibly occur in 2 years or less for values greater than 10 uA/cm^2 (Clear, K.C., 1989). Most mean i_{corr} values were within the range of 1 to 10 uA/cm^2 for three specified days which Clear states that corrosion damage is possible within 2 to 10 years. These values signify that corrosion, formation of the passive layer, is occurring throughout the 273 day test time period. Statistical differences were not detected for the connected and unconnected states and possessed standard deviations and coefficients of variation that were relatively small and consistent.

Table 15 – Corrosion Current Density at Different Spacing Arrangements

Days After Casting	Clear Spacing mm (in)	Connected i_{corr} (uA/cm^2)				Unconnected i_{corr} (uA/cm^2)			
		Number of Measurements (N)	Mean i_{corr} (uA/cm^2)	Standard Deviation	Coefficient of Variation (%)	Number of Measurements (N)	Mean i_{corr} (uA/cm^2)	Standard Deviation	Coefficient of Variation (%)
105	50.8 (2)	18	13.13	3.95	30.08	18	11.69	3.16	27.03
105	76.2 (3)	18	10.89	3.49	32.05	18	8.04	2.81	34.95
105	101.6 (4)	18	12.41	3.69	29.73	18	10.04	3.85	38.35
189	50.8 (2)	18	8.98	1.92	21.38	18	7.73	1.77	22.90
189	76.2 (3)	18	7.79	1.99	25.55	18	5.86	1.72	29.35
189	101.6 (4)	18	9.55	3.36	35.18	18	6.92	2.58	37.28
245	50.8 (2)	18	7.77	2.27	29.21	18	6.86	1.70	24.78
245	76.2 (3)	18	6.64	1.70	25.60	18	4.97	1.51	30.38
245	101.6 (4)	18	8.70	3.35	38.51	18	6.92	2.60	37.57

Stay-in-Place Forms

Corrosion current density was also observed with and without SIP at specified days after placement for the connected and unconnected states. Statistical differences were not observed between the corrosion current densities regardless of SIP for the unconnected and connected states and the standard deviations and coefficients of variation were relatively small. Once again, the data generally ranged between 1 and 10 uA/cm^2 which signifies the passive layer continues to form throughout the 273 day test period.

Table 16 – Corrosion Current Density Measurements with SIP

Days After Casting	Clear Spacing mm (in)	SIP							
		Connected i_{corr} (uA/cm^2)				Unconnected i_{corr} (uA/cm^2)			
		Number of Measurements (N)	Mean i_{corr} (uA/cm^2)	Standard Deviation	Coefficient of Variation (%)	Number of Measurements (N)	Mean i_{corr} (uA/cm^2)	Standard Deviation	Coefficient of Variation (%)
105	50.8 (2)	12	12.65	3.63	28.70	12	11.56	3.49	30.19
105	76.2 (3)	12	9.76	3.29	33.71	12	7.24	2.79	38.54
105	101.6 (4)	12	12.75	3.59	28.16	12	10.36	3.69	35.62
189	50.8 (2)	12	8.63	1.56	18.08	12	7.64	1.34	17.54
189	76.2 (3)	12	7.27	1.84	25.31	12	5.39	1.73	32.10
189	101.6 (4)	12	8.46	2.04	24.11	12	6.36	1.96	30.82
245	50.8 (2)	12	6.88	1.67	24.27	12	6.55	1.49	22.75
245	76.2 (3)	12	6.71	2.04	30.40	12	4.71	1.61	34.18
245	101.6 (4)	12	8.79	3.45	39.25	12	6.90	2.30	33.33

Table 17 – Corrosion Current Density Measurements Without SIP

Days After Casting	Clear Spacing mm (in)	NSIP							
		Connected i_{corr} (uA/cm^2)				Unconnected i_{corr} (uA/cm^2)			
		Number of Measurements (N)	Mean i_{corr} (uA/cm^2)	Standard Deviation	Coefficient of Variation (%)	Number of Measurements (N)	Mean i_{corr} (uA/cm^2)	Standard Deviation	Coefficient of Variation (%)
105	50.8 (2)	6	14.09	4.73	33.57	6	11.96	2.68	22.41
105	76.2 (3)	6	13.16	2.90	22.04	6	9.62	2.28	23.70
105	101.6 (4)	6	11.72	4.14	35.32	6	9.41	4.43	47.08
189	50.8 (2)	6	9.68	2.52	26.03	6	7.92	2.57	32.45
189	76.2 (3)	6	8.83	1.99	22.54	6	6.81	1.37	20.12
189	101.6 (4)	6	9.13	3.18	34.83	6	6.25	2.82	45.12
245	50.8 (2)	6	8.84	2.24	25.34	6	7.22	1.95	27.01
245	76.2 (3)	6	6.86	1.23	17.93	6	5.86	0.87	14.85
245	101.6 (4)	6	8.51	3.46	40.66	6	6.96	3.38	48.56

Cathode Bar to Anode Bar Ratio

The last comparison made was the ratio of the cathode bars to the anode bars in each connected and unconnected specimen. Statistical differences were not observed between the different cathode-to-anode ratios in both the connected and unconnected states. Once again, the standard deviations and coefficients of variation are relatively small. The corrosion current density (i_{corr}) measurements regardless of C/A ratios also generally ranged between 1 and 10 uA/cm^2 signifying that corrosion, the formation of the passive layer, continued throughout the 273 day test period.

Table 18 – Corrosion Current Density Measurements for C/A = 2/1

Days After Casting	Clear Spacing mm (in)	C/A = 2/1							
		SIP							
		Connected i_{corr} (uA/cm^2)				Unconnected i_{corr} (uA/cm^2)			
		Number of Measurements (N)	Mean i_{corr} (uA/cm^2)	Standard Deviation	Coefficient of Variation (%)	Number of Measurements (N)	Mean i_{corr} (uA/cm^2)	Standard Deviation	Coefficient of Variation (%)
105	50.8 (2)	6	13.98	4.49	32.12	6	12.51	4.19	33.49
105	76.2 (3)	6	10.84	2.75	25.37	6	7.33	2.81	38.34
105	101.6 (4)	6	13.47	4.19	31.11	6	10.56	4.28	40.53
189	50.8 (2)	6	9.50	1.13	11.89	6	7.40	1.22	16.49
189	76.2 (3)	6	7.80	1.36	17.44	6	5.31	1.30	24.48
189	101.6 (4)	6	10.39	4.55	43.79	6	7.12	3.12	43.82
245	50.8 (2)	6	7.23	2.17	30.01	6	6.90	1.93	2.80
245	76.2 (3)	6	7.51	2.13	28.36	6	4.87	1.64	33.68
245	101.6 (4)	6	8.74	3.68	42.11	6	6.98	2.90	41.55

Table 19 – Corrosion Current Density Measurements for C/A = 1/1

Days After Casting	Clear Spacing mm (in)	C/A = 1/1							
		SIP							
		Connected i_{corr} (uA/cm^2)				Unconnected i_{corr} (uA/cm^2)			
		Number of Measurements (N)	Mean i_{corr} (uA/cm^2)	Standard Deviation	Coefficient of Variation (%)	Number of Measurements (N)	Mean i_{corr} (uA/cm^2)	Standard Deviation	Coefficient of Variation (%)
105	50.8 (2)	6	11.32	2.14	18.90	6	10.50	2.73	26.00
105	76.2 (3)	6	8.68	3.66	42.17	6	7.16	3.03	42.32
105	101.6 (4)	6	12.03	3.09	25.69	6	10.16	3.40	33.46
189	50.8 (2)	6	7.75	1.50	19.35	6	7.88	1.53	19.42
189	76.2 (3)	6	6.75	2.23	33.04	6	5.47	2.21	40.40
189	101.6 (4)	6	9.13	2.50	27.38	6	7.41	2.02	27.26
245	50.8 (2)	6	6.53	1.06	16.23	6	6.20	0.931	15.02
245	76.2 (3)	6	5.90	1.75	29.66	6	4.56	1.71	37.50
245	101.6 (4)	6	9.00	3.29	36.56	6	6.63	2.11	31.83

Tables 15 through 19 support the statement that the, i_{corr} measurements, regardless of differences in the presence of SIP and the C/A ratio when compared to different spacing arrangements at specific ages, contain insignificant differences. The lack of differences infers that the i_{corr} measured is that of the top bar only.

Also important was the time period that the initial decrease in i_{corr} values occurred. Almost all specimens experienced a high rate of decrease in the initial i_{corr} values until approximately 105 days when the rate of decrease in the corrosion current density measurements decreased significantly. It appears that the greatest portion of the formation of the passive layer took place within 105 days after casting. The higher the i_{corr} value the more likely that corrosion is occurring (Clear, K.C. 1989). The formation of the passive layer in itself is a corrosion process. The values greater than 10 uA/cm^2 indicate that corrosion is occurring at a rapid rate, thus the passive layer thickens and becomes more uniform when the rate of corrosion current density decreases. It is

reasoned that once the passive layer is disrupted by the intrusion of chlorides that the i_{corr} values will once again increase (Clear, K.C. 1989).

As for the resistivity and half-cell potential measurements, the corrosion current density measurements were divided into two groups for comparison. The first comparison was between those with SIP with C/A = 2/1 and C/A = 1/1. All of the corrosion current densities with SIP, connected and unconnected, and reinforcing steel spacings are presented in Figure 30.

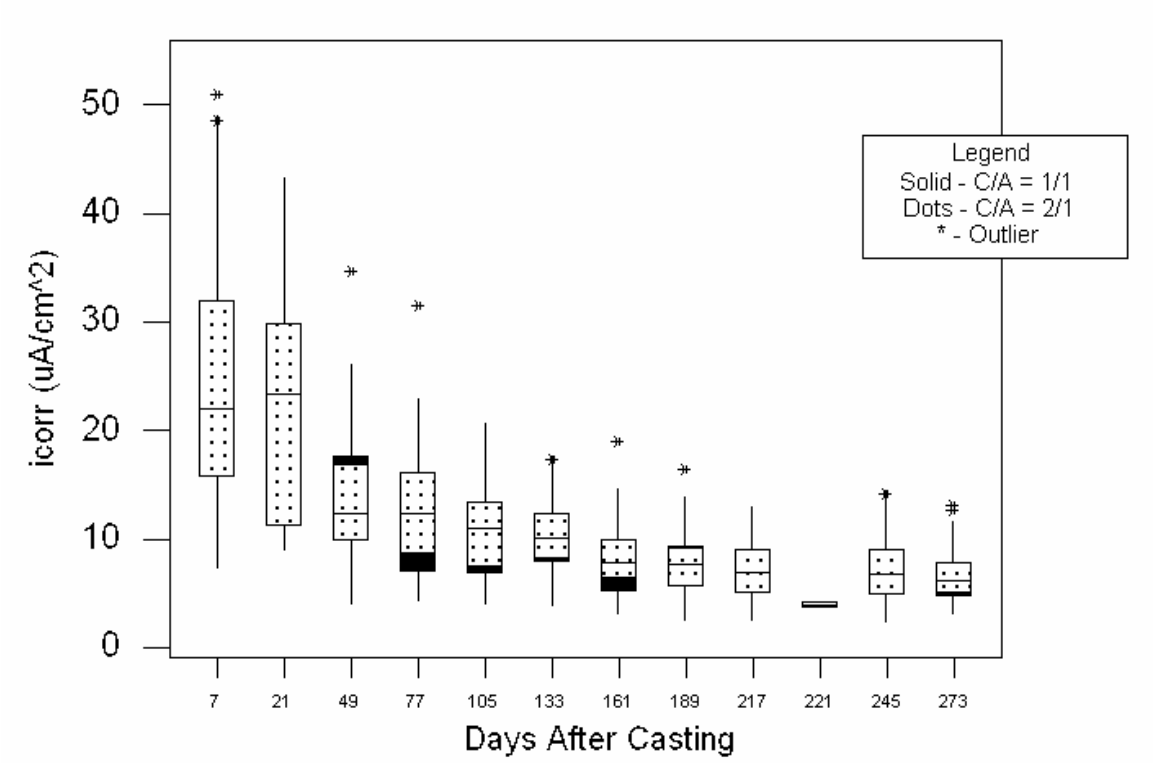

Figure 30 – i_{corr} Measurements With SIP (C/A = 1/1 v. C/A = 2/1)

Regardless of the C/A ratio, the i_{corr} values follow the same trend of initially decreasing until approximately day 105 where they stabilized in the range of 21 to 2 uA/cm^2. The minor differences indicate that an increase of the cathode area by 50% did not significantly affect the formation of the passive layer over the 273 day time period.

When the presence of SIP was compared, the i_{corr} values followed a similar trend as those of the other variables that were compared, Figure 31. The values initially decreased until

day 105 where they stabilized between 22 and 1 uA/cm^2. The differences between those specimens with SIP and those without SIP are insignificant. After day 105, the variability amongst the specimens remained relatively uniform. Therefore, it appears that the presence of SIP or lack there of, did not influence the formation of the passive layer.

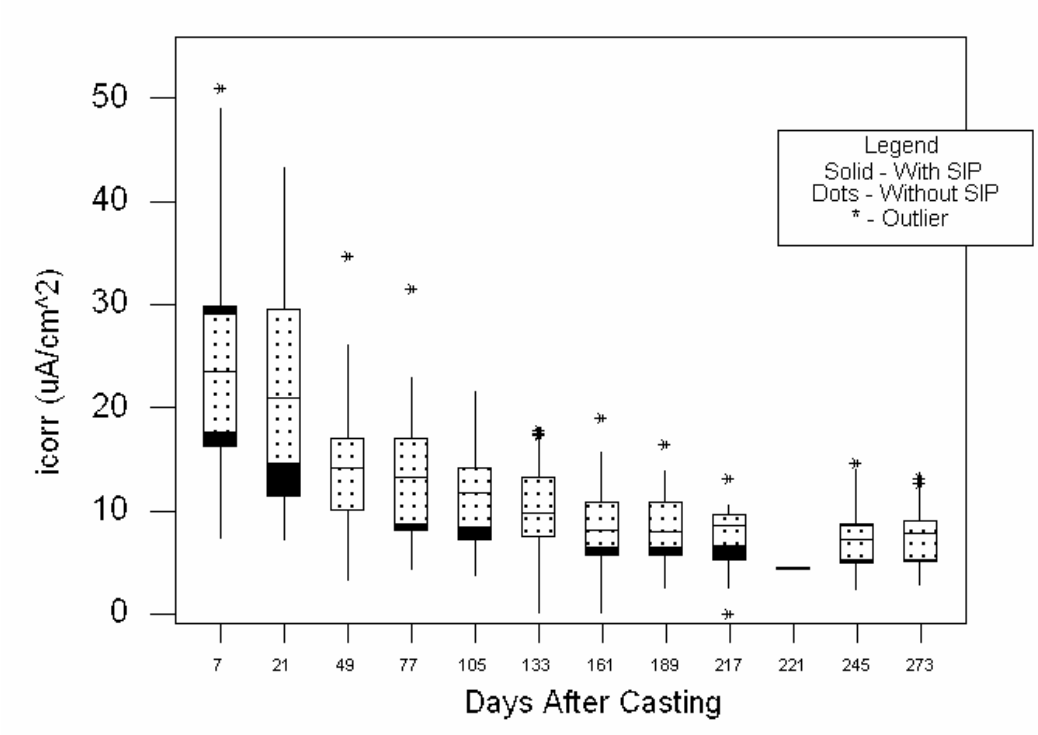

Figure 31 – Corrosion Current Density Measurements (SIP v. NSIP)

It is important to note that the values measured in this experiment somewhat contradict those used by Kenneth C. Clear to predict the rate of corrosion in reinforced concrete. These differences can be attributed to the environment in which the measurements were taken. A majority of the measurements taken by Kenneth C. Clear to obtain predicted corrosion rates were of actual bridge decks versus specimen in a controlled laboratory environment as in this experiment. In the laboratory environment, the area of polarization was known, where in a real world environment it is unknown as polarization currents move to the lowest potential which may be outside of the area being measured (S. Feliu et al. 2005). Also, the bottom of the top reinforcing bar is not polarized. Therefore, it can be inferred that Kenneth C. Clear's predicted corrosion rates will vary slightly from those in a laboratory environment during the formation of the passive layer.

Macrocell Current

Macrocell potentials were measured for each spacing arrangement throughout the 273 day time period. The potentials were then converted into current using ohm's law and a known resistivity of 100 ohms. Figure 32 represents the macrocell currents measured for the 2-inch spacing arrangement. A majority of the macrocell currents measured occurred before the 105 day time period which are to be considered typical of all the macrocell measurements. The macrocell current measurements occurred within the same time period of the rapid rate of formation of the passive layer as the half-cell potentials and corrosion current densities. However, as time progressed the measurements remained at zero. The measured macrocell currents may influence the initial corrosion reaction, the formation of the passive layer, but they do not support the continued occurrence of the corrosion reaction as it became relatively uniform. Because the rate that the currents occurred was not consistent, varying between positive and negative values, and because the measurements did not follow any specific trend they can be considered insignificant.

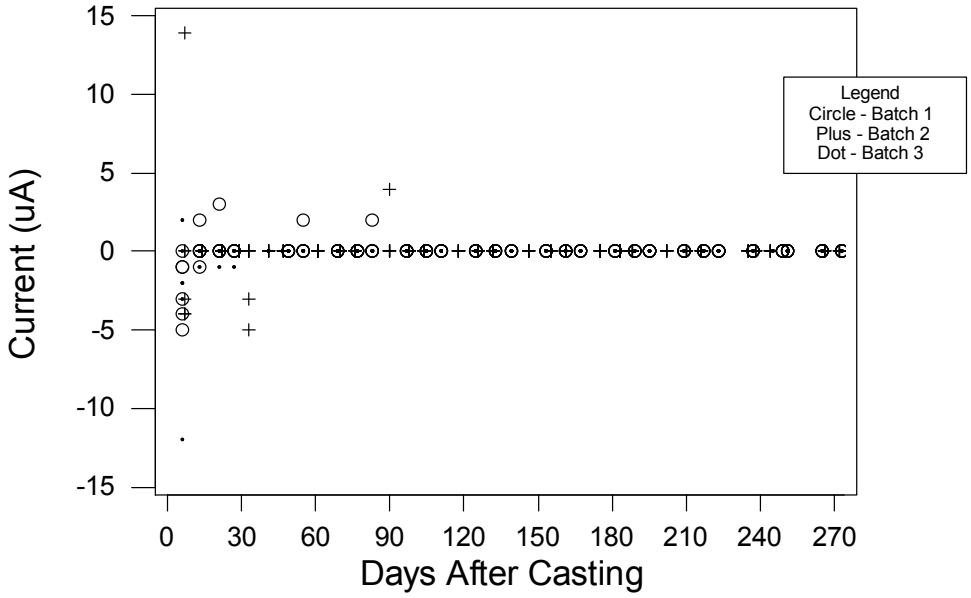

Figure 32 – Macrocell Current (2-inch Spacing)

CONCLUSIONS

Three parameters were modified amongst specimens to determine their influence on the microcell and macrocell current. The effect of the parameters was monitored utilizing four different methods of evaluation.

Resistivity

The resistivity of each specimen was measured and compared with different spacing arrangements, the presence of SIP, and different C/A ratios. No significant differences were detected between the parameters as they were modified. The consistency amongst resistivities signifies the consistencies amongst each batch of concrete and its mixture parameters. The final resistivities measured after a 273 day time period still displayed the concrete's ability to sustain a corrosion reaction.

Half-Cell Potentials

The half-cell potentials of each specimen were measured and compared with different spacing arrangements, the presence of SIP, and different C/A ratios. Measurements were recorded in both the connected and unconnected states to determine the macrocell effect. Significant differences were not detected amongst half-cell measurements for any observed parameter, including the connected and unconnected states. The lack of differences between the connected and unconnected states signified that the measured potentials could only be attributed to the microcell effect or from the corrosion reaction formed on the top reinforcing bar. The trend of the potentials becoming more positive at a relatively rapid rate and then becoming relatively uniform supported the conclusion that the passive layer was becoming more uniform and denser with time.

Corrosion Current Density

The corrosion current density of each specimen was measured and compared with different spacing arrangements, the presence of SIP, and different C/A ratios. The readings were taken in the connected and unconnected states. As in the half-cell potentials measurements, a lack of significant differences were observed between

parameters. The lack of differences between the connected and unconnected states signified that the measured corrosion current density may be attributed to that of the top reinforcing bar or microcell corrosion activity. The corrosion current density also supported the formation of the passive layer in that the measurements decreased at a relatively rapid rate and then became relatively uniform over the same time period in which the half-cell potentials began to stabilize. It was also determined that Kenneth C. Clear's predicted corrosion rates are slightly different than those values observed in this experiment because the polarized area is known in this laboratory environment.

RECOMMENDATIONS FOR FUTURE RESEARCH

It is important that this study continue as there were questions that were left unanswered. Primarily, chloride induced corrosion had not taken place in any of the specimen over the 273 day time period. Hence, it is not known what the effects of differences in spacing arrangements, C/A ratios, or SIP will have on the specimens once the bars begin to corrode. It is also unknown what effect macrocell corrosion had on the spacing arrangments and the presence of SIP because besides the continued formation of the passive layer, corrosion had not taken place. It is recommended that the ponding cycles continue until corrosion values peak. Then, further comparison should be made between the three variables, typical spacing arrangements, the presence of SIP, and differences in C/A ratios, in this experiment as well as the influence of the macrocell corrosion versus the microcell corrosion.

It is also recommended that if this study is to be repeated that the ponding cycles commence immediately after casting in order to allow the chlorides to reach the passive layer much more quickly. This will allow the specimen to corrode much more quickly and record results in a shorter period of time.

REFERENCES

Andrade, C., I.R. Maribona, S. Feliu, J.A. Gonzalez, and S. Felieu Jr. "The Effect of Macrocells Between Active and Passive Areas of Steel Reinforcements." *Corrosion Science* 33 (1991): 237-249.

Anon., ACI Committee 222, Corrosion of Metals in Concrete. 1996. Detroit, MI, American Concrete Institute. ACI Manual of Concrete Practice, Part I.

ASTM, American Society for Testing and Materials, "C 876-91, Standard Test Method for Half-Cell Potentials of Uncoated Reinforcing Steel in Concrete," *Annual Book of ASTM Standards* Vol. 04.02 Concrete and Aggregates (1991).

Bentur, Arnon, Sidney Diamond, and Neal Berke. *Steel Corrosion In Concrete.* London: E&FN Spon, 1997.

Berke, N. S. and Hicks, M. C., "Predicting Times to Corrosion From Field and Laboratory Chloride Data," Berke, N. S., Escalante, E., Nmai, C. K., Whiting, D. Ed., TECHNIQUE TO ASSESS THE CORROSION ACTIVITY OF STEEL REINFORCED CONCRETE STRUCTURES, 41-57. 1996. W Consohocken, American Society Testing and Materials. AMERICAN SOCIETY FOR TESTING AND MATERIALS SPECIAL TECHNICAL PUBLICATION.

Berkeley, K and S. Pathmanaban. *Cathodic Protection of Reinforcement Steel in Concrete.* London: Butterworth & Co. Ltd, 1990.

Bertolini, L., B. Elsener, P. Pedeferri, and R. Polder. *Corrosion of Steel in Concrete – Prevention, Diagnosis, Repair.* Weinheim, Germany: Wiley-VCH Verlag GmbH & Co. KGaA, 2004.

Broomfield, John P. *Corrosion of Steel in Concrete.* London: E&FN Spon, 1997.

Brown, Michael C. (1999). "Assessment of Commercial Corrosion Inhibiting Admixtures for Reinforced Concrete." Master of Science Thesis in Civil and Environmental Engineering, Virginia Polytechnic Institute and State University.

Brown, Michael C. (2002). "Corrosion Protection Service Life of Epoxy Coated Reinforcing Steel in Virginia Bridge Decks." Dissertation in Civil and Environmental Engineering, Virginia Polytechnic Institute and State University.

Castro, P, E. Pazini, C. Andrade, and C. Alonso. "Macrocell Activity in Slightly Chloride-Contaminated Concrete Induced by Reinforcement Primers." *Corrosion* 59 (June 2003): 535-545.

Chess, Paul. *Cathodic Protection of Steel in Concrete.* New York: Routledge, 1998.

Clear, Kenneth C. (1989). "Measuring Rate of Corrosion of Steel in Field Concrete Structures." Kenneth C. Clear, Inc. Concrete Materials and Corrosion Specialists, Sterling, Virginia (1989).

Clemena, Gerardo G. (2003). "Investigation of the Resistiance of Several New Metallic Reinforcing Bars to the Chloride-Induced Corrosion in Concrete." Virgnia Transportation Research Council, Report Number VTRC 04-R7.

Elsener, B. "Macrocell Corrosion of Steel in Concrete – Implications for Corrosion Monitoring." *Cement & Concrete Composites* 24 (2002): 65-72.

Feliu, S., J.A. Gonzalez, J.M. Miranda, V. Feliu. "Possibilities and Problems of in Situ Techniques for Measuring Steel Corrosion Rates in Large Reinforced Concrete Structures." *Corrosion Science* 47 (2005): 217-238.

Keddam, M., X.R. Novoa, L. Soler, C. Andrade, and H. Takenouti. "An Equivalent Electrical Circuit of Macrocell Activity in Facing Electrodes Embedded in Cement Mortar." *Corrosion Science* 36 (1994): 1155-1166.

Mehta, K.P. *Concrete: Microstructure, Properties, and Materials.* 3rd Edition, New York: The McGraw-Hill Companies, 2005.

Ramniceanu, Andrei (2004). "Correlation of Corrosion Measurements and Bridge Conditions with NBIS Deck Rating." Master of Science Thesis in Civil and Environmental Engineering, Virginia Polytechnic Institute and State University.

Raupach, M. "Chlrodie-Induced Macrocell Corrosion of Steel in Concrete – Theoretical Background and Practical Consequences." *Construction and Building Materials* 10 (1996): 329-338.

Revie, R. Winston. *Uhlig's Corrosion Handbook.* 2nd Edition, New York: Wiley-Interscience, 2000.

Schiessl, Peter. "Chloride-Induced Corrosion of Steel in Concrete: Development of a Concrete Corrosion Testing Cell." *Concrete Precasting Plant and Technology* 52 (1986): 626-635.

Shiessel, Peter. *Corrosion of Steel in Concrete.* London, New York: Chapman and Hall, 1998.

Weingroff, Richard F., "FHWA By Day: A Look at the History of the Federal Highway Administration." 1996. www.fhwa.dot.gov/byday/ghbd1215.htm. 2006.

Zemajtis, Jerzy, Modeling the Time to Corrosion Initiation for Concretes with Mineral Admixtures and/or Corrosion Inhibitors in Chloride-Laden Environments, Virginia Polytechnic Institute and State University, (1998).

APPENDICES

A – Mixture Parameters & Compressive Strengths

Table A-1
Mix Design for Batch 1

Basic Mix Design - 1 Cubic Yard (0.76 m^3)

Constituents	Weight	Volume (lb/ft^3)	Specifications		Acutal
Coarse Aggregate	1419.66 lb	52.58	w/c	0.5	0.49
Fine Aggregate	1539.40 lb	57.01	Entrained Air	6%	6.4%
Cement	600.00 lb	22.22	Slump	3-4 in.	3.5 in.
Water	300.00 lb	11.11		s.g.	Absorp.
HRWR	60.3 oz	0.14	C.A.	2.82	0.30%
Air Entrainer	25.4 oz	0.06	F.A.	2.61	0.80%
			Mix Temperature		72º F
Total	3864 pcy	113 pcf	Bar Ribbing		Thick

Batch Size - 2.5 Cubic Feet (0.07 m^3)

Constituents	Design Mix	Additional During Mix	Actual Mix
Coarse Aggregate	131.45 lb	0.00 lb	131.45 lb
Fine Aggregate	142.53 lb	0.00 lb	142.53 lb
Water	27.78 lb	(0.74) lb	27.04 lb
Cement	55.55 lb	0.00 lb	55.55 lb
HRWR	165 mL	0.00 mL	165 mL
AEA	27.78 mL	(5.28) mL	22.5 mL
Total	**357.72 lb**	**(0.75) lb**	**356.97 lb**

Table A-2
Mix Design for Batch 2

Basic Mix Design - 1 Cubic Yard (0.76 m^3)

Constituents	Weight	Volume (lb/ft^3)	Specifications		Acutal
Coarse Aggregate	1419.66 lb	52.58	w/c	0.5	0.5
Fine Aggregate	1539.40 lb	57.01	Entrained Air	6%	6.2%
Cement	600.00 lb	22.22	Slump	3-4 in.	7.75 in.
Water	300.00 lb	11.11		s.g.	Absorp.
HRWR	60.3 oz	0.14	C.A.	2.82	0.30%
Air Entrainer	25.4 oz	0.06	F.A.	2.61	0.80%
			Mix Temperature		73º F
Total	3864 pcy	113 pcf	Bar Ribbing		Thick

Batch Size - 2.5 Cubic Feet (0.07 m^3)

Constituents	Design Mix	Additional During Mix	Actual Mix
Coarse Aggregate	131.45 lb	0.00 lb	131.45 lb
Fine Aggregate	142.53 lb	0.00 lb	142.53 lb
Water	27.78 lb	0.00 lb	27.78 lb
Cement	55.55 lb	0.00 lb	55.55 lb
HRWR	165 mL	0.00 mL	165 mL
AEA	27.78 mL	(5.28) mL	22.5 mL
Total	**357.72 lb**	**(0.01) lb**	**357.71 lb**

Table A-3
Mix Design for Batch 3

Basic Mix Design - 1 Cubic Yard (0.76 m^3)

Constituents	Weight	Volume (lb/ft^3)	Specifications		Acutal
Coarse Aggregate	1419.66 lb	52.58	w/c	0.5	0.5
Fine Aggregate	1539.40 lb	57.01	Entrained Air	6%	6.4%
Cement	600.00 lb	22.22	Slump	3-4 in.	4.0 in.
Water	300.00 lb	11.11		s.g.	Absorp.
HRWR	60.3 oz	0.14	C.A.	2.82	0.30%
Air Entrainer	25.4 oz	0.06	F.A.	2.61	0.80%
			Mix Temperature		77º F
Total	3864 pcy	113 pcf	Bar Ribbing		Thin

Batch Size - 2.5 Cubic Feet (0.07 m^3)

Constituents	Design Mix	Additional During Mix	Actual Mix
Coarse Aggregate	131.45 lb	0.00 lb	131.45 lb
Fine Aggregate	142.53 lb	0.00 lb	142.53 lb
Water	27.78 lb	0.00 lb	27.78 lb
Cement	55.55 lb	0.00 lb	55.55 lb
HRWR	165 mL	(115) mL	50 mL
AEA	27.78 mL	(5.28) mL	22.5 mL
Total	**357.72 lb**	**(0.12) lb**	**357.6 lb**

Table A-4
Mix Design for Batch 4

Basic Mix Design - 1 Cubic Yard (0.76 m^3)

Constituents	Weight	Volume (lb/ft^3)	Specifications		Acutal
Coarse Aggregate	1419.66 lb	52.58	w/c	0.5	0.5
Fine Aggregate	1539.40 lb	57.01	Entrained Air	6%	6.4%
Cement	600.00 lb	22.22	Slump	3-4 in.	4.5 in.
Water	300.00 lb	11.11		s.g.	Absorp.
HRWR	60.3 oz	0.14	C.A.	2.82	0.30%
Air Entrainer	25.4 oz	0.06	F.A.	2.61	0.80%
			Mix Temperature		77º F
Total	3864 pcy	113 pcf	Bar Ribbing		Thick

Batch Size - 2.5 Cubic Feet (0.07 m^3)

Constituents	Design Mix	Additional During Mix	Actual Mix
Coarse Aggregate	131.45 lb	0.00 lb	131.45 lb
Fine Aggregate	142.53 lb	0.00 lb	142.53 lb
Water	27.78 lb	0.00 lb	27.78 lb
Cement	55.55 lb	0.00 lb	55.55 lb
HRWR	165 mL	(115) mL	50 mL
AEA	27.78 mL	(5.28) mL	22.5 mL
Total	**357.72 lb**	**(0.12) lb**	**357.6 lb**

Table A-5
Mix Design for Batch 5

Basic Mix Design - 1 Cubic Yard (0.76 m^3)

Constituents	Weight	Volume (lb/ft^3)	Specifications		Acutal
Coarse Aggregate	1419.66 lb	52.58	w/c	0.5	0.5
Fine Aggregate	1539.40 lb	57.01	Entrained Air	6%	6.6%
Cement	600.00 lb	22.22	Slump	3-4 in.	3.0 in.
Water	300.00 lb	11.11		s.g.	Absorp.
HRWR	60.3 oz	0.14	C.A.	2.82	0.30%
Air Entrainer	25.4 oz	0.06	F.A.	2.61	0.80%
			Mix Temperature		72º F
Total	3864 pcy	113 pcf	Bar Ribbing		Thin

Batch Size - 2.5 Cubic Feet (0.07 m^3)

Constituents	Design Mix	Additional During Mix	Actual Mix
Coarse Aggregate	131.45 lb	0.00 lb	131.45 lb
Fine Aggregate	142.53 lb	0.00 lb	142.53 lb
Water	27.78 lb	0.00 lb	27.78 lb
Cement	55.55 lb	0.00 lb	55.55 lb
HRWR	165 mL	(115) mL	50 mL
AEA	27.78 mL	(5.28) mL	22.5 mL
Total	**357.72 lb**	**(0.12) lb**	**357.6 lb**

Table A-6
Mix Design for Batch 6

Basic Mix Design - 1 Cubic Yard (0.76 m^3)

Constituents	Weight	Volume (lb/ft^3)	Specifications		Acutal
Coarse Aggregate	1419.66 lb	52.58	w/c	0.5	0.5
Fine Aggregate	1539.40 lb	57.01	Entrained Air	6%	5.5%
Cement	600.00 lb	22.22	Slump	3-4 in.	7.0 in.
Water	300.00 lb	11.11		s.g.	Absorp.
HRWR	60.3 oz	0.14	C.A.	2.82	0.30%
Air Entrainer	25.4 oz	0.06	F.A.	2.61	0.80%
			Mix Temperature		72º F
Total	3864 pcy	113 pcf	Bar Ribbing		Thin

Batch Size – 2.65 Cubic Feet (0.08 m^3)

Constituents	Design Mix	Additional During Mix	Actual Mix
Coarse Aggregate	139.34 lb	0.00 lb	131.45 lb
Fine Aggregate	151.08 lb	0.00 lb	142.53 lb
Water	29.44 lb	0.00 lb	27.78 lb
Cement	58.88 lb	0.00 lb	55.55 lb
HRWR	174.9 mL	(122.5) mL	52.4 mL
AEA	29.44 mL	(5.59) mL	23.85 mL
Total	**379.17 lb**	**(0.27) lb**	**378.9 lb**

Table A-7
Mix Design for Batch 7

Basic Mix Design - 1 Cubic Yard (0.76 m^3)

Constituents	Weight	Volume (lb/ft^3)	Specifications		Acutal
Coarse Aggregate	1419.66 lb	52.58	w/c	0.5	0.5
Fine Aggregate	1539.40 lb	57.01	Entrained Air	6%	6.4%
Cement	600.00 lb	22.22	Slump	3-4 in.	4.5 in.
Water	300.00 lb	11.11		s.g.	Absorp.
HRWR	60.3 oz	0.14	C.A.	2.82	0.30%
Air Entrainer	25.4 oz	0.06	F.A.	2.61	0.80%
Total	3864 pcy	113 pcf	Mix Temperature Bar Ribbing		76º F Thick

Batch Size - 2.5 Cubic Feet (0.07 m^3)

Constituents	Design Mix	Additional During Mix	Actual Mix
Coarse Aggregate	131.45 lb	0.00 lb	131.45 lb
Fine Aggregate	142.53 lb	0.00 lb	142.53 lb
Water	27.78 lb	0.00 lb	27.78 lb
Cement	55.55 lb	0.00 lb	55.55 lb
HRWR	165 mL	(105) mL	60 mL
AEA	27.78 mL	(5.28) mL	22.5 mL
Total	**357.72 lb**	**(0.23) lb**	**357.49 lb**

Table A-8
Mix Design for Batch 8

Basic Mix Design - 1 Cubic Yard (0.76 m^3)

Constituents	Weight	Volume (lb/ft^3)	Specifications		Acutal
Coarse Aggregate	1419.66 lb	52.58	w/c	0.5	0.5
Fine Aggregate	1539.40 lb	57.01	Entrained Air	6%	6.9%
Cement	600.00 lb	22.22	Slump	3-4 in.	4.5 in.
Water	300.00 lb	11.11		s.g.	Absorp.
HRWR	60.3 oz	0.14	C.A.	2.82	0.30%
Air Entrainer	25.4 oz	0.06	F.A.	2.61	0.80%
			Mix Temperature		73º F
Total	3864 pcy	113 pcf	Bar Ribbing		Thick

Batch Size – 2.65 Cubic Feet (0.08 m^3)

Constituents	Design Mix	Additional During Mix	Actual Mix
Coarse Aggregate	139.34 lb	0.00 lb	131.45 lb
Fine Aggregate	151.08 lb	0.00 lb	142.53 lb
Water	29.44 lb	0.00 lb	27.78 lb
Cement	58.88 lb	0.00 lb	55.55 lb
HRWR	174.9 mL	(109.9) mL	65 mL
AEA	29.44 mL	(5.59) mL	23.85 mL
Total	**379.17 lb**	**(0.24) lb**	**378.93 lb**

Table A-9
Mix Design for Batch 9

Basic Mix Design - 1 Cubic Yard (0.76 m^3)

Constituents	Weight	Volume (lb/ft^3)	Specifications		Acutal
Coarse Aggregate	1419.66 lb	52.58	w/c	0.5	0.5
Fine Aggregate	1539.40 lb	57.01	Entrained Air	6%	6.4%
Cement	600.00 lb	22.22	Slump	3-4 in.	5.5 in.
Water	300.00 lb	11.11		s.g.	Absorp.
HRWR	60.3 oz	0.14	C.A.	2.82	0.30%
Air Entrainer	25.4 oz	0.06	F.A.	2.61	0.80%
			Mix Temperature		70º F
Total	3864 pcy	113 pcf	Bar Ribbing		Thin

Batch Size – 2.65 Cubic Feet (0.08 m^3)

Constituents	Design Mix	Additional During Mix	Actual Mix
Coarse Aggregate	139.34 lb	0.00 lb	131.45 lb
Fine Aggregate	151.08 lb	0.00 lb	142.53 lb
Water	29.44 lb	0.00 lb	27.78 lb
Cement	58.88 lb	0.00 lb	55.55 lb
HRWR	174.9 mL	(114.9) mL	60 mL
AEA	29.44 mL	(5.59) mL	23.85 mL
Total	**379.17 lb**	**(0.25) lb**	**378.92 lb**

Table A-10

Cylinder Compressive Strengths

Batch	Compressive Strength MPa (psi)	
	7-day	28-day
1	27.4 (3980)	35.1 (5090)
2	24.1 (3500)	29.9 (4340)
3	27.4 (3980)	34.0 (4930)
4	26.9 (3900)	34.4 (4990)
5	27.4 (3980)	31.6 (4580)
6	25.8 (3740)	31.4 (4560)
7	27.4 (3980)	34.8 (5050)
8	29.1 (4220)	34.3 (4970)
9	27.4 (3980)	34.7 (5030)
Average Compressive Strength	27.0 (3920)	33.4 (4840)

B – Resistivity Measurements

Figure B-1

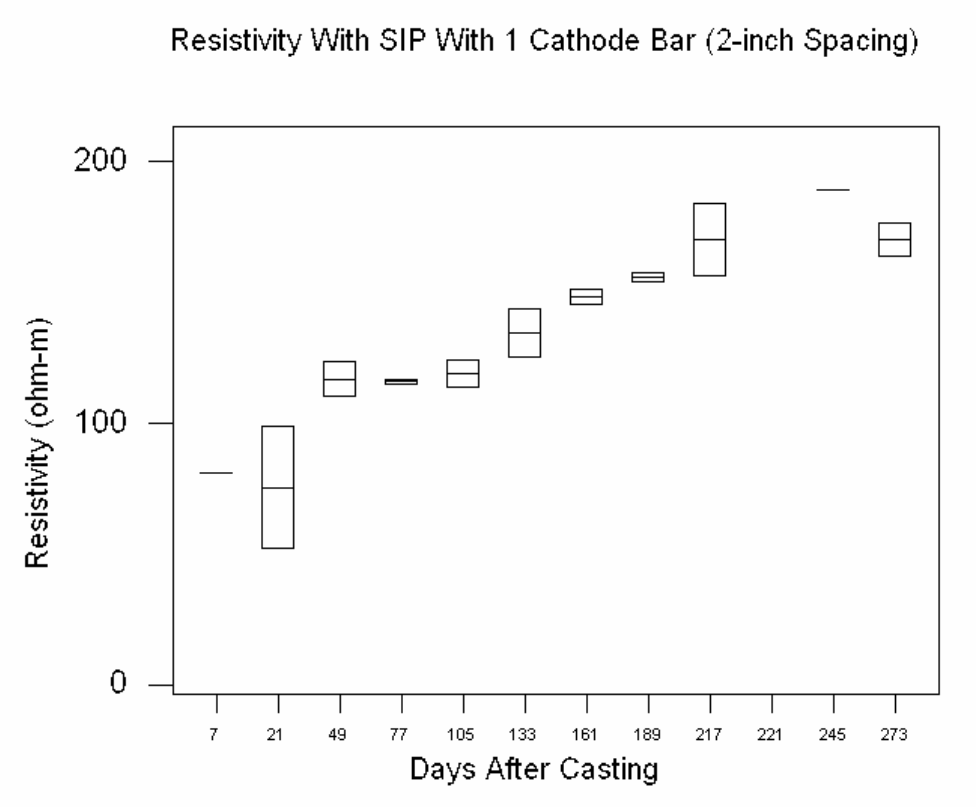

Figure B-2

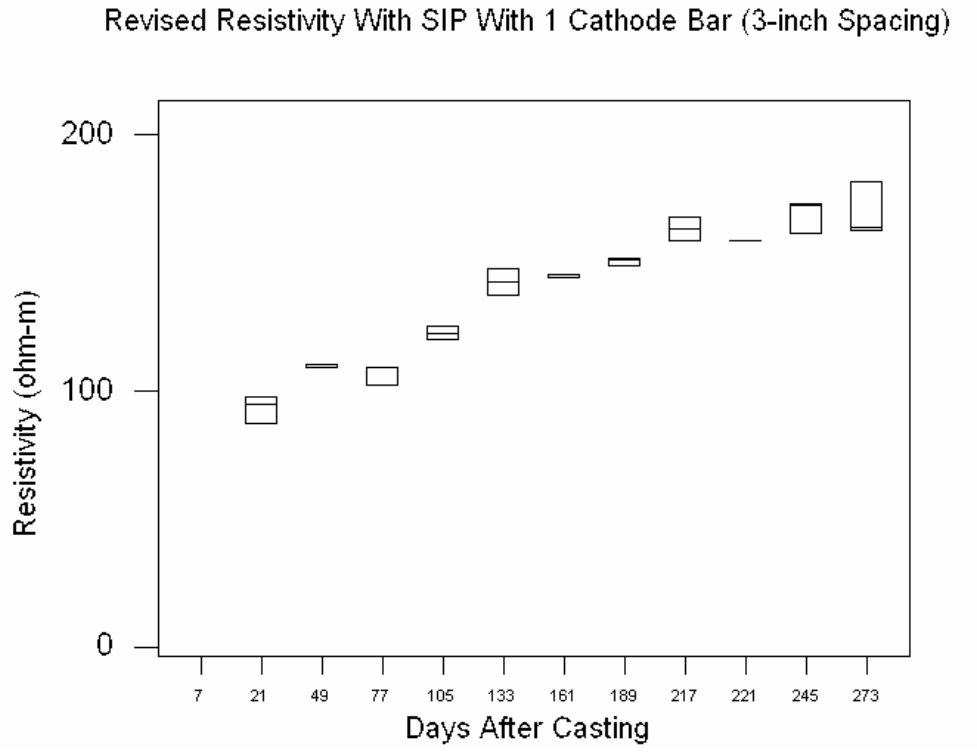

Figure B-3

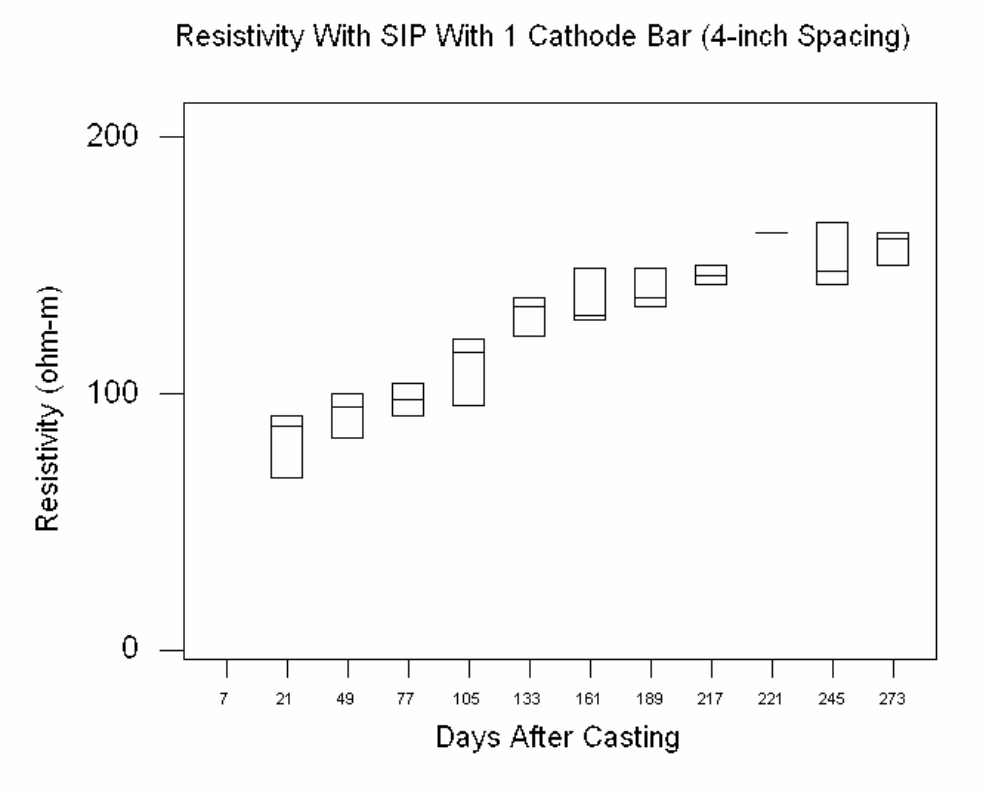

Figure B-4

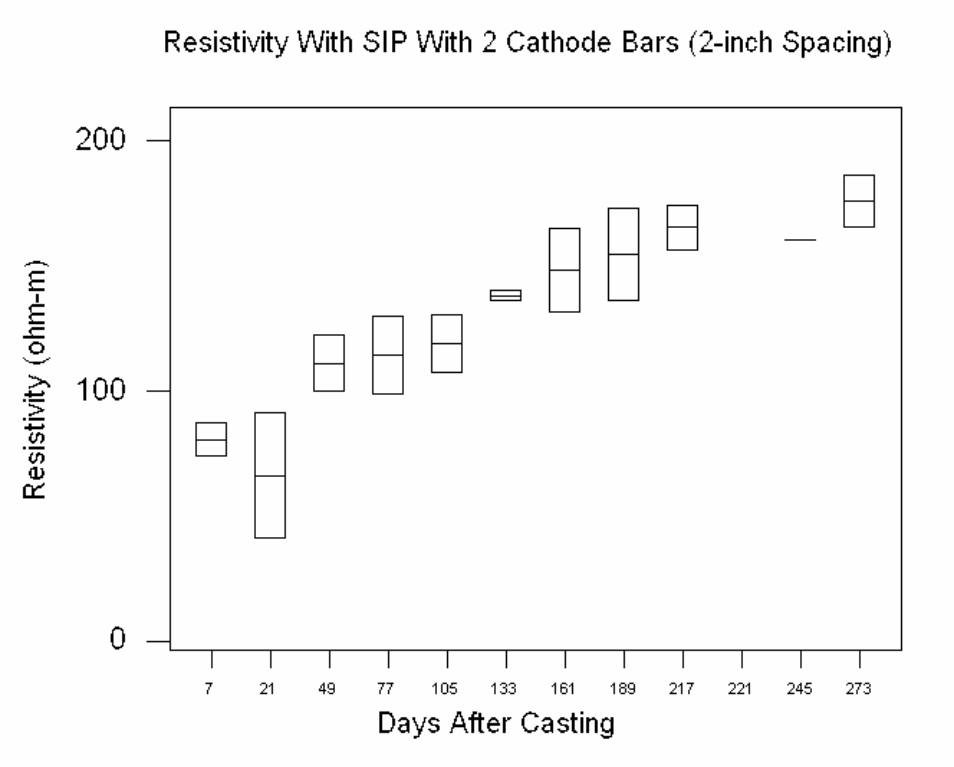

Figure B-5

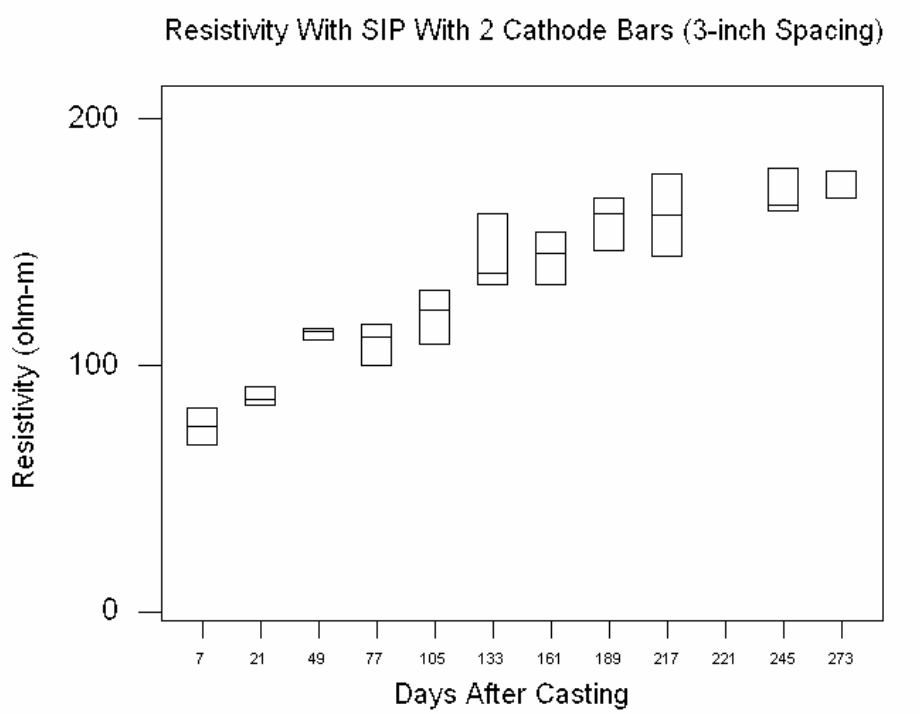

Figure B-6

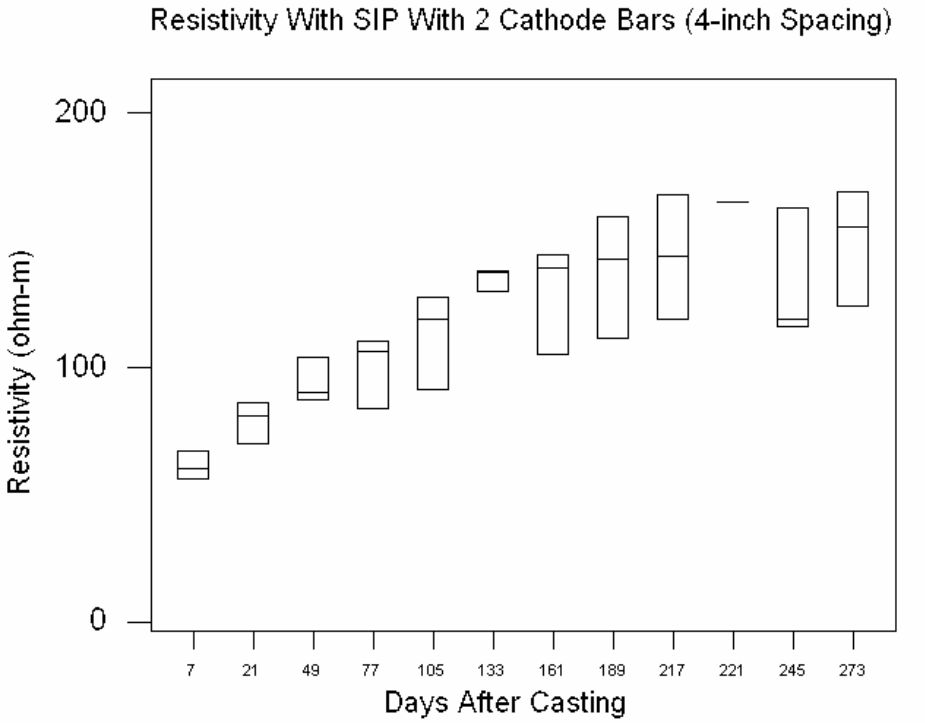

Figure B-7

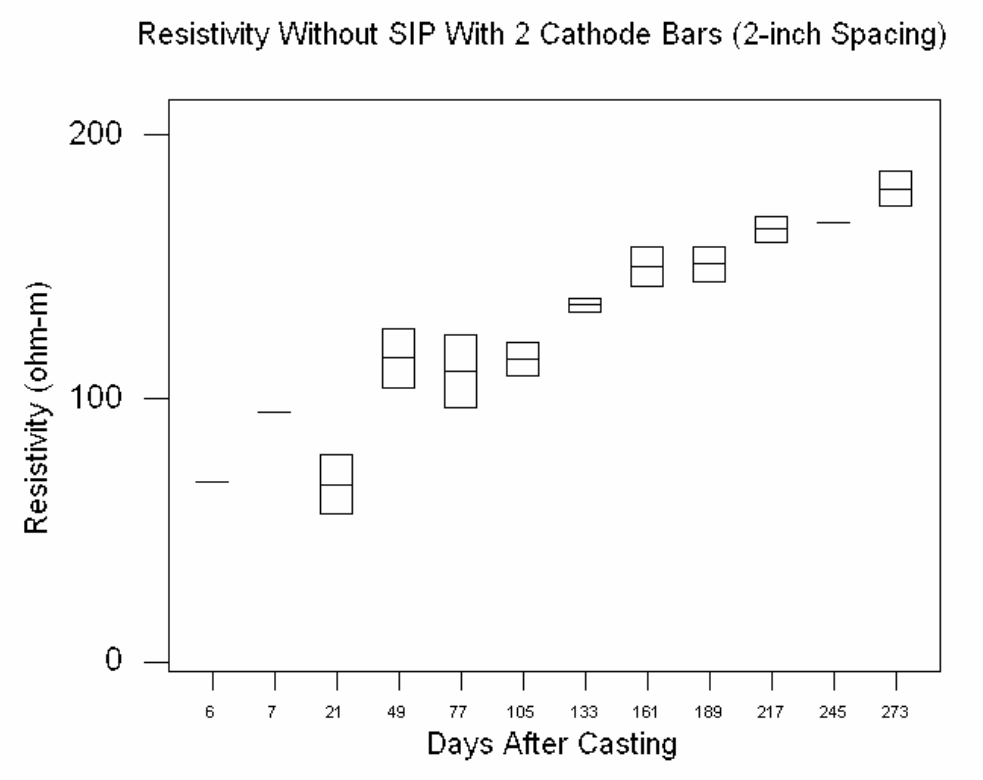

Figure B-8

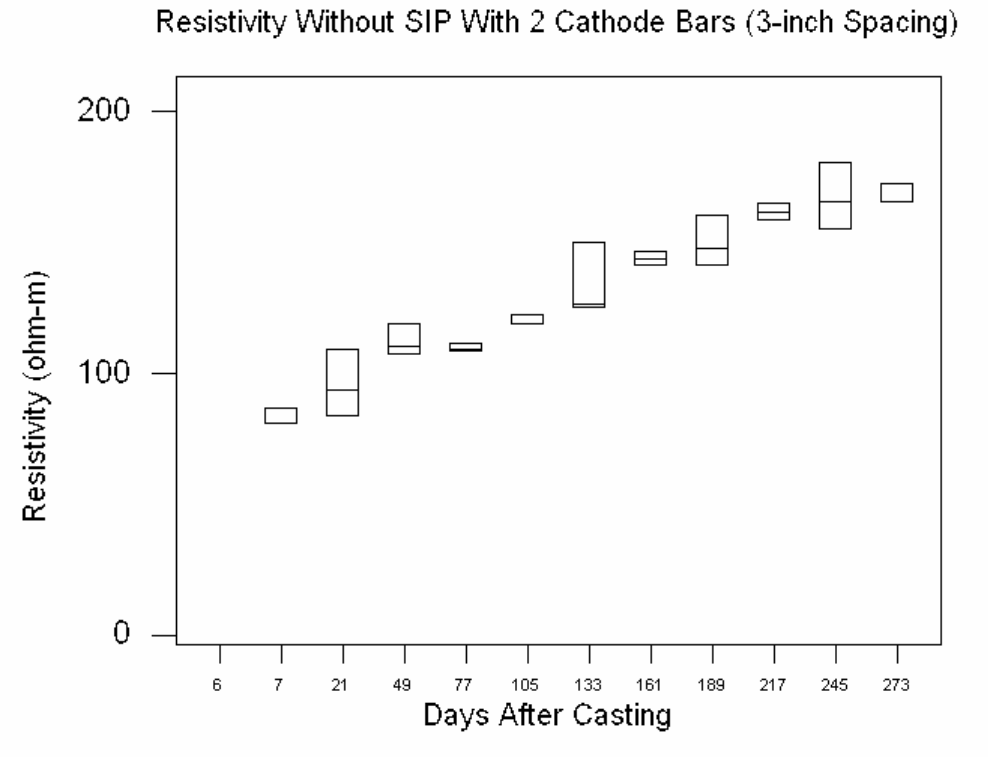

Figure B-9

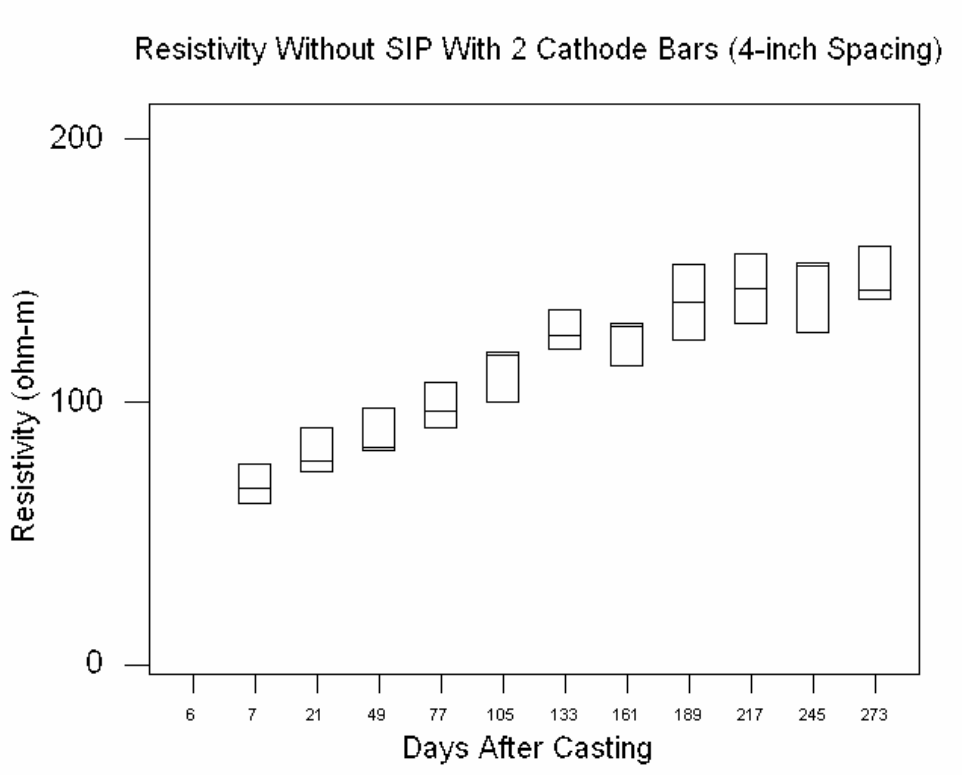
Resistivity Without SIP With 2 Cathode Bars (4-inch Spacing)
Resistivity (ohm-m)
200
100
0
6
7
21
49
77
105
133
161
189
217
245
273
Days After Casting

C – Half-Cell Potential Measurements

Figure C-1

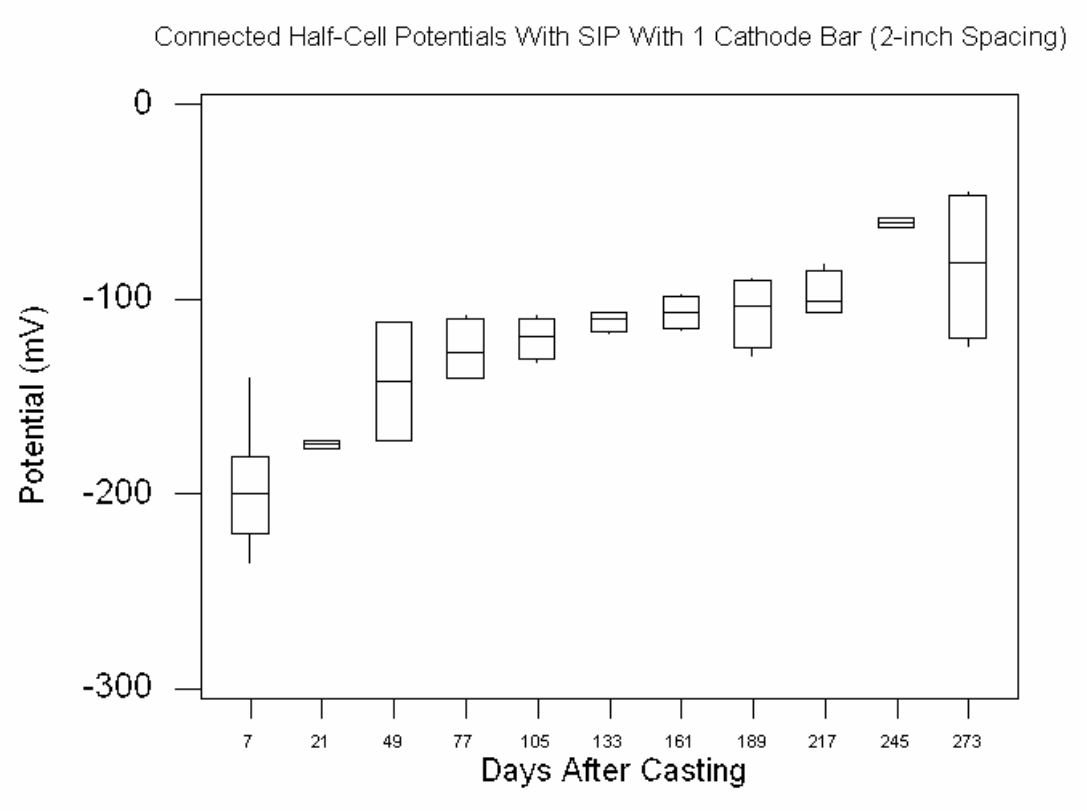

Figure C-2

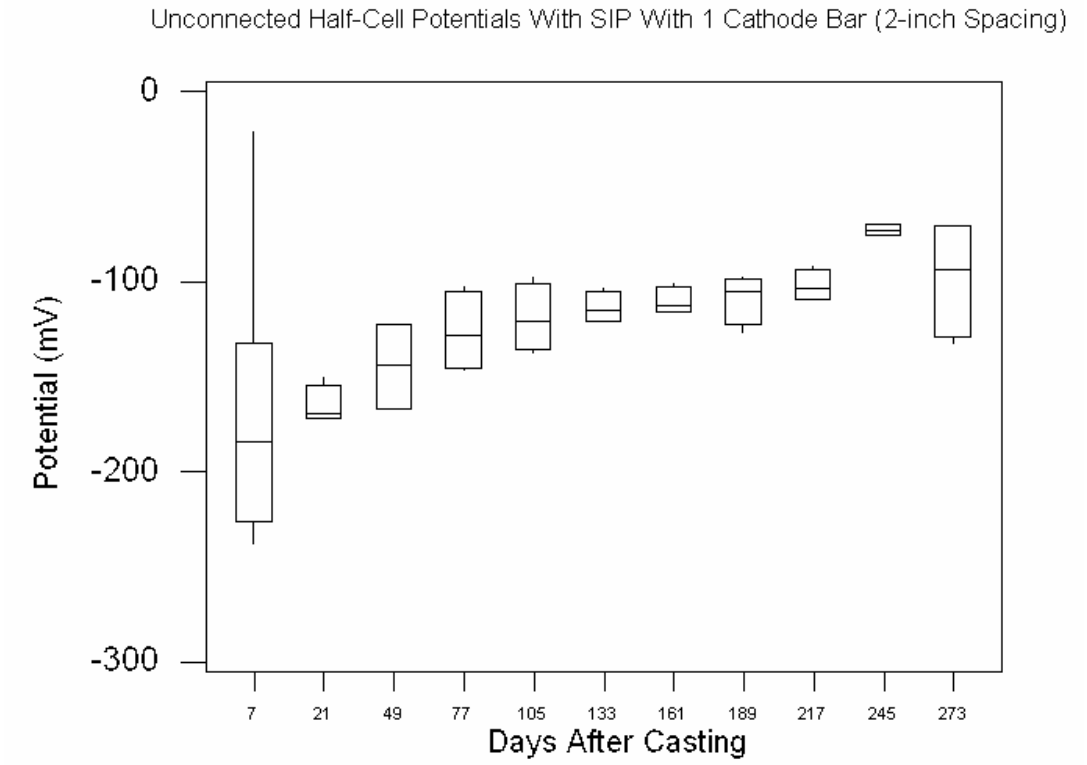

Figure C-3

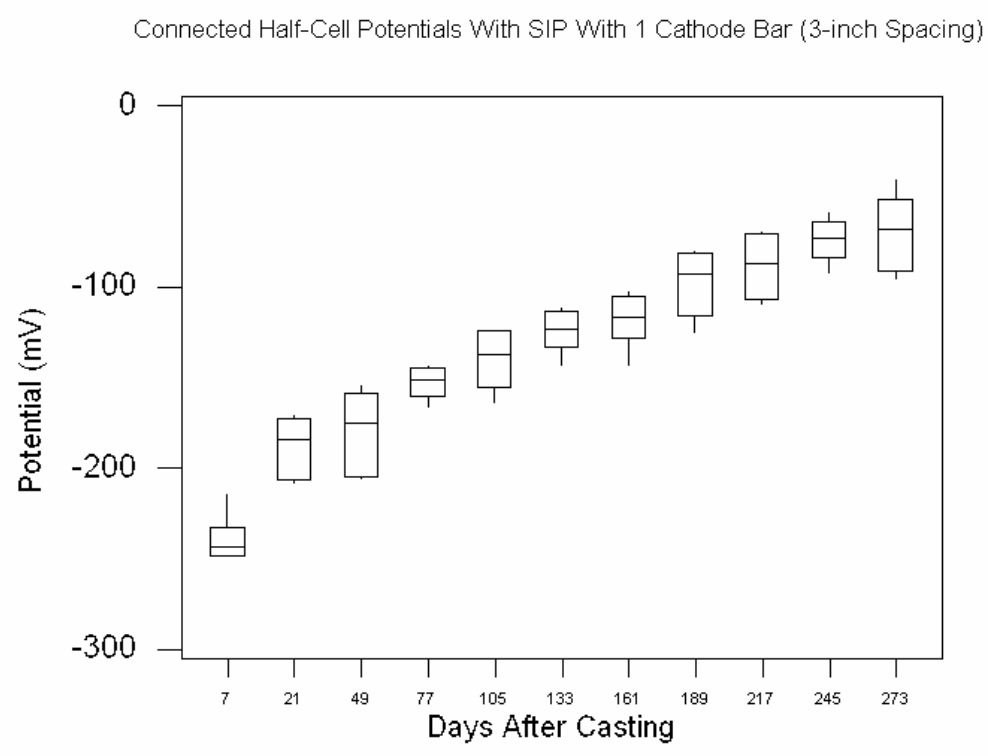

Figure C-4

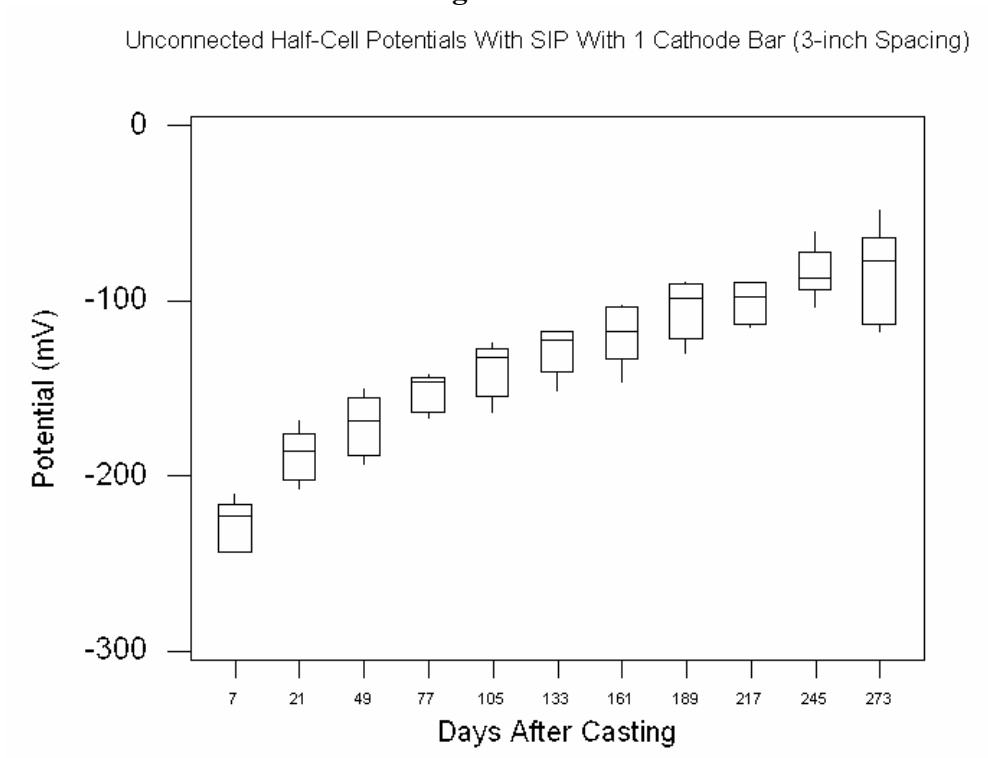

Figure C-5

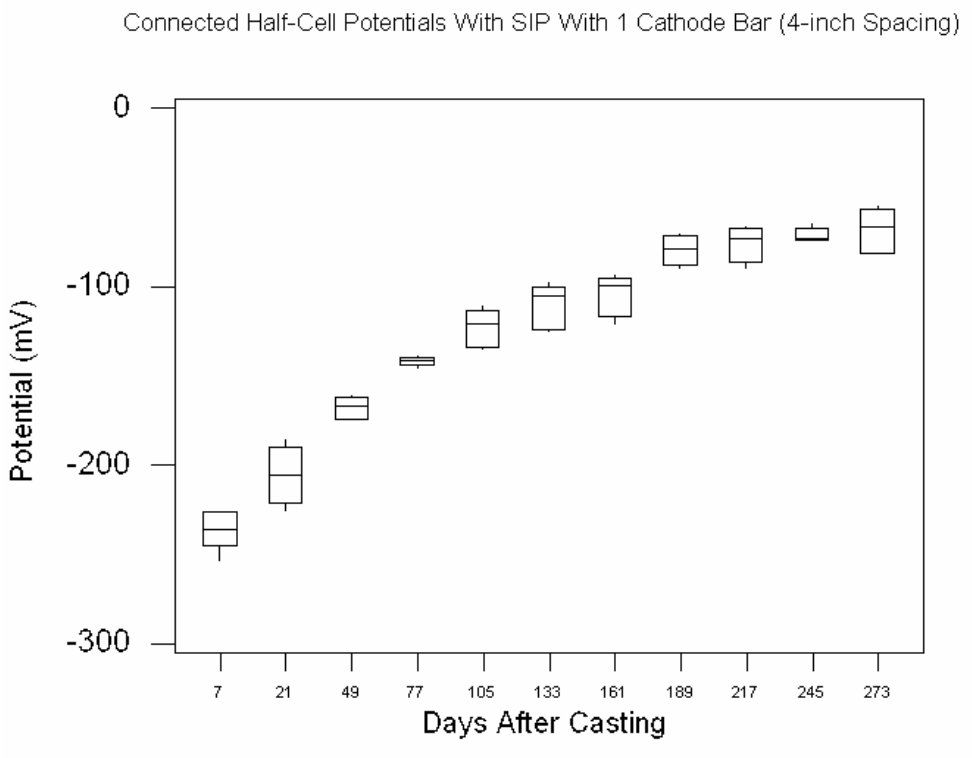

Figure C-6

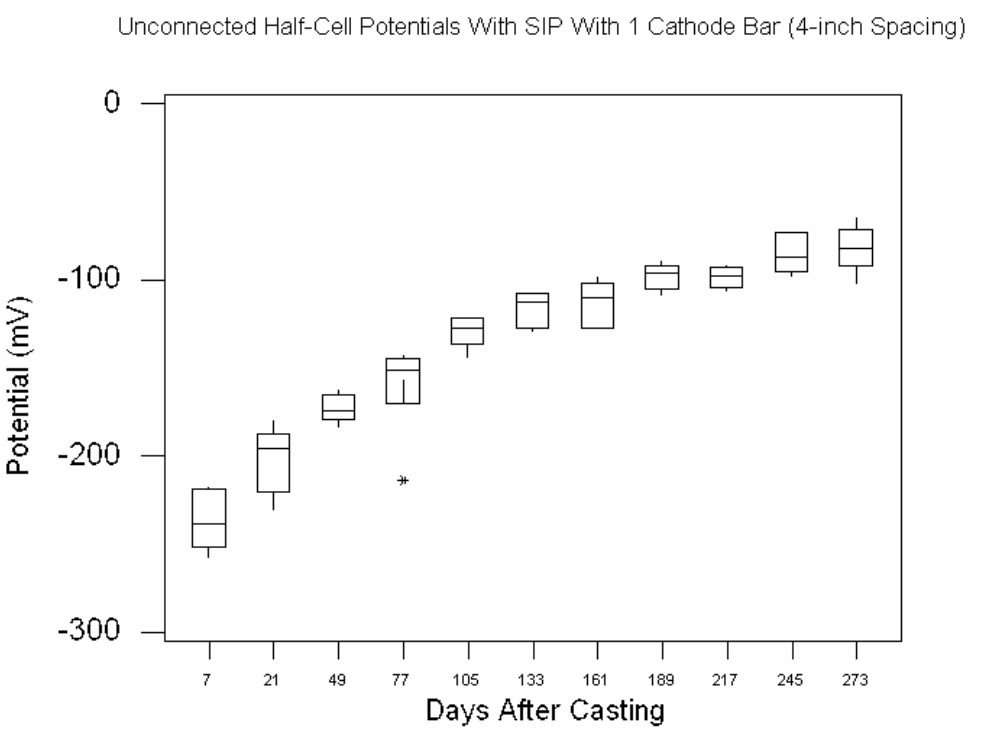

Figure C-7

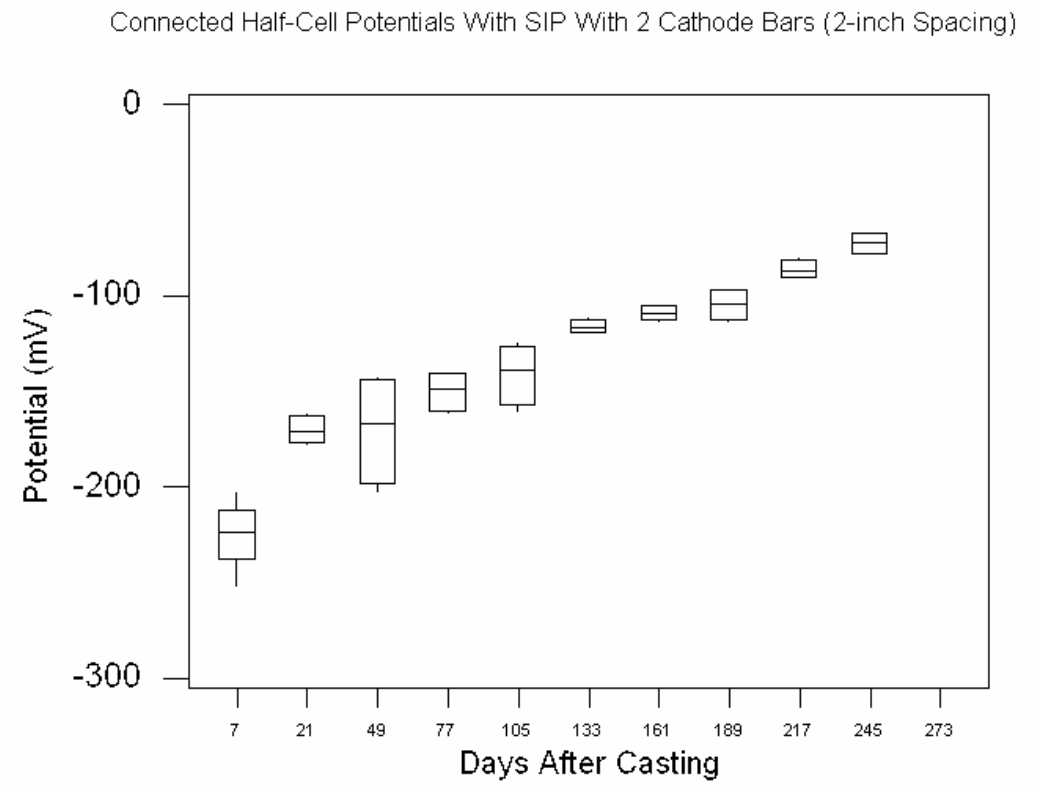

Figure C-8

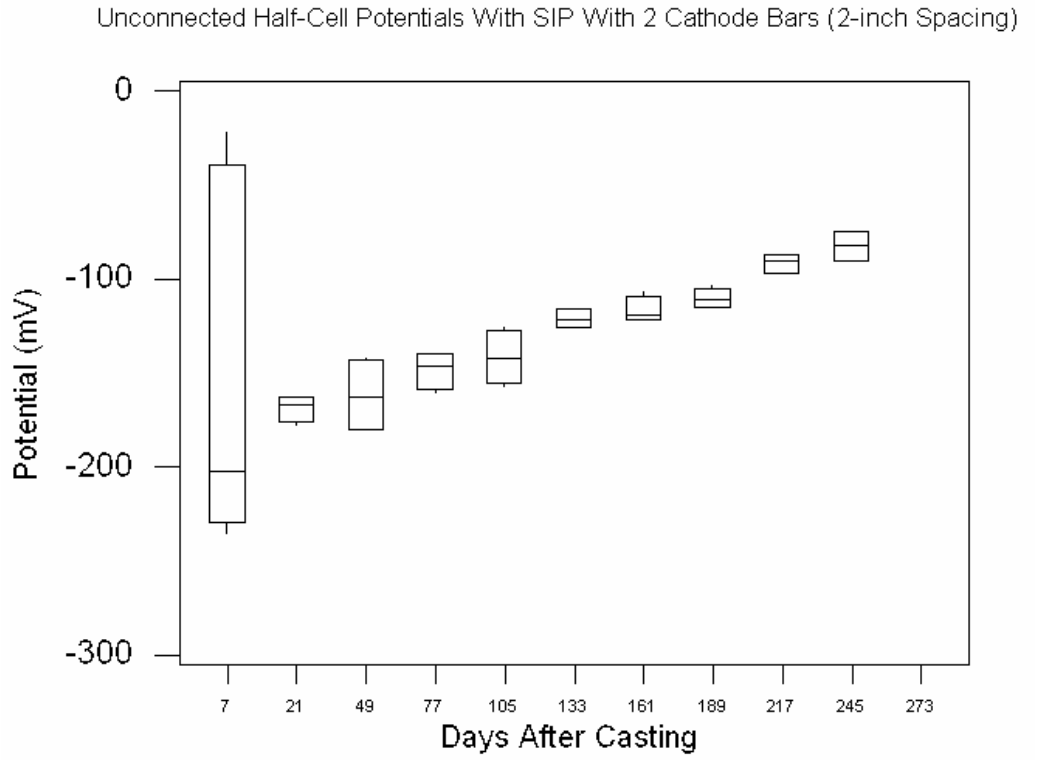

Figure C-9

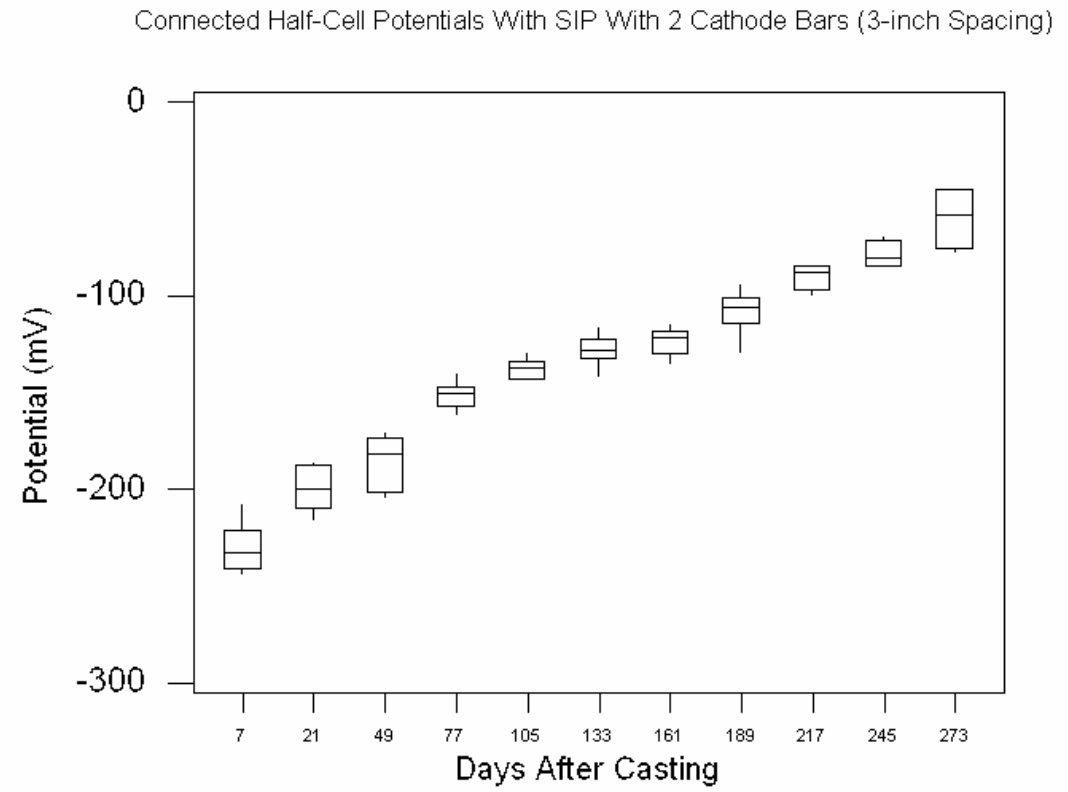

Figure C-10

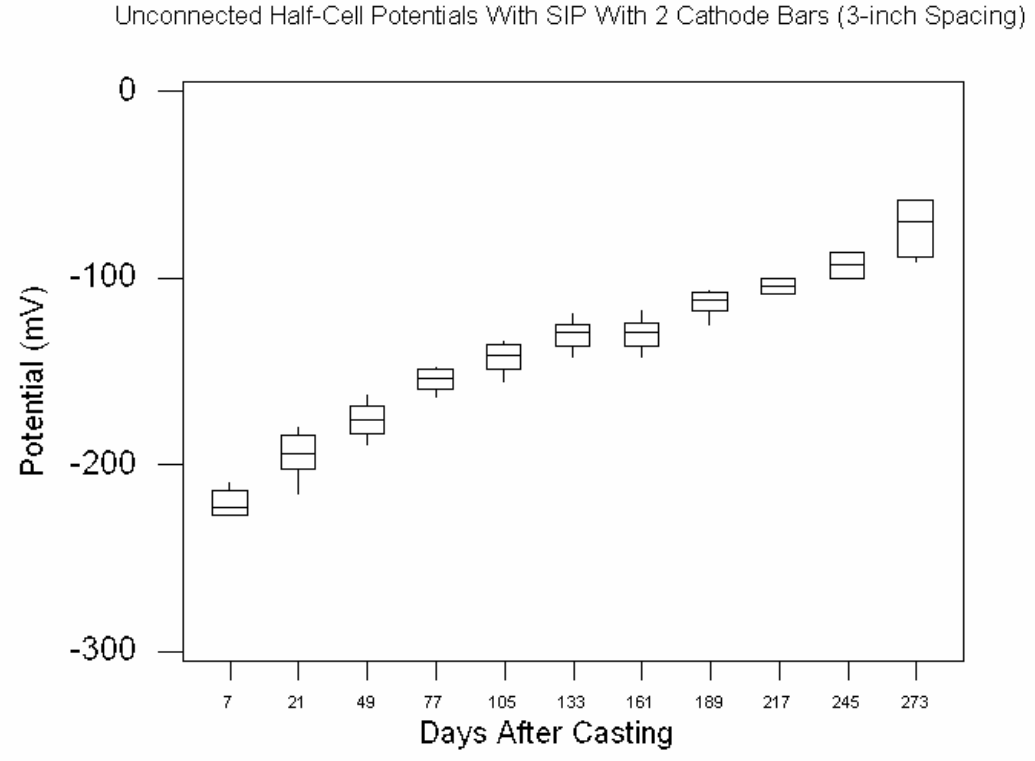

Figure C-11

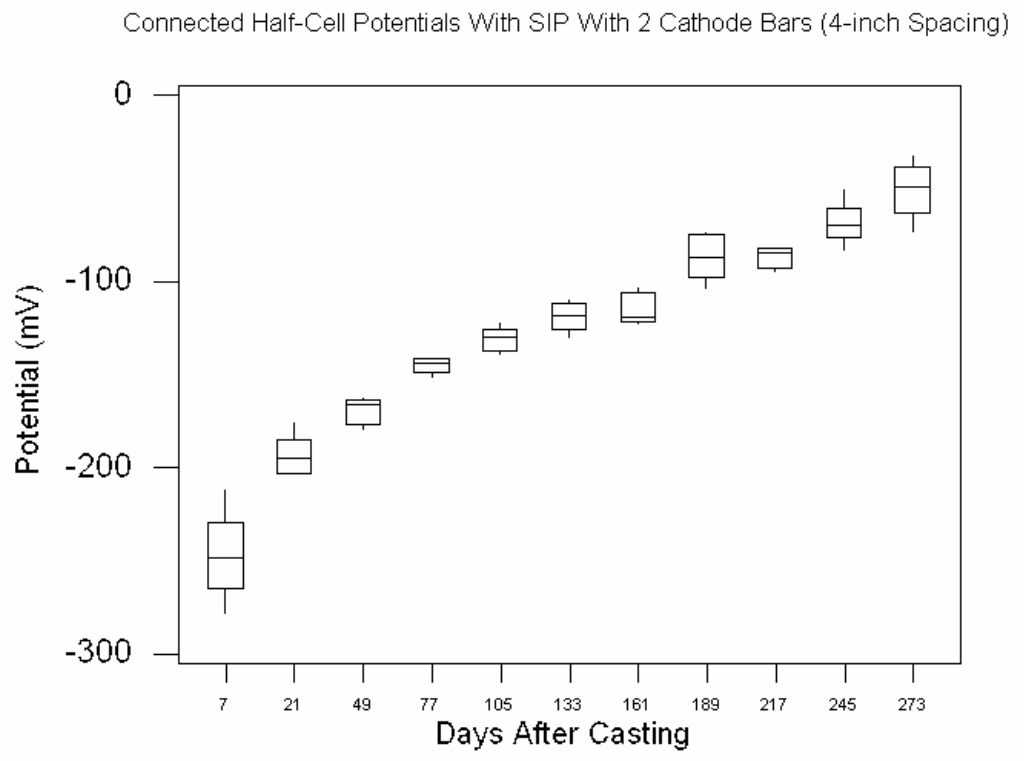

Figure C-12

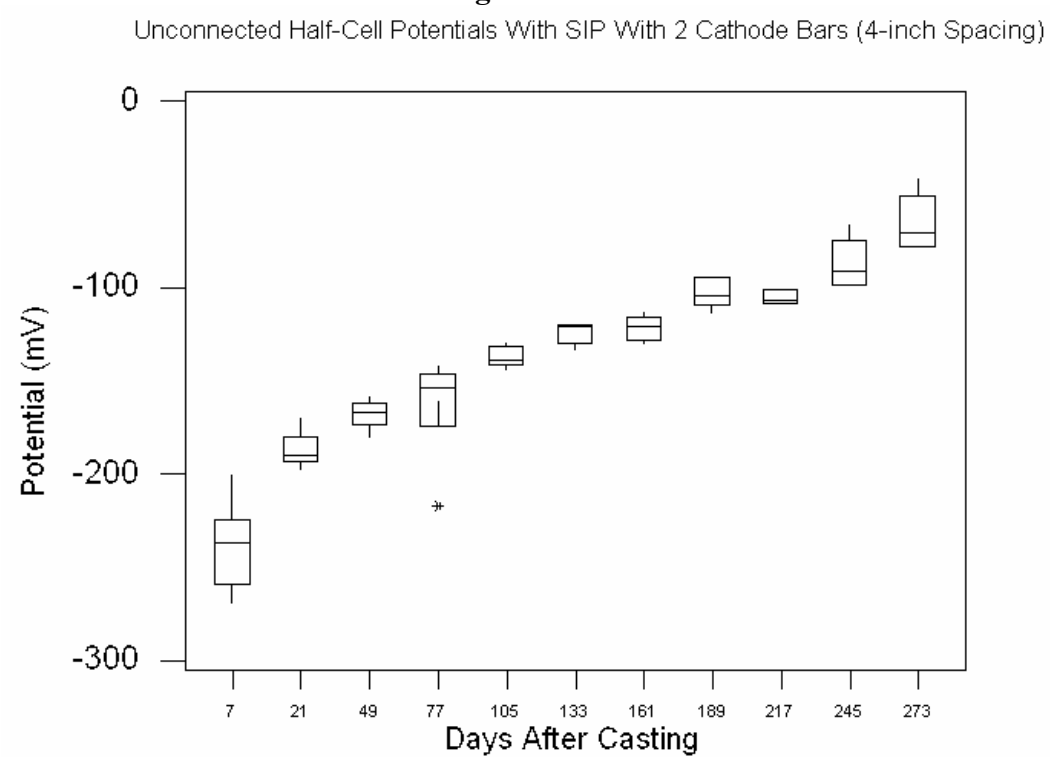

Figure C-13

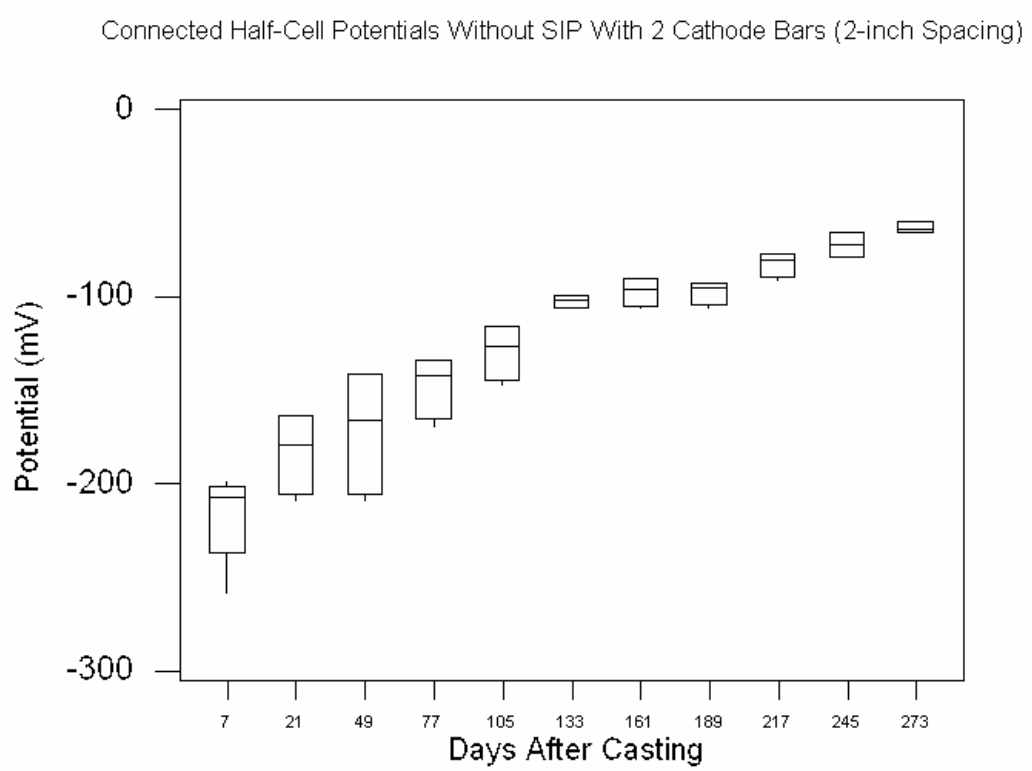

Figure C-14

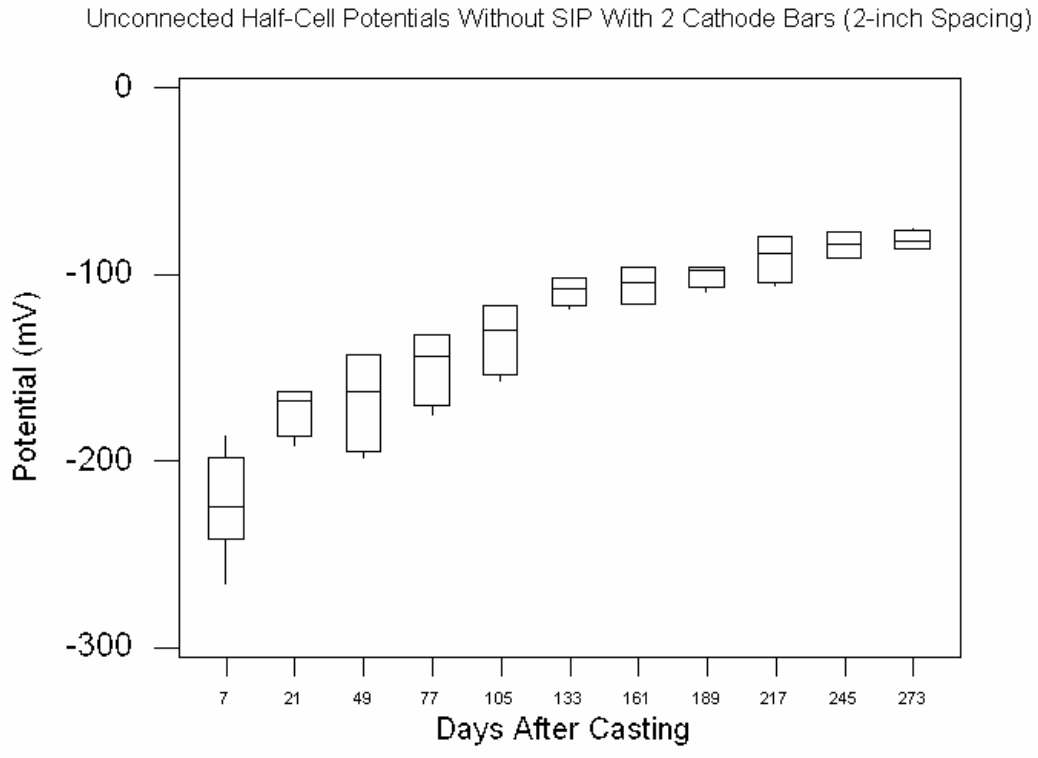

Figure C-15

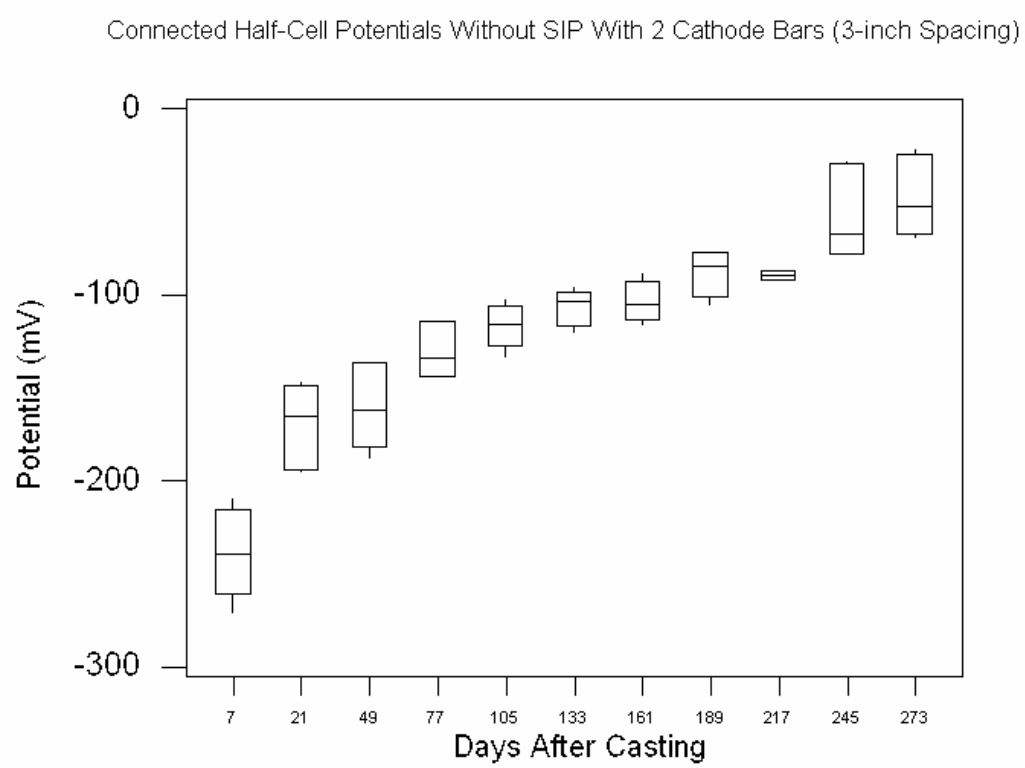

Figure C-16

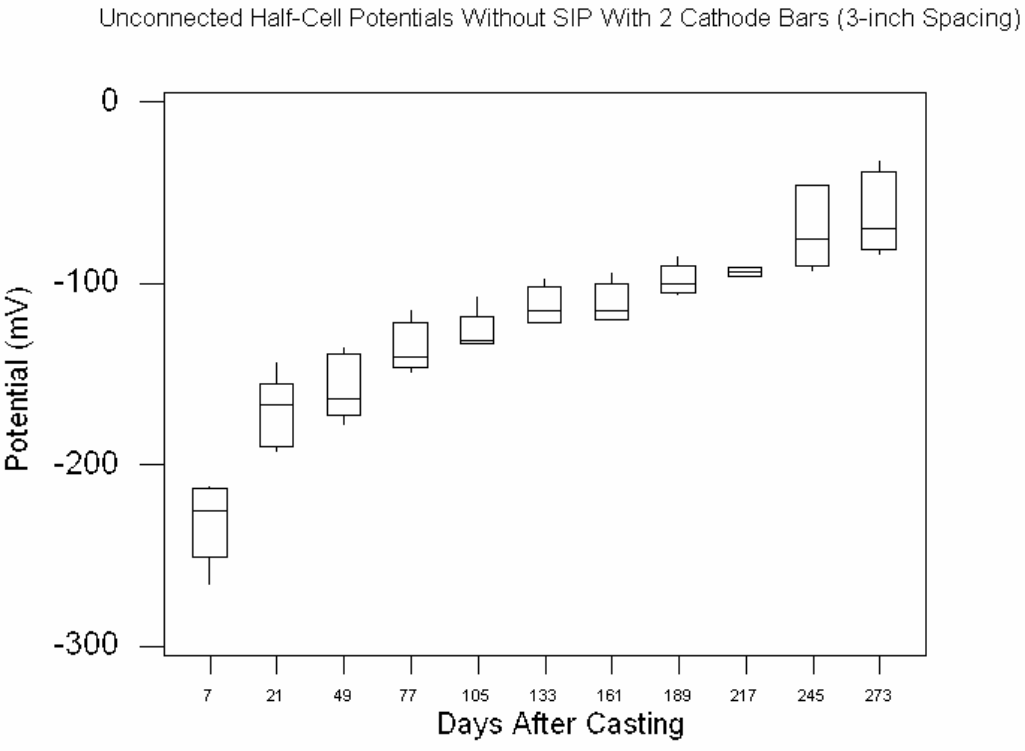

Figure C-17

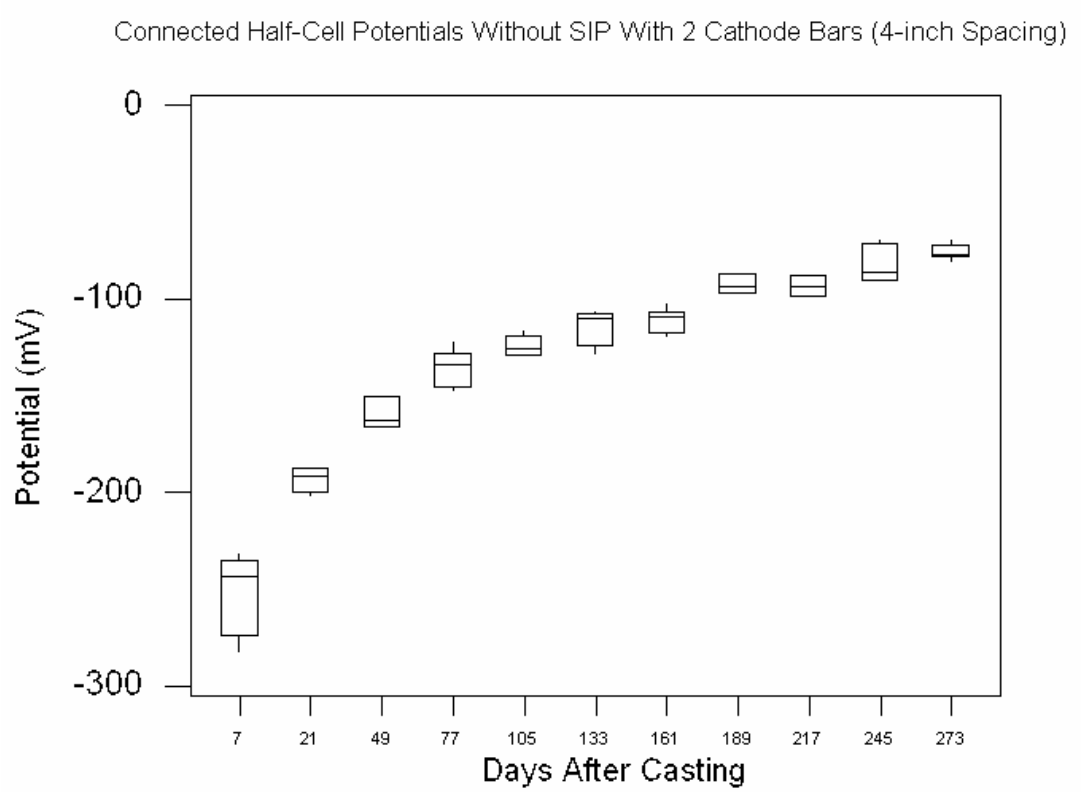

Figure C-18

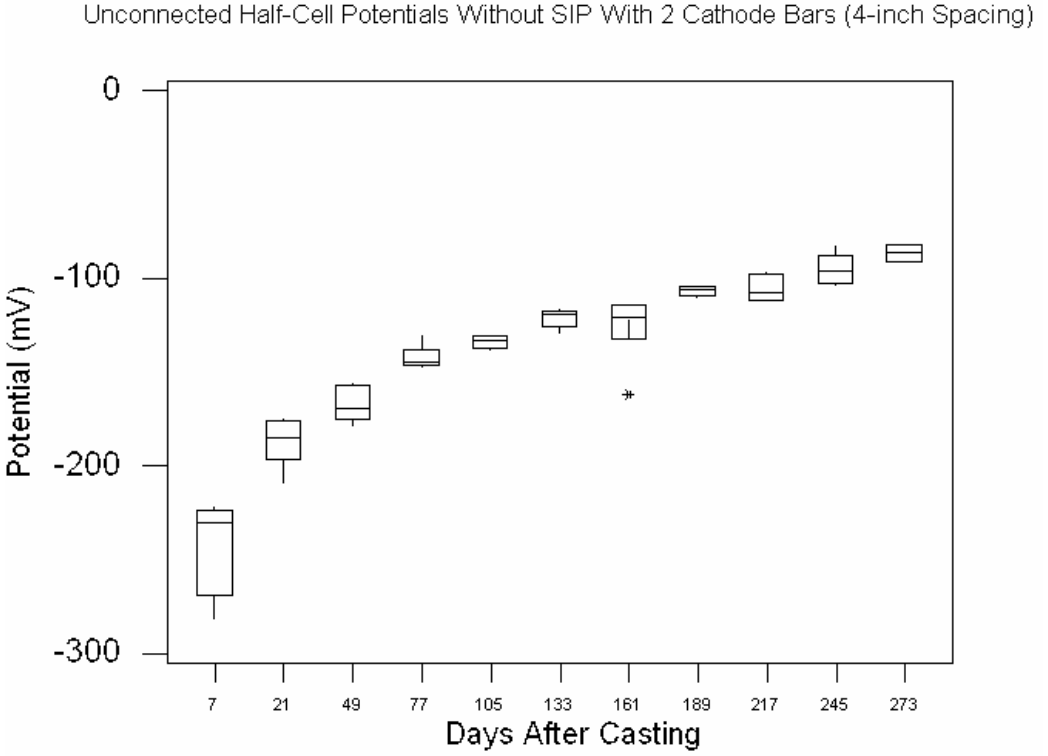

D – Corrosion Current Density Measurements

Figure D-1

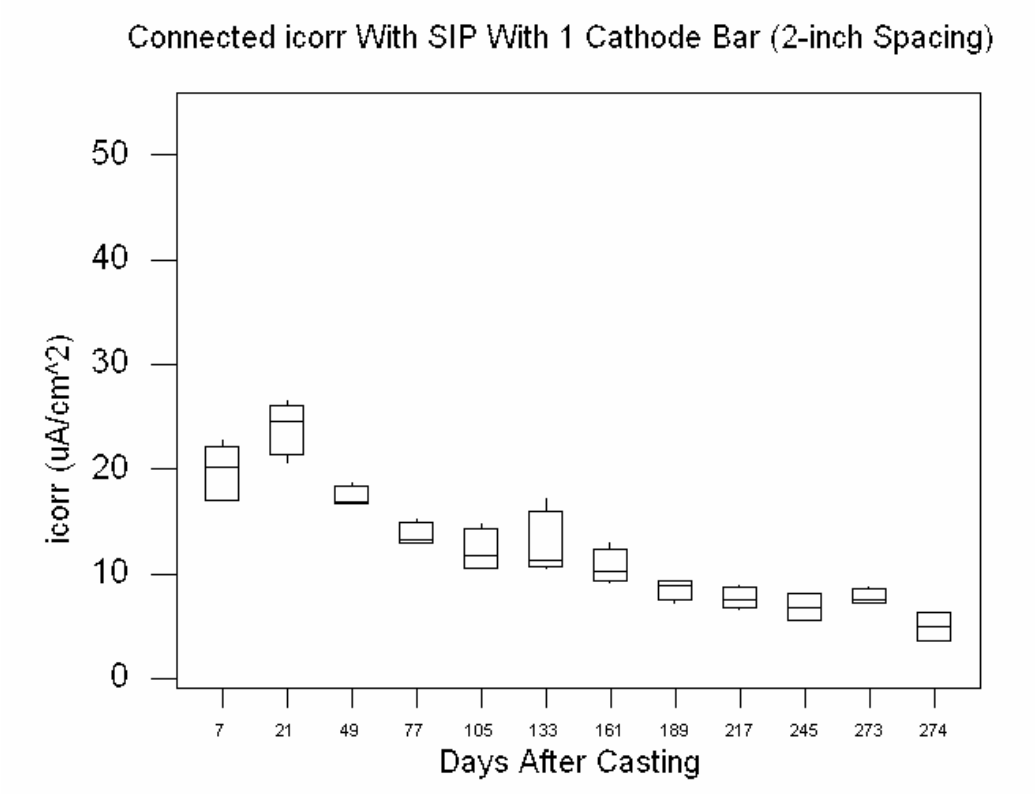

Figure D-2

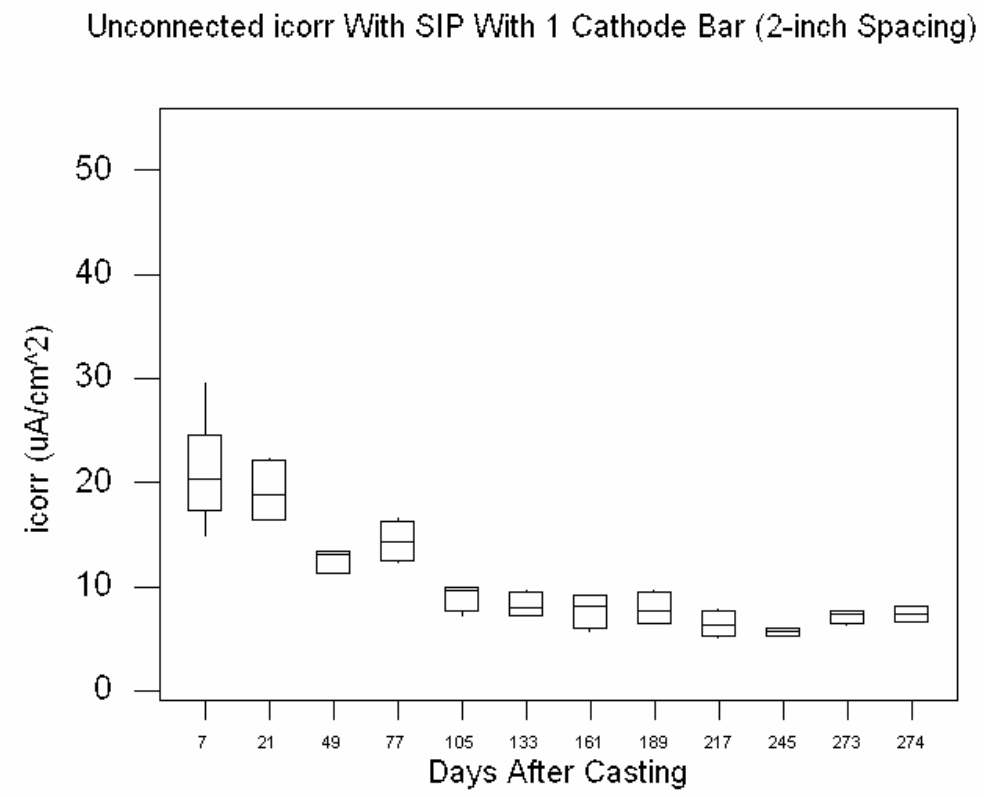

Figure D-3

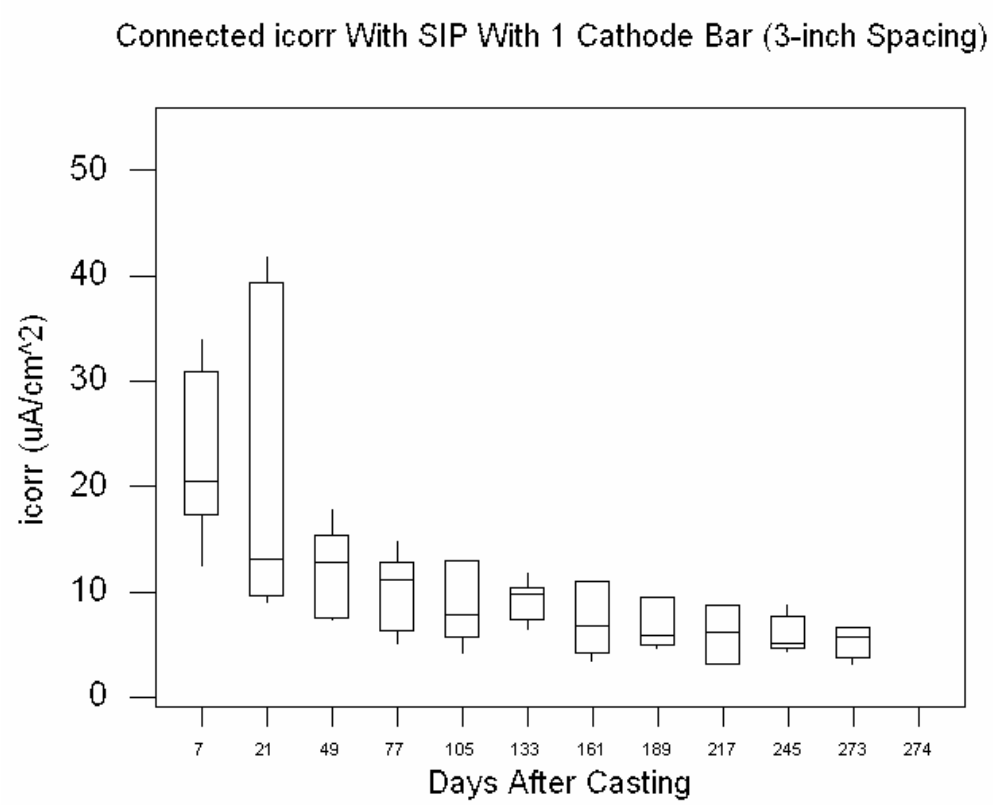

Figure D-4

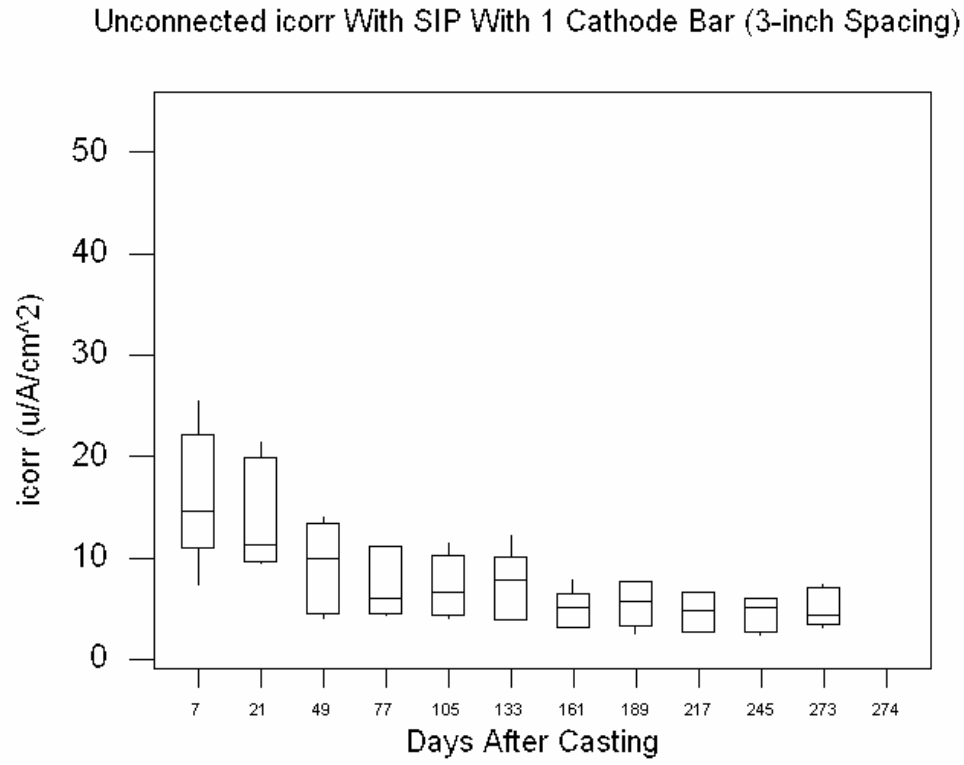

Figure D-5

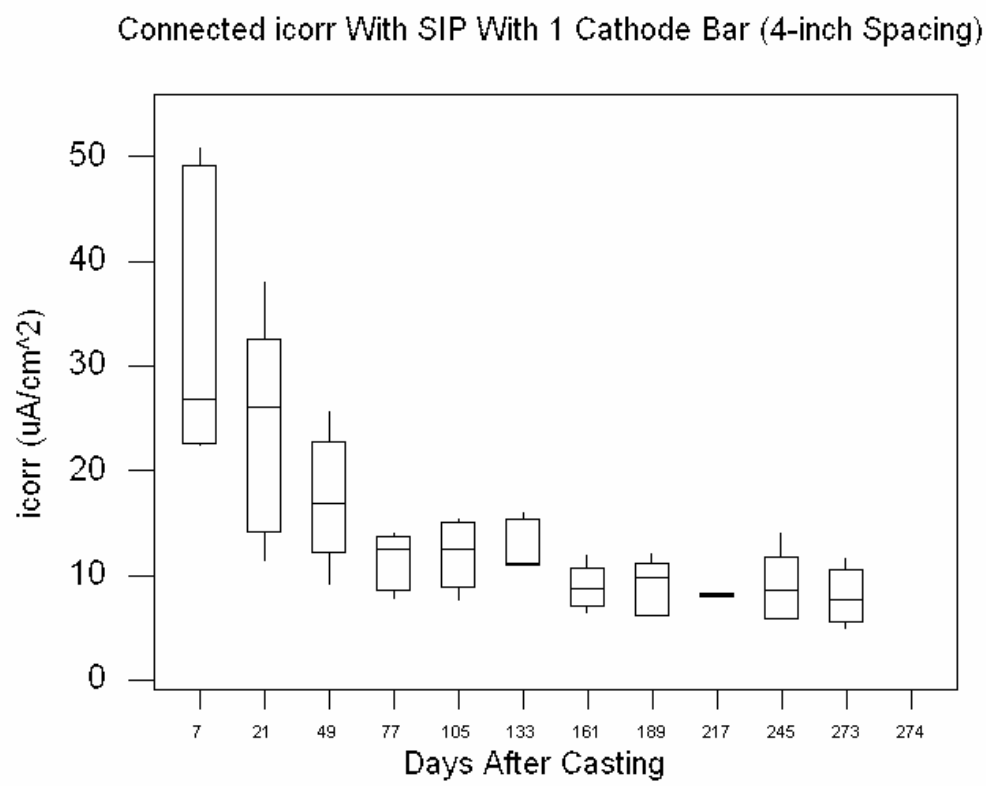

Figure D-6

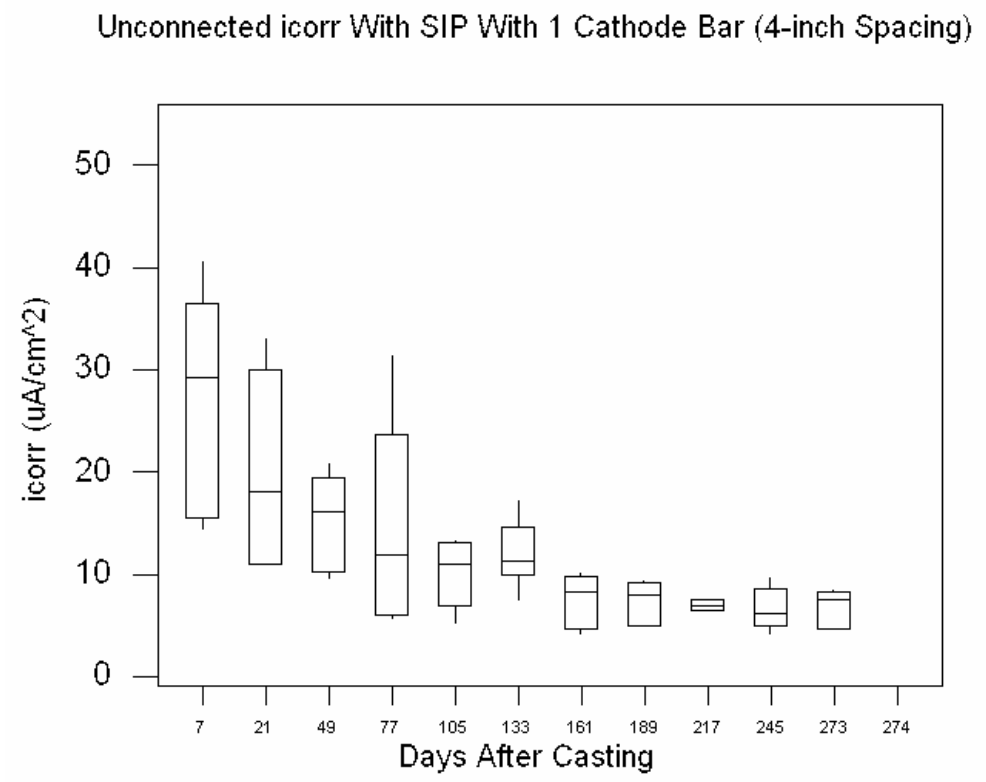

Figure D-7

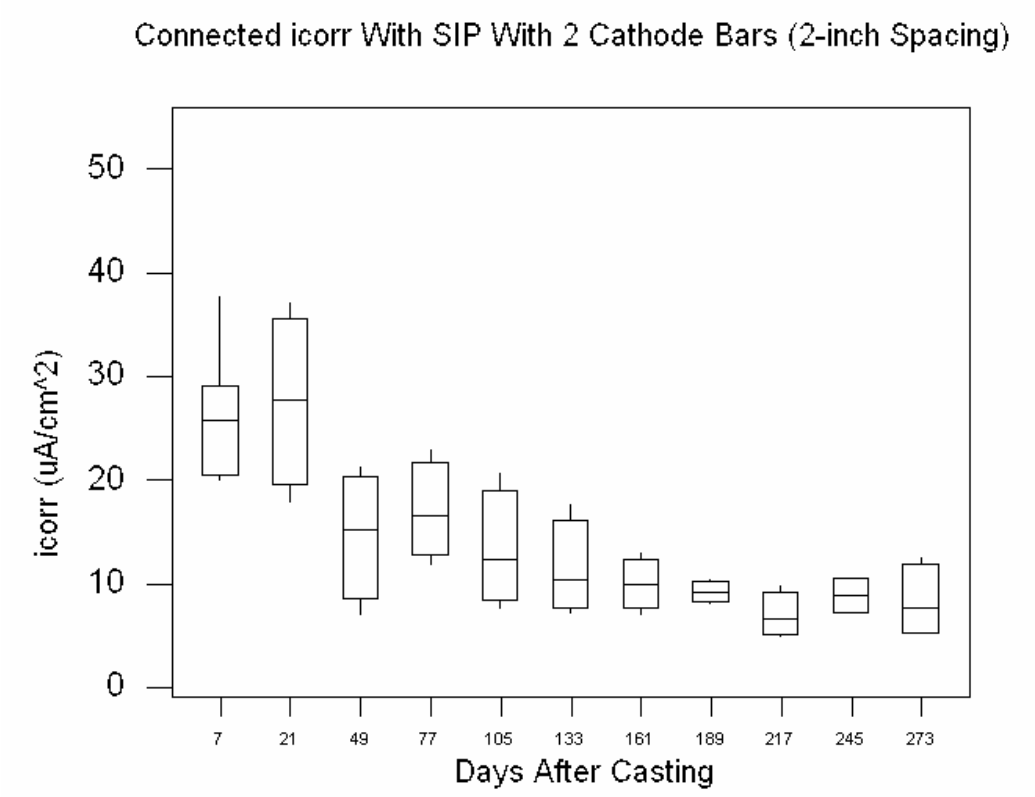

Figure D-8

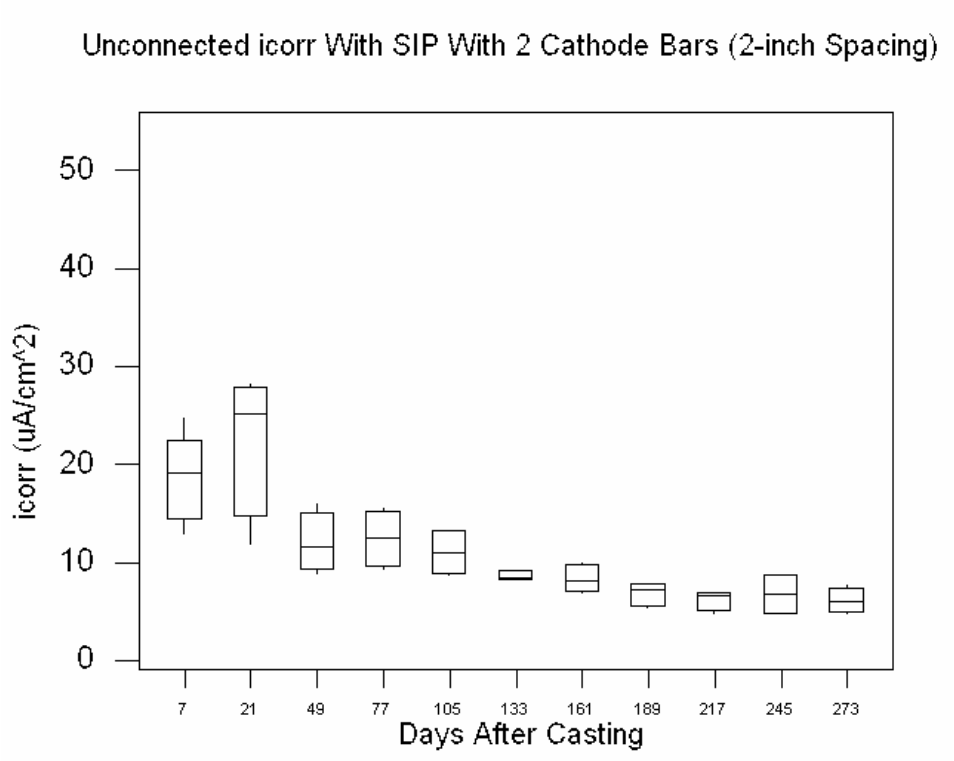

Figure D-9

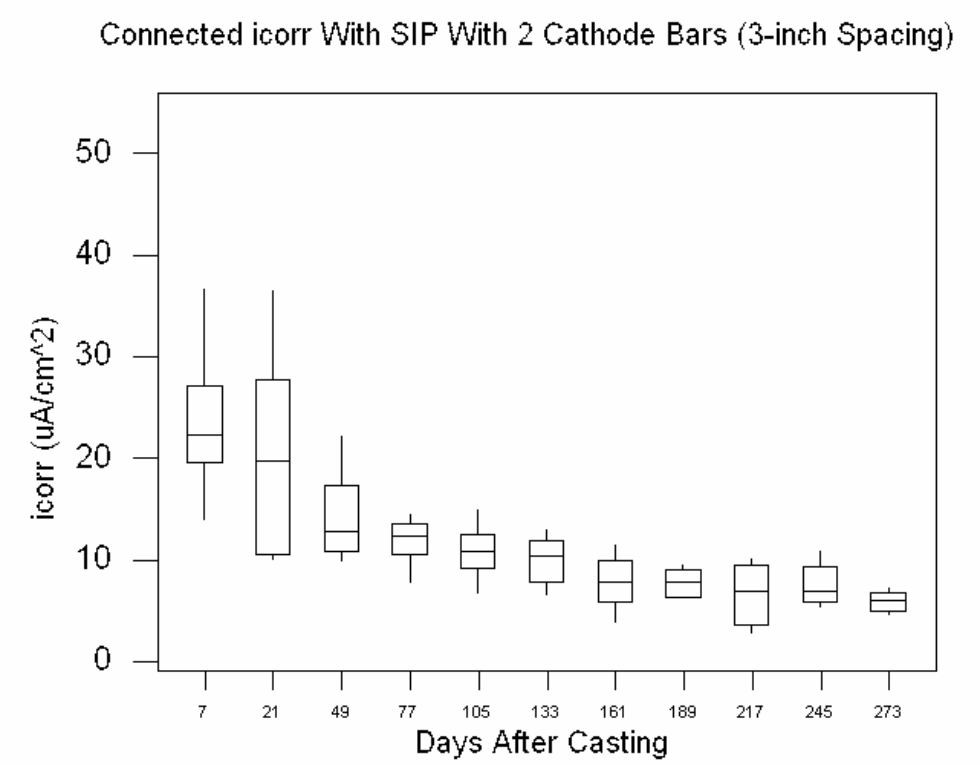

Figure D-10

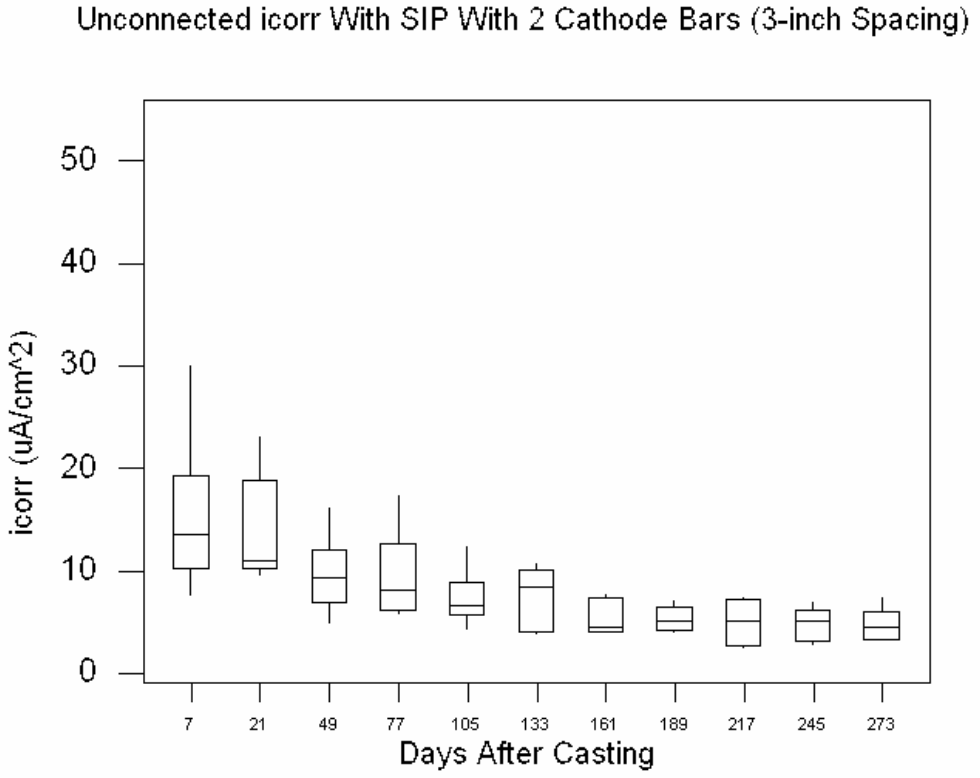

Figure D-11

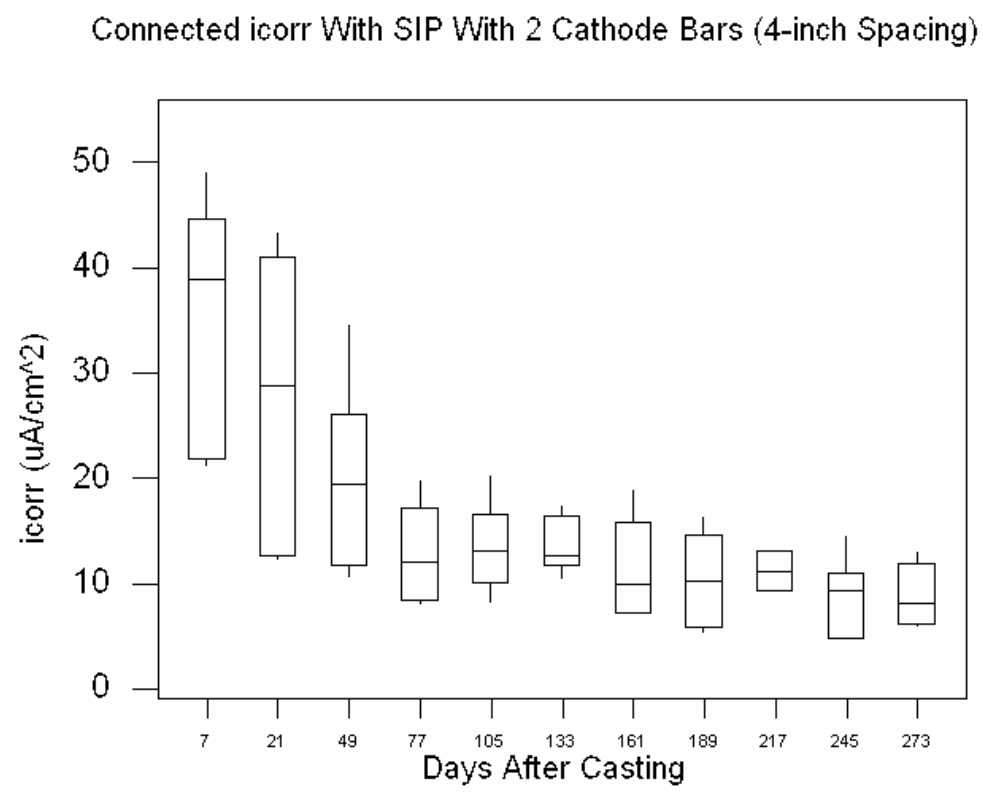

Figure D-12

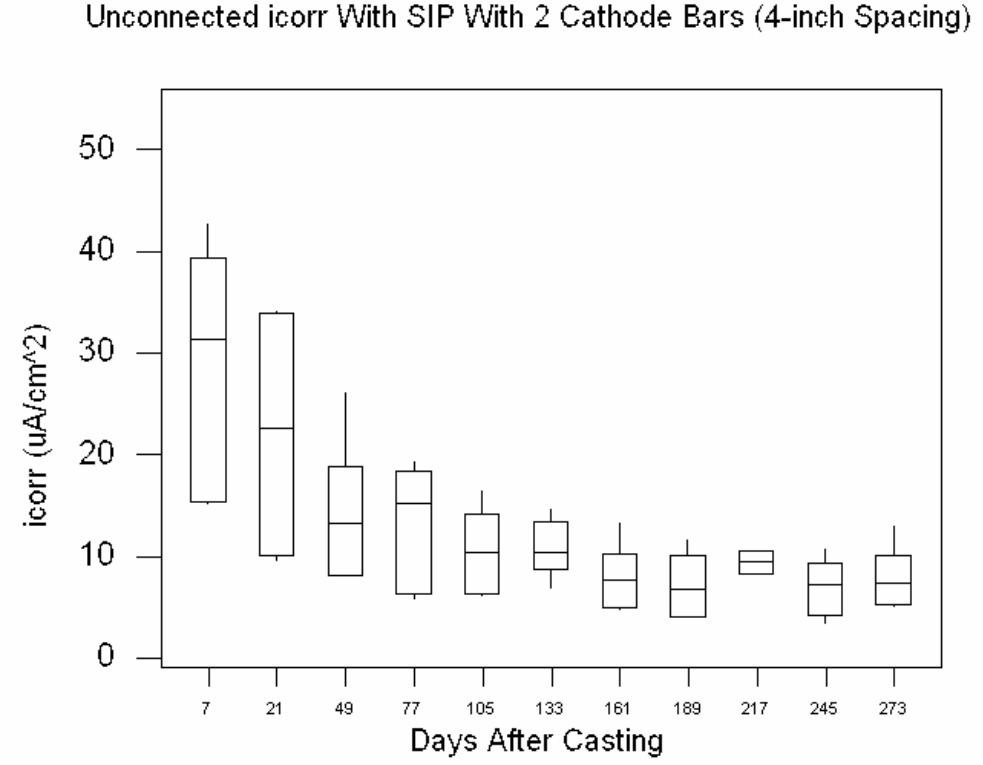

Figure D-13

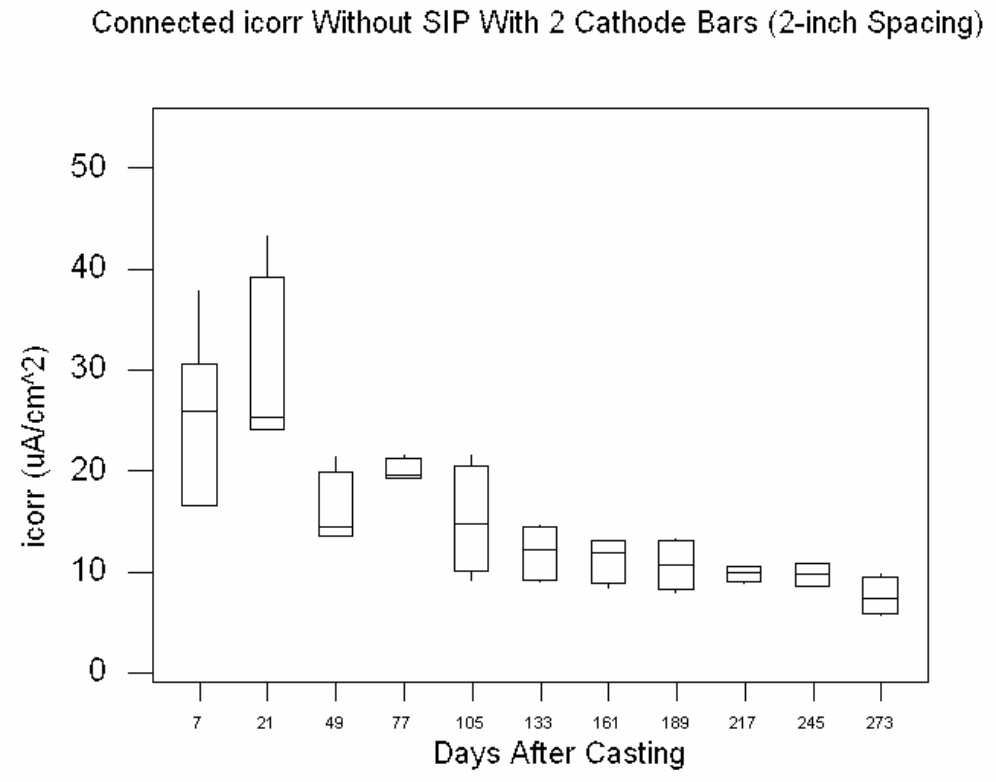

Figure D-14

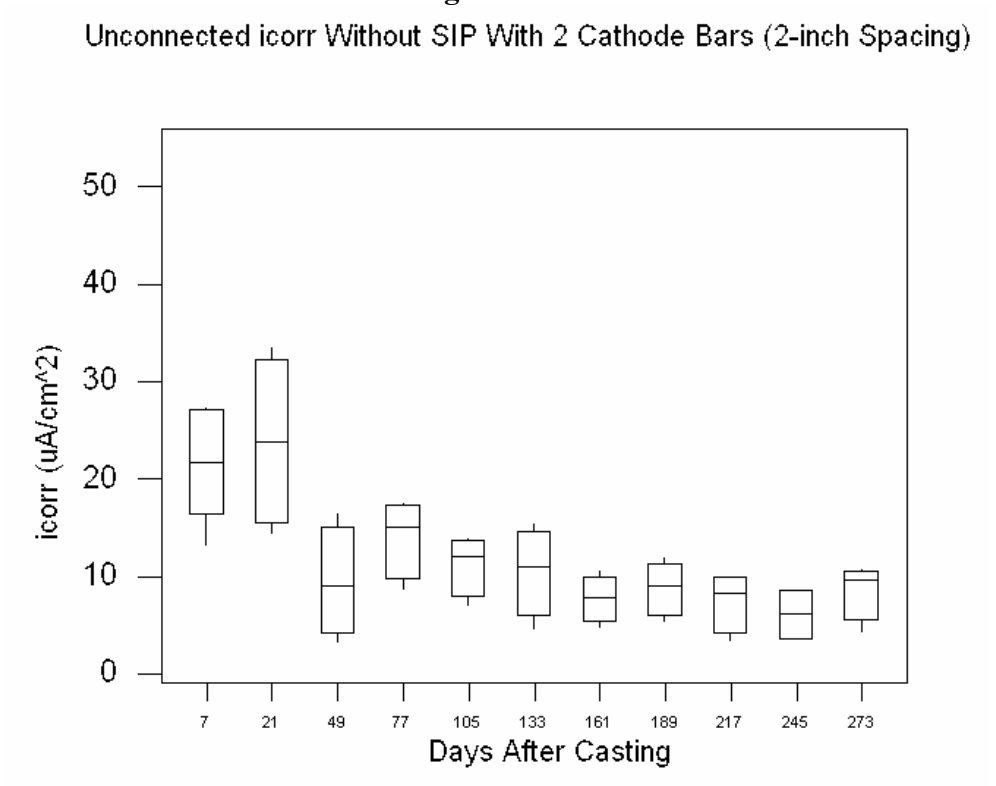

Figure D-15

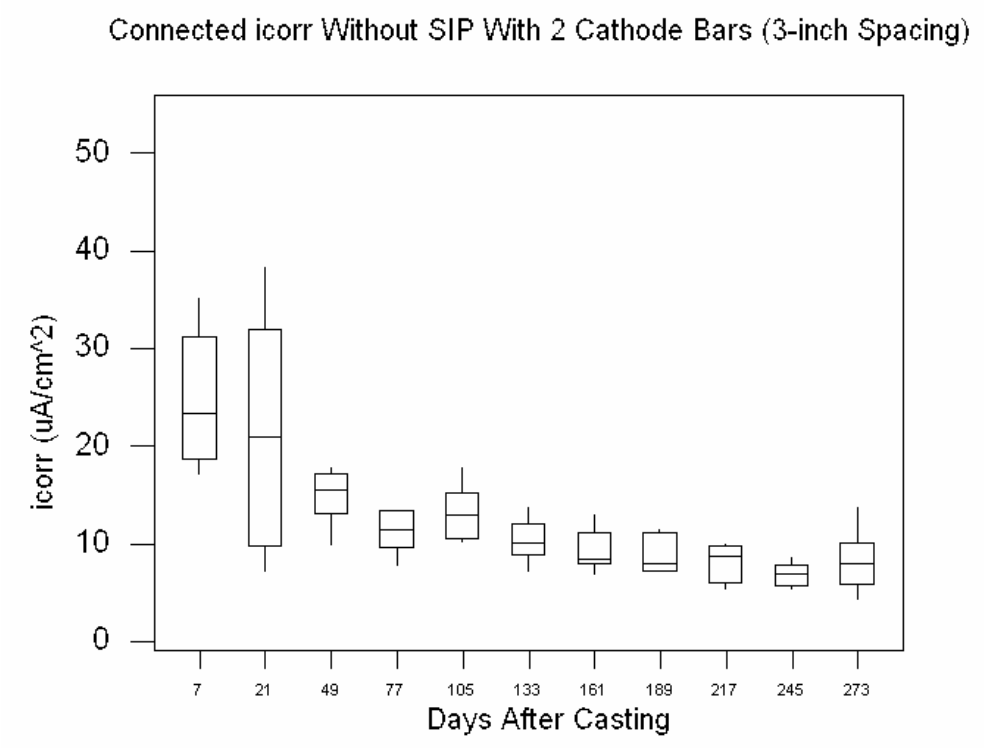

Figure D-16

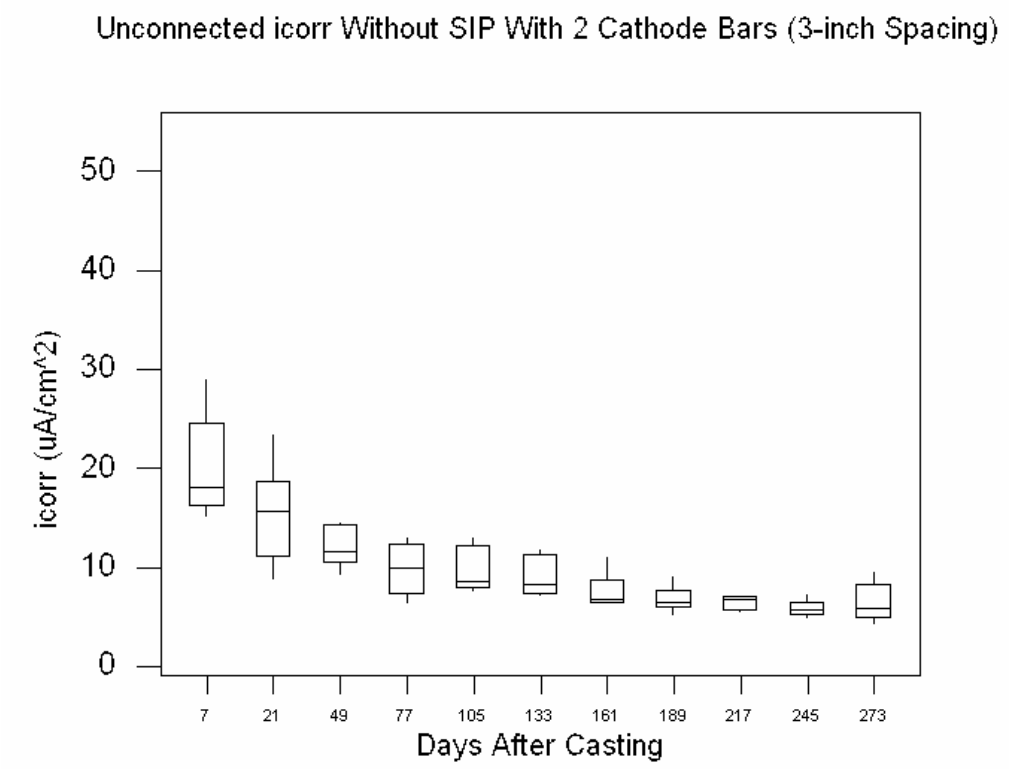

Figure D-17

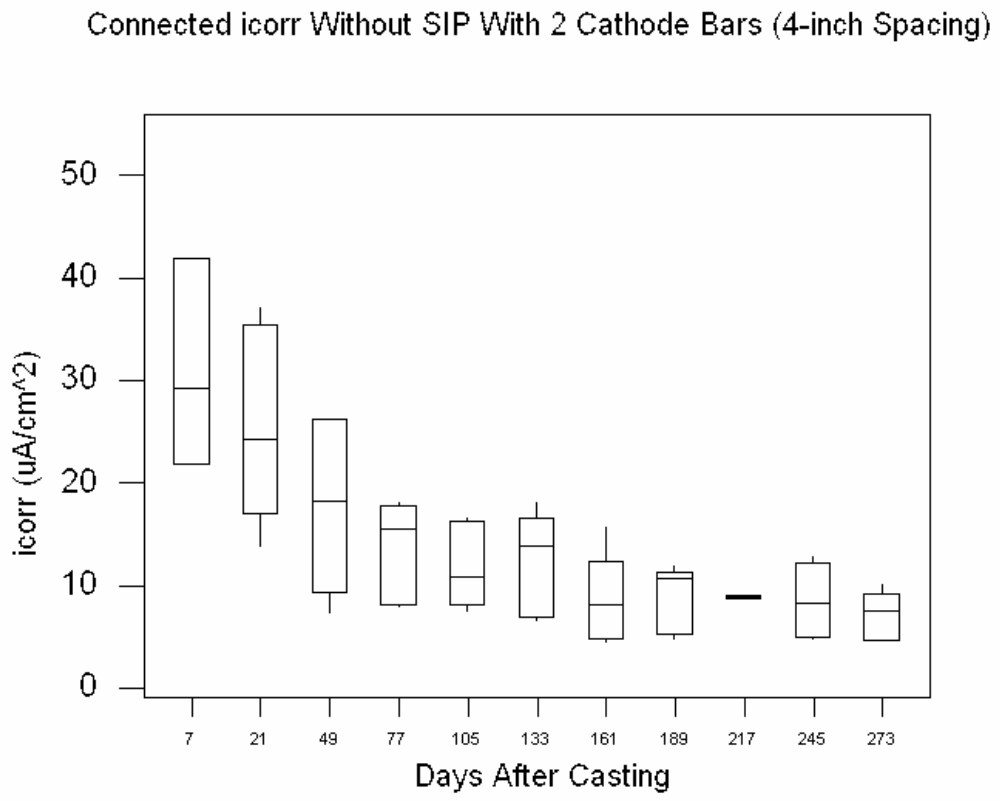

Figure D-18

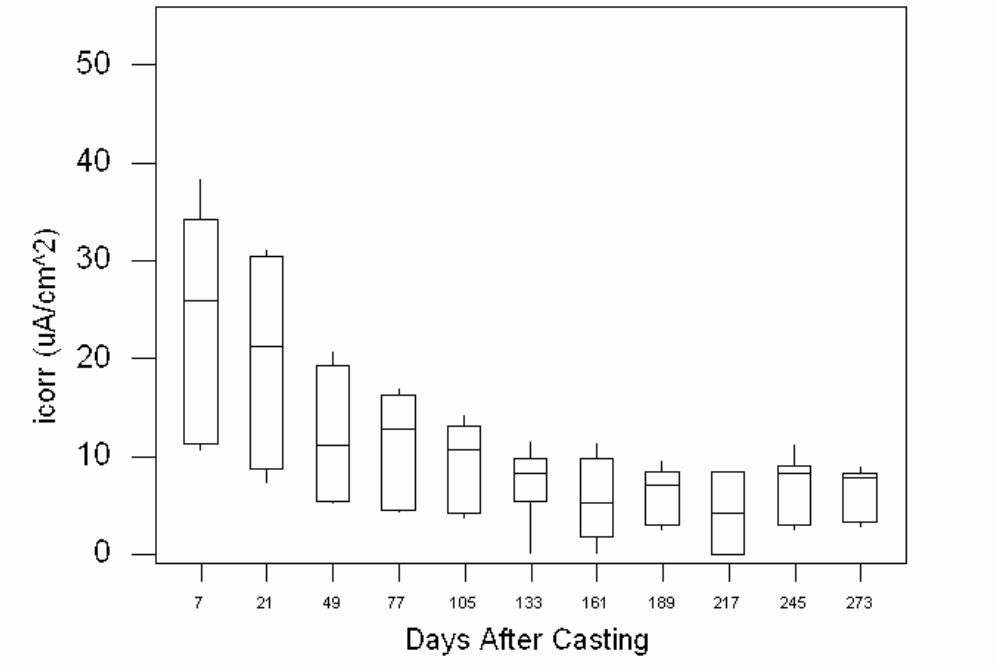

Appendix E – Macrocell Current Measurements

Figure E-1

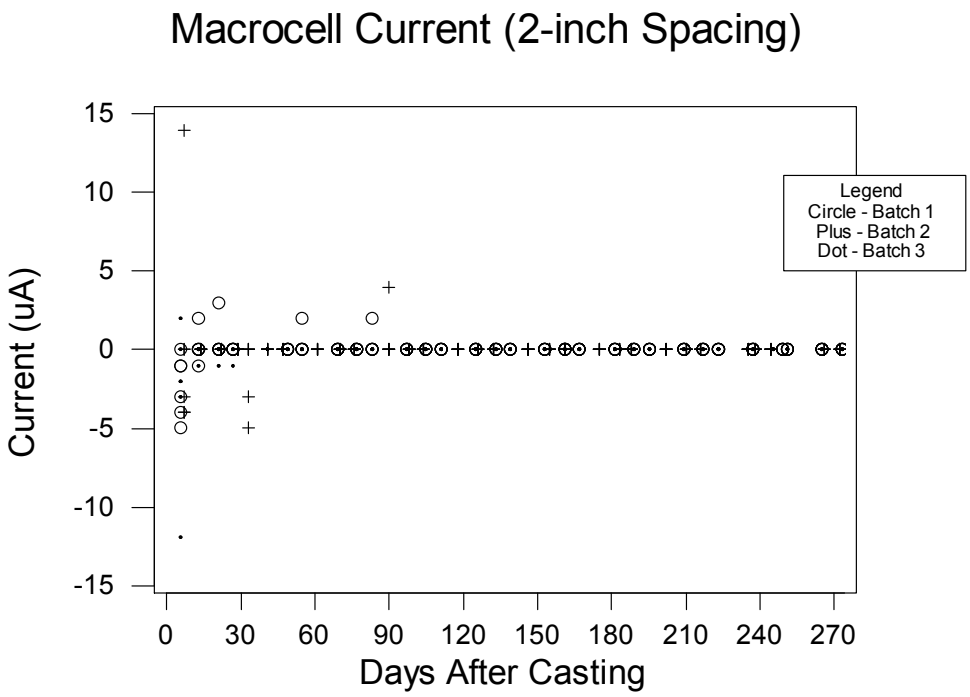

Figure E-2

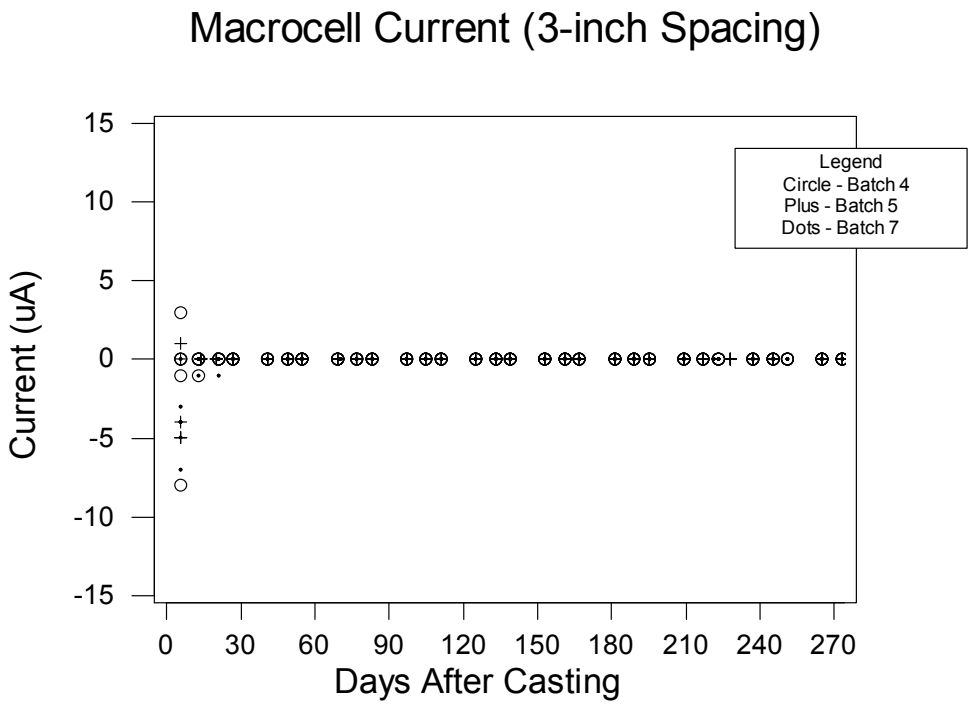

Figure E-3

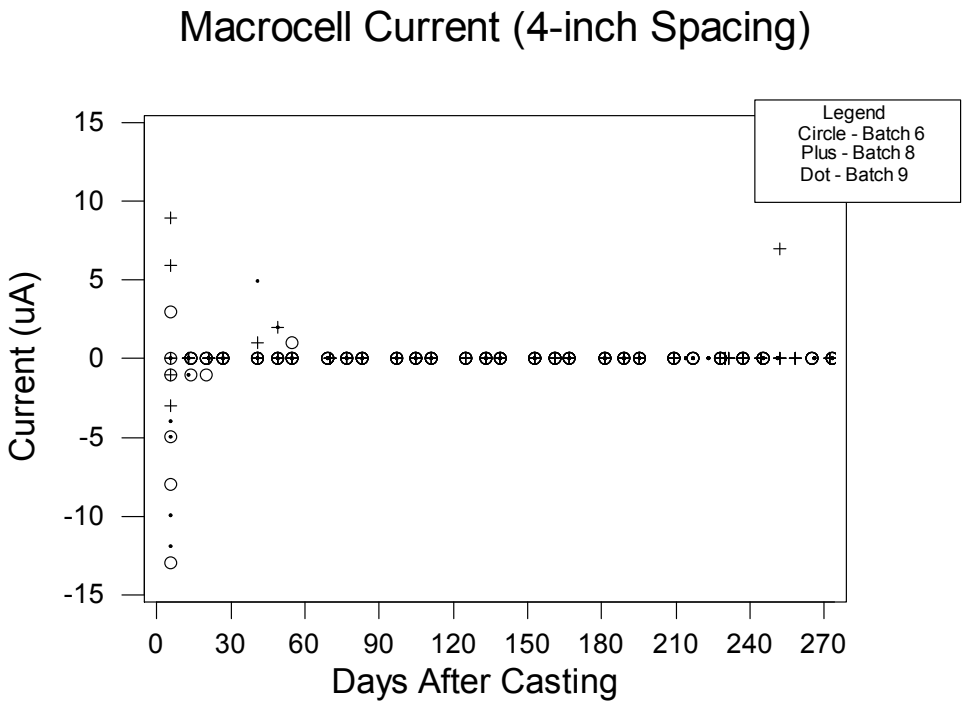
Macrocell Current (4-inch Spacing)
Legend
Circle - Batch 6
Plus - Batch 8
Dot - Batch 9
Current (uA)
15
10
5
0
-5
-10
-15
0
30
60
90
120
150
180
210
240
270
Days After Casting

Appendix F – Statistical Analysis

Statistical Analysis

Statistical analysis was performed using the MINITAB Software package to compare the mean resistivities, mean half-cell potentials, and mean corrosion current densities amongst each spacing arrangement against the presence and absence of SIP and different cathode to anode ratios.

Resistivity

Table F-1 - Differences in Mean Resistivity for Different Spacing Arrangements

Days After Casting	Spacing Arrangement Comparison mm (in)	Number of Measurements (N)	Differences in Mean Resistivity (Ω-m)	Paired t-test	Confidence Interval (%)
105	50.8 (2) v. 76.2 (3)	9	7.57	0.10	95
105	50.8 (2) v. 101.6 (4)	9	1.89	0.79	95
105	76.2 (3) v. 101.6 (4)	9	9.46	0.02	95
189	50.8 (2) v. 76.2 (3)	9	4.60	0.40	95
189	50.8 (2) v. 101.6 (4)	9	9.88	0.06	95
189	76.2 (3) v. 101.6 (4)	9	14.49	0.03	95
245	50.8 (2) v. 76.2 (3)	9	6.03	0.27	95
245	50.8 (2) v. 101.6 (4)	9	31.54	0.00	95
245	76.2 (3) v. 101.6 (4)	9	25.51	0.01	95

As can be seen from Table F-1, at a 95% confidence interval, few comparisons displayed significant differences between the mean resistivities at different spacing arrangements. It should be noted that the 50.8 mm (2 in) to 101.6 mm (4 in) comparison at days 105 and 245 display the greatest differences in the mean resistivities. However, these differences may be attributed to the outlying data and relatively large variability as presented in the figures in Appendix B.

Table F-2 – Differences in Mean Resistivity for Specimen With and Without SIP

Days After Casting	Spacing Arrangement Comparison mm (in)	SIP				NSIP			
		Number of Measurements (N)	Differences in Mean Resistivity (Ω-m)	Paired t-test	Confidence Interval (%)	Number of Measurements (N)	Differences in Mean Resistivity (Ω-m)	Paired t-test	Confidence Interval (%)
105	50.8 (2) v. 76.2 (3)	6	6.91	0.35	95	3	8.87	0.15	95
105	50.8 (2) v. 101.6 (4)	6	2.84	0.77	95	3	31.57	1.00	95
105	76.2 (3) v. 101.6 (4)	6	9.75	0.04	95	3	22.70	0.32	95
189	50.8 (2) v. 76.2 (3)	6	5.14	0.60	95	3	3.55	0.47	95
189	50.8 (2) v. 101.6 (4)	6	10.64	0.44	95	3	8.37	0.62	95
189	76.2 (3) v. 101.6 (4)	6	15.78	0.03	95	3	11.92	0.45	95
245	50.8 (2) v. 76.2 (3)	6	7.62	0.38	95	3	2.83	0.50	95
245	50.8 (2) v. 101.6 (4)	6	34.09	0.04	95	3	26.24	0.18	95
245	76.2 (3) v. 101.6 (4)	6	26.57	0.03	95	3	23.41	0.27	95

Few differences exist in the mean resistivity for specimens with and without SIP at specific days after casting, as can be seen in Table F-2. The greatest differences exists between the 76.2 mm (3 in) v. 101.6 mm (4 in) spacing with SIP at day 189 and the 76.2 mm (3 in) v. 101.6 mm (4 in) spacing without SIP at 245. However, the differences are relatively small and are inconsistent with previous data and may therefore, be considered insignificant.

Table F-3 – Differences in Mean Resistivity for Specimen with Different Cathode-to-Anode Ratios

Days After Casting	Spacing Arrangement Comparison mm (in)	C/A = 2/1				C/A = 1/1			
		SIP				SIP			
		Number of Measurements (N)	Differences in Mean Resistivity (Ω-m)	Paired t-test	Confidence Interval (%)	Number of Measurements (N)	Differences in Mean Resistivity (Ω-m)	Paired t-test	Confidence Interval (%)
105	50.8 (2) v. 76.2 (3)	3	7.09	0.68	95	3	6.74	0.18	95
105	50.8 (2) v. 101.6 (4)	3	0.69	0.97	95	3	4.96	0.56	95
105	76.2 (3) v. 101.6 (4)	3	7.78	0.23	95	3	11.70	0.21	95
189	50.8 (2) v. 76.2 (3)	3	11.38	0.61	95	3	1.06	0.83	95
189	50.8 (2) v. 101.6 (4)	3	9.5	0.75	95	3	11.70	0.30	95
189	76.2 (3) v. 101.6 (4)	3	20.88	0.17	95	3	10.64	0.13	95
245	50.8 (2) v. 76.2 (3)	3	7.43	0.67	95	3	7.80	0.54	95
245	50.8 (2) v. 101.6 (4)	3	43.9	0.21	95	3	24.47	0.16	95
245	76.2 (3) v. 101.6 (4)	3	36.47	0.07	95	3	16.67	0.09	95

As can be seen in Table F-3, the differences between the spacing arrangements for the mean resistivities of specimens with and without SIP and with different C/A ratios at specific days after casting varied only slightly. The paired t-test at all spacing arrangement comparisons was relatively strong, meaning few differences were likely for the mean resistivities, for all observed values in Table F-3 regardless of the presence or absence of SIP and different C/A ratios.

Half-Cell Potentials

Table F-4 – Differences in Mean Half-Cell Potentials for Specimen with Different Spacing Arrangements

Days After Casting	Spacing Arrangement Comparisons mm (in)	Connected Half-Cell Potentials (mV)				Unconnected Half-Cell Potentials (mV)			
		Number of Measurements (N)	Differences in Potential (mV)	Paired t-test	Confidence Interval (%)	Number of Measurements (N)	Differences in Potential (mV)	Paired t-test	Confidence Interval (%)
105	50.8 (2) v. 76.2 (3)	18	5.39	0.31	95	18	6.66	0.25	95
105	50.8 (2) v. 101.6 (4)	18	0.17	0.97	95	18	4.39	0.31	95
105	76.2 (3) v. 101.6 (4)	18	5.56	0.23	95	18	2.27	0.56	95
189	50.8 (2) v. 76.2 (3)	18	5.73	0.13	95	18	2.28	0.36	95
189	50.8 (2) v. 101.6 (4)	18	17.28	0.00	95	18	4.78	0.10	95
189	76.2 (3) v. 101.6 (4)	18	11.55	0.03	95	18	2.50	0.50	95
245	50.8 (2) v. 76.2 (3)	18	14.56	0.01	95	18	11.05	0.07	95
245	50.8 (2) v. 101.6 (4)	18	9.33	0.15	95	18	1.83	0.80	95
245	76.2 (3) v. 101.6 (4)	18	5.23	0.37	95	18	9.22	0.11	95

The differences in the mean half-cell potentials were compared for the connected and unconnected states and slight variances were observed, the greatest being between the 50.8 mm (2 in) v. 101.6 mm (4 in) spacing at day 189 and between the 50.8 mm (2 in) v. 76.2 in (3 in) spacing at day 245. However, a trend did not exist when compared with the other specific days after casting. Therefore, it may be assumed that outlying data and some variability contributed to the weak t-test values at a 95% confidence interval.

Table F-5 – Differences in Mean Half-Cell Potentials for Specimen With SIP

Days After Casting	Spacing Arrangement Comparisons mm (in)	SIP							
		Connected Half-Cell Potentials (mV)				Unconnected Half-Cell Potentials (mV)			
		Number of Measurements (N)	Differences in Potential (mV)	Paired t-test	Confidence Interval (%)	Number of Measurements (N)	Differences in Potential (mV)	Paired t-test	Confidence Interval (%)
105	50.8 (2) v. 76.2 (3)	12	12.67	0.05	95	12	13.83	0.07	95
105	50.8 (2) v. 101.6 (4)	12	0.50	0.94	95	12	6.66	0.28	95
105	76.2 (3) v. 101.6 (4)	12	12.17	0.03	95	12	7.17	0.17	95
189	50.8 (2) v. 76.2 (3)	12	2.75	0.53	95	12	1.00	0.73	95
189	50.8 (2) v. 101.6 (4)	12	22.33	0.00	95	12	9.08	0.02	95
189	76.2 (3) v. 101.6 (4)	12	19.58	0.01	95	12	8.08	0.17	95
245	50.8 (2) v. 76.2 (3)	12	13.67	0.02	95	12	4.67	0.53	95
245	50.8 (2) v. 101.6 (4)	12	0.08	0.05	95	12	8.00	0.41	95
245	76.2 (3) v. 101.6 (4)	12	13.75	0.45	95	12	3.33	0.31	95

Table F-6 – Differences in Mean Half-Cell Potentials Without SIP

Days After Casting	Spacing Arrangement Comparisons mm (in)	NSIP							
		Connected Half-Cell Potentials (mV)				Unconnected Half-Cell Potentials (mV)			
		Number of Measurements (N)	Differences in Potential (mV)	Paired t-test	Confidence Interval (%)	Number of Measurements (N)	Differences in Potential (mV)	Paired t-test	Confidence Interval (%)
105	50.8 (2) v. 76.2 (3)	6	9.16	0.37	95	6	4.83	0.64	95
105	50.8 (2) v. 101.6 (4)	6	1.50	0.80	95	6	2.67	0.74	95
105	76.2 (3) v. 101.6 (4)	6	7.66	0.15	95	6	7.50	0.10	95
189	50.8 (2) v. 76.2 (3)	6	11.66	0.14	95	6	4.83	0.35	95
189	50.8 (2) v. 101.6 (4)	6	7.16	0.13	95	6	3.83	0.23	95
189	76.2 (3) v. 101.6 (4)	6	4.50	0.33	95	6	8.66	0.05	95
245	50.8 (2) v. 76.2 (3)	6	19.00	0.07	95	6	13.67	0.12	95
245	50.8 (2) v. 101.6 (4)	6	5.17	0.55	95	6	10.50	0.31	95
245	76.2 (3) v. 101.6 (4)	6	24.17	0.10	95	6	24.17	0.04	95

The differences in the mean half-cell potentials in the connected and unconnected states with SIP and without SIP vary only slightly at the specified days after casting. The weakest relationships were present amongst the connected mean half-cell potentials with SIP at day 189 between the 50.8 mm (2 in) v. 101.6 mm (4 in) spacing and the 76.2 mm (3 in) v. 101.6 mm (4 in) spacing. However, in the unconnected state with SIP and both the connected and unconnected states with and without SIP, the large differences in the mean half-cell potentials do not exist. Therefore, it may be assumed that the differences are insignificant.

Table F-7 – Differences in Mean Half-Cell Potentials with C/A = 2/1

Days After Casting	Spacing Arrangement Comparisons mm (in)	C/A = 2/1							
		SIP							
		Connected Half-Cell Potentials (mV)				Unconnected Half-Cell Potentials (mV)			
		Number of Measurements (N)	Differences in Potential (mV)	Paired t-test	Confidence Interval (%)	Number of Measurements (N)	Differences in Potential (mV)	Paired t-test	Confidence Interval (%)
105	50.8 (2) v. 76.2 (3)	6	8.67	0.30	95	6	8.33	0.30	95
105	50.8 (2) v. 101.6 (4)	6	1.67	0.88	95	6	3.17	0.67	95
105	76.2 (3) v. 101.6 (4)	6	7.00	0.16	95	6	5.16	0.24	95
189	50.8 (2) v. 76.2 (3)	6	4.83	0.22	95	6	2.33	0.54	95
189	50.8 (2) v. 101.6 (4)	6	16.17	0.01	95	6	7.34	0.08	95
189	76.2 (3) v. 101.6 (4)	6	21.00	0.01	95	6	9.67	0.03	95
245	50.8 (2) v. 76.2 (3)	6	10.08	0.34	95	6	4.20	0.74	95
245	50.8 (2) v. 101.6 (4)	6	20.33	0.09	95	6	9.87	0.45	95
245	76.2 (3) v. 101.6 (4)	6	10.25	0.13	95	6	5.67	0.41	95

Table F-8 – Differences in Mean Half-Cell Potentials with C/A = 1/1

Days After Casting	Spacing Arrangement Comparisons mm (in)	C/A = 1/1							
		SIP							
		Connected Half-Cell Potentials (mV)				Unconnected Half-Cell Potentials (mV)			
		Number of Measurements (N)	Differences in Potential (mV)	Paired t-test	Confidence Interval (%)	Number of Measurements (N)	Differences in Potential (mV)	Paired t-test	Confidence Interval (%)
105	50.8 (2) v. 76.2 (3)	6	16.66	0.17	95	6	16.50	0.22	95
105	50.8 (2) v. 101.6 (4)	6	0.67	0.88	95	6	7.33	0.24	95
105	76.2 (3) v. 101.6 (4)	6	17.33	0.14	95	6	9.17	0.35	95
189	50.8 (2) v. 76.2 (3)	6	10.33	0.24	95	6	4.33	0.51	95
189	50.8 (2) v. 101.6 (4)	6	28.50	0.01	95	6	10.83	0.13	95
189	76.2 (3) v. 101.6 (4)	6	18.17	0.12	95	6	6.50	0.48	95
245	50.8 (2) v. 76.2 (3)	6	10.00	0.09	95	6	7.66	0.13	95
245	50.8 (2) v. 101.6 (4)	6	12.83	0.19	95	6	6.16	0.59	95
245	76.2 (3) v. 101.6 (4)	6	2.83	0.56	95	6	1.50	0.87	95

As can be seen in Table F-7 and F-8, the differences between the half-cell potentials at different spacing arrangements, with and without SIP, and with different C/A ratios varied only slightly. Generally, the t-test for a 95% confidence interval presented very strong relationships that few differences existed between the mean half-cell potentials. It should be noted that at day 189 in the connected state with SIP between the 50.8 mm (2 in) v. 101.6 mm (4 in) spacing displayed a large difference and weak t-test value in both C/A = 2/1 and C/A = 1/1. A slight difference may exist between the resistivities at this time period after casting but the value, a difference of approximately 16 to 29 mV does not appear significant enough to warrant further evaluation.

Corrosion Current Density

Table F-9 – Differences in Mean Corrosion Current Density for Specimen with Different Spacing Arrangements

Days After Casting	Spacing Arrangement Comparisons mm (in)	Connected i_{corr} (uA/cm^2)				Unconnected i_{corr} (uA/cm^2)			
		Number of Measurements (N)	Differences in Mean i_{corr} (uA/cm^2)	Paired t-test	Confidence Interval (%)	Number of Measurements (N)	Differences in Mean i_{corr} (uA/cm^2)	Paired t-test	Confidence Interval (%)
105	50.8 (2) v. 76.2 (3)	18	2.24	0.09	95	18	3.65	0.00	95
105	50.8 (2) v. 101.6 (4)	18	0.72	0.61	95	18	1.65	0.28	95
105	76.2 (3) v. 101.6 (4)	18	1.52	0.30	95	18	2.00	0.18	95
189	50.8 (2) v. 76.2 (3)	18	1.19	0.12	95	18	1.87	0.01	95
189	50.8 (2) v. 101.6 (4)	18	0.57	0.49	95	18	0.81	0.25	95
189	76.2 (3) v. 101.6 (4)	18	1.76	0.13	95	18	1.06	0.24	95
245	50.8 (2) v. 76.2 (3)	18	1.13	0.08	95	18	1.89	0.00	95
245	50.8 (2) v. 101.6 (4)	18	0.93	0.40	95	18	0.06	0.95	95
245	76.2 (3) v. 101.6 (4)	18	2.06	0.07	95	18	1.95	0.02	95

The mean differences in the corrosion current density for all spacing arrangement comparisons were relatively strong when compared in a paired t-test for the connected state. However, the unconnected state presented some differences between 50.8 mm (2 in) v. 76.2 mm (3 in) spacing arrangements at day 105 and at day 245. The large differences and weak t-test may be attributed to the relatively large variability that existed at days 105 and 245 for these spacing arrangements, as seen in Appendix D, and can therefore be considered insignificant.

Table F-10 – Differences in Mean Corrosion Current Density for Specimen with SIP

Days After Casting	Spacing Arrangement Comparisons mm (in)	SIP							
		Connected i_{corr} (uA/cm^2)				Unconnected i_{corr} (uA/cm^2)			
		Number of Measurements (N)	Differences in Mean i_{corr} (uA/cm^2)	Paired t-test	Confidence Interval (%)	Number of Measurements (N)	Differences in Mean i_{corr} (uA/cm^2)	Paired t-test	Confidence Interval (%)
105	50.8 (2) v. 76.2 (3)	12	2.89	0.04	95	12	4.32	0.01	95
105	50.8 (2) v. 101.6 (4)	12	0.10	0.95	95	12	1.20	0.53	95
105	76.2 (3) v. 101.6 (4)	12	2.99	0.11	95	12	3.12	0.09	95
189	50.8 (2) v. 76.2 (3)	12	1.36	0.11	95	12	2.25	0.01	95
189	50.8 (2) v. 101.6 (4)	12	0.17	0.80	95	12	1.28	0.07	95
189	76.2 (3) v. 101.6 (4)	12	1.19	0.24	95	12	0.97	0.26	95
245	50.8 (2) v. 76.2 (3)	12	0.17	0.85	95	12	1.84	0.01	95
245	50.8 (2) v. 101.6 (4)	12	1.91	0.06	95	12	0.35	0.62	95
245	76.2 (3) v. 101.6 (4)	12	2.08	0.14	95	12	2.19	0.01	95

Table F-11 – Differences in Mean Corrosion Current Density for Specimen without SIP

Days After Casting	Spacing Arrangement Comparisons mm (in)	NSIP							
		Connected i_{corr} (uA/cm^2)				Unconnected i_{corr} (uA/cm^2)			
		Number of Measurements (N)	Differences in Mean i_{corr} (uA/cm^2)	Paired t-test	Confidence Interval (%)	Number of Measurements (N)	Differences in Mean i_{corr} (uA/cm^2)	Paired t-test	Confidence Interval (%)
105	50.8 (2) v. 76.2 (3)	6	0.93	0.76	95	6	2.34	0.07	95
105	50.8 (2) v. 101.6 (4)	6	2.37	0.44	95	6	2.55	0.38	95
105	76.2 (3) v. 101.6 (4)	6	1.44	0.52	95	6	0.21	0.94	95
189	50.8 (2) v. 76.2 (3)	6	0.85	0.63	95	6	1.11	0.36	95
189	50.8 (2) v. 101.6 (4)	6	0.55	0.66	95	6	1.67	0.15	95
189	76.2 (3) v. 101.6 (4)	6	0.30	0.89	95	6	0.56	0.73	95
245	50.8 (2) v. 76.2 (3)	6	1.98	0.10	95	6	1.36	0.10	95
245	50.8 (2) v. 101.6 (4)	6	0.33	0.88	95	6	0.26	0.90	95
245	76.2 (3) v. 101.6 (4)	6	1.65	0.39	95	6	1.10	0.54	95

The differences in the mean corrosion current densities in Tables F-10 and Table F-11 are relatively small and possess strong t-test values for all specimen without SIP in the connected and unconnected states and for specimen with SIP in the connected state. Relatively larger differences existed in the unconnected state with SIP. These differences were prevalent between the 50.8 mm (2 in) v. 76.2 mm (3 in) spacing arrangements at days 105, 189, and 245. However, these differences appear to be isolated instances as they do not appear to display a trend when compared with the other half-cell potential data.

Table F-12 – Differences in Mean Corrosion Current Density for Specimen with C/A = 2/1

Days After Casting	Spacing Arrangement Comparisons mm (in)	C/A = 2/1							
		SIP							
		Connected i_{corr} (uA/cm^2)				Unconnected i_{corr} (uA/cm^2)			
		Number of Measurements (N)	Differences in Mean i_{corr} (uA/cm^2)	Paired t-test	Confidence Interval (%)	Number of Measurements (N)	Differences in Mean i_{corr} (uA/cm^2)	Paired t-test	Confidence Interval (%)
105	50.8 (2) v. 76.2 (3)	6	3.14	0.13	95	6	5.18	0.07	95
105	50.8 (2) v. 101.6 (4)	6	0.51	0.88	95	6	1.95	0.57	95
105	76.2 (3) v. 101.6 (4)	6	2.63	0.33	95	6	3.23	0.24	95
189	50.8 (2) v. 76.2 (3)	6	1.70	0.08	95	6	2.09	0.01	95
189	50.8 (2) v. 101.6 (4)	6	0.89	0.70	95	6	0.28	0.86	95
189	76.2 (3) v. 101.6 (4)	6	2.59	0.25	95	6	1.81	0.27	95
245	50.8 (2) v. 76.2 (3)	6	0.28	0.81	95	6	2.03	0.05	95
245	50.8 (2) v. 101.6 (4)	6	1.51	0.46	95	6	0.08	0.96	95
245	76.2 (3) v. 101.6 (4)	6	1.23	0.79	95	6	2.11	0.24	95

Table F-13 – Differences in Mean Corrosion Current Density for Specimen with C/A = 1/1

Days After Casting	Spacing Arrangement Comparisons mm (in)	C/A = 1/1							
		SIP							
		Connected i_{corr} (uA/cm^2)				Unconnected i_{corr} (uA/cm^2)			
		Number of Measurements (N)	Differences in Mean i_{corr} (uA/cm^2)	Paired t-test	Confidence Interval (%)	Number of Measurements (N)	Differences in Mean i_{corr} (uA/cm^2)	Paired t-test	Confidence Interval (%)
105	50.8 (2) v. 76.2 (3)	6	2.64	0.24	95	6	3.34	0.01	95
105	50.8 (2) v. 101.6 (4)	6	0.71	0.56	95	6	0.34	0.90	95
105	76.2 (3) v. 101.6 (4)	6	3.35	0.27	95	6	3.00	0.28	95
189	50.8 (2) v. 76.2 (3)	6	1.00	0.52	95	6	2.41	0.08	95
189	50.8 (2) v. 101.6 (4)	6	1.38	0.04	95	6	0.47	0.69	95
189	76.2 (3) v. 101.6 (4)	6	2.38	0.26	95	6	1.94	0.28	95
245	50.8 (2) v. 76.2 (3)	6	0.63	0.45	95	6	1.64	0.04	95
245	50.8 (2) v. 101.6 (4)	6	2.47	0.10	95	6	0.43	0.72	95
245	76.2 (3) v. 101.6 (4)	6	3.10	0.16	95	6	2.07	0.12	95

As can be seen from Tables F-11 and F-12, the differences between the mean corrosion current densities with different C/A ratios varies only slightly. The paired t-test at the specified confidence interval supports the relatively small differences. Therefore, it may be assumed that the mean corrosion current densities differences are insignificant regardless of the C/A ratio, the presence of SIP, and at specific days after casting for both the connected and unconnected states.